EXPLORATION GEOPHYSICS
https://doi.org/10.1080/08123985.2021.1951117

The magnetic field and magnetic gradient tensor for a right circular cylinder

K. Blair McKenzie[a,b]

[a]Department of Earth and Environmental Sciences, Macquarie University, Sydney, Australia; [b]Tensor Research Pty Ltd, Greenwich, Australia

ABSTRACT

Expressions for the magnetic scalar potential, the magnetic field vector and the magnetic gradient tensor due to a uniformly magnetised semi-infinite right circular vertical cylinder are presented based on an application of Poisson's relation to the gravity gradient tensor. The superposition principle allows for the theory to be extended to finite length and concentrically zoned right circular cylinders. This formulation provides an accurate and computationally efficient means of modelling the magnetic response of vertical or plunging right circular cylinders or pipes in which the total magnetisation is assumed to be homogeneous. This modelling technique lends itself to inversion applications in magnetic exploration. Furthermore, the theory presented here considers some important special cases including expressions for the magnetic gradient tensor on the axis of a vertical cylinder or pipe. This leads to expressions for estimating the direction of magnetisation within a uniformly magnetised pipe. This theory provides a basis for mapping magnetisation directions over quasi-vertical pipe-like bodies.

ARTICLE HISTORY
Received 17 December 2020
Accepted 30 June 2021

KEYWORDS
Pipe; gravity gradient tensor; magnetic gradient tensor; magnetisation; superposition

Introduction

The finite and semi-infinite, right circular cylinder model in geophysical exploration can provide a useful representation of pipe-like bodies in both gravity and magnetic modelling. For example right circular vertical pipes provide a useful representation for many quasi-circular kimberlite pipes, some near-vertical basaltic pipe swarms and some pipe-like magnetite and pyrrhotite bearing ore bodies (Clark 2012, 2013, 2014; Pratt, McKenzie, and White 2014).

In this paper, I derive expressions for the magnetic scalar potential, the magnetic field vector and the magnetic gradient tensor of the semi-infinite right circular vertical cylinder or pipe. Expressions for the finite length circular cylinder (or pipe) may then be deduced using the principle of superposition. Importantly, I note that the following two descriptive terms referred to throughout this paper, namely, right circular vertical cylinder and right circular vertical pipe are identical magnetic sources.

This work has its basis in papers by Singh (1977b) and Singh and Sabina (1978) who used a Fourier–Hankel transform of Poisson's equation to derive a closed form expression for the gravitational potential at points on or above the top face of the cylinder. This development enabled Singh and Sabina (1978) to derive closed form expressions for the total anomalous magnetic field due to a right circular vertical cylinder with uniform total magnetisation via an application of Poisson's relation. Prior to this research, papers on the magnetic response of right circular vertical cylinders were rather uncommon in the literature with most attention focussed on the derivation of expressions for the vertical component of gravitational attraction due to right circular vertical cylinder sources [see for example, Nabighian 1962; Nagy 1965; Singh 1977a,b]. Reilly (1969) and Woodward (1973) presented expressions for the anomalous gravitational and magnetic effects of right circular cylinders. Importantly, Reilly (1969) derived expressions for the anomalous gravitational potential, the gravitational field, the gravity gradient tensor and the components of the anomalous magnetic field due to a finite length right circular cylinder with arbitrary orientation and uniform magnetisation but his formulation was based on infinite series of Legendre polynomials which presented some computational difficulties and convergence problems (Woodward 1973; Siew 1990).

More recently Damiata and Lee (2002a, 2002b) have derived expressions for the components of the gravitational field due to both vertical and plunging circular cylinders using the gravitational potential given in Singh (1977b). In their second paper, Damiata and Lee (2002b) noted but did not elaborate in detail how this theory may be extended to computation of the magnetic field components. Finally, Rim and Li (2016) have derived expressions for the gravity gradient tensor due to a plunging circular cylinder, however, these expressions were not extended to the magnetic field or magnetic gradient tensor cases.

CONTACT K. Blair McKenzie keith.mckenzie@students.mq.edu.au Department of Earth and Environmental Sciences, Macquarie University, North Ryde, NSW 2109, Australia; Tensor Research Pty Ltd, P.O. Box 5189, Greenwich, NSW 2065, Australia

An important theoretical investigation of the anomalous magnetic field due to a vertical cylinder was given in Siew (1990) and also in Siew (1997) in which he outlined a methodology for differentiating between cylinders and discs. In his earlier paper, Siew (1990) showed that expressions for the anomalous potential due to a vertical cylinder can be expressed as a pair of axisymmetric and non-symmetric potentials which arise from its top planar surface and from its curved vertical face respectively. Siew (1990) did not provide explicit expressions for the magnetic field components in his paper but he was able to confirm that for low susceptibility sources, the expressions for the pair of axisymmetric and non-symmetric magnetic scalar potentials (in Equations (5.6) and (5.7) of his paper) were in agreement with Singh and Sabina (1978). An important aspect of Siew's (1990) paper is an investigation of the logarithmic singularity on the rim of the cylinder which leads to expressions for the magnetic scalar potential both inside and outside a permeable magnetic cylinder with the former providing a basis for the computing the self demagnetisation effects of a vertical cylinder in which the relative magnetic permeability μ/μ_0 exceeds 1.

As noted above the development of theory for calculating both the full gravitational and magnetic fields and their respective gradient tensors for a right circular cylinder has been both slow and fragmented. This paper presents a more unified overview of the theory filling in gaps not covered in previous papers and culminating in theory for the magnetic gradient tensor of a right circular cylinder. First I will use Poisson's relation to derive an expression for the magnetic scalar potential due to a right circular cylinder using expressions for its gravitational field components. Second I will again use Poisson's relation to derive expressions for the magnetic field components due to a uniformly magnetised cylinder using expressions for the gravity gradient tensor due to a right circular cylinder. The expressions for the magnetic gradient tensor may be derived from either the scalar magnetic potential or from the gravity gradient tensor. Here I use the second approach which allows me to highlight the relation between the gravity gradient tensor and the magnetic field components for three orthogonal magnetisation directions which leads to a definition of the magnetic field-magnetisation matrix for a vertical cylinder.

The expressions for the magnetic scalar potential, the magnetic field vector and the magnetic gradient tensor of a circular pipe contain a total of six Lipschitz–Hankel integrals which involve products of pairs of Bessel functions. Closed form expressions for each of these integrals which necessarily involve elliptic integral functions have been derived by Eason, Noble, and Sneddon (1955). In addition to presenting these results, I shall discuss the numerical accuracy of these formulae for various geometries of observation points relative to the centre of the top face of the cylinder. The results will be compared with those derived from using a facetted circular pipe model where the number of sides in polygonal section is allowed to increase.

The theory presented in this paper gives expressions for the magnetic field and gradient tensor at an external observation point in both Cartesian and cylindrical coordinates. This includes some important special cases including observation points which may be axial or coplanar with a right circular vertical pipe. Most importantly the axial cases lead to expressions for calculating the direction of magnetisation in a vertical pipe. Furthermore, the use of cylindrical coordinates facilitates the extension of theory to calculating the anomalous magnetic field and the magnetic gradient tensor for a plunging right circular cylinder or pipe.

In addition I shall show that the superposition principle not only allows for the modelling of the magnetic fields and gradient tensors due to finite length right circular pipes, but it also facilitates the modelling of circular pipes which possess concentric zoning of magnetisation properties or alternatively it enables the modelling of pipes which change radius and bulk magnetisation properties vertically or along the axis of the pipe.

Finally I present images showing the symmetry relations between various magnetic field components and gradient tensor elements when the resultant magnetisation directions in a right circular vertical pipe are aligned north, east and vertically down.

Theory

A closed expression for the gravitational potential $U(\mathbf{r})$ due to a semi-infinite right circular vertical cylinder of radius a and uniform density or density contrast ρ at a measurement point $\mathrm{P}(\mathbf{r})\,;\mathbf{r}=(x,y,z)^T$ located on or above the top surface of the cylinder ($z \leq 0$) was derived by Singh (1977b) and restated in Singh and Sabina (1978) using a new nomenclature and a new Cartesian coordinate system (consistent with geomagnetism) in which the vertical or z axis is defined as positive downwards rather than positive upwards. The expression derived by Singh (1977b) for the gravitational potential comprises an integral of the Lipschitz–Hankel type involving the product of a pair of Bessel functions which often arise from systems of axial or cylindrical symmetry (Eason, Noble, and Sneddon 1955). In this instance,

$$U(\mathbf{r}) = 2\pi\, \mathrm{G}\rho a \int_0^\infty \mathrm{J}_1(ap)\, \mathrm{J}_0(rp) \mathrm{e}^{-|z|p}\, p^{-2}\, \mathrm{d}p, \qquad (1)$$

where the radial coordinate $r = \sqrt{x^2 + y^2}$ is the horizontal distance from the origin located at the centre of the top face of the cylinder (see Figure 1), z is the vertical coordinate of the observation station $\mathrm{P}(\mathbf{r})$, and G is the universal gravitational constant. As shown in Figure 1, the Cartesian coordinate system adopted here follows the normal geomagnetic field convention, namely, it

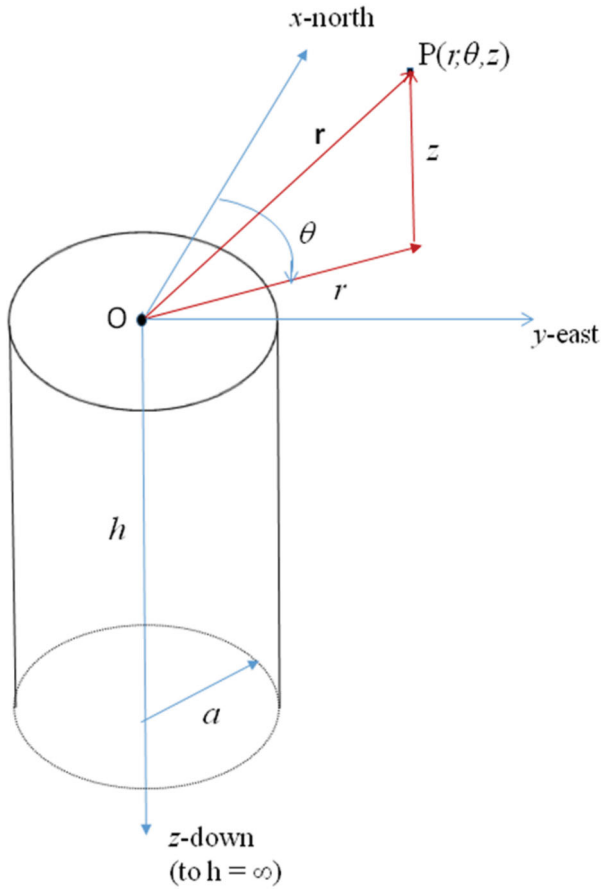

Figure 1. Coordinate system for evaluating the magnetic response of a right circular vertical cylinder of radius a, axial length h at a measurement station P(**r**). In cylindrical coordinates the observation point is P(r,θ,z) where r is the radial or horizontal distance of P from the origin; θ is the horizontal azimuth of P measured positive clockwise from north; and $|z|$ is the elevation of P above the top surface of the cylinder.

is a right-hand clockwise system in which the x axis points north ($x-N$), the y axis points east ($y-E$) and the z axis points vertically down ($z-D$). The integral equation in (1) may be rewritten more efficiently following Eason, Noble, and Sneddon (1955), in which the Lipschitz–Hankel integral $I(\mu,\nu;\lambda)$ is defined as:

$$I(\mu,\nu;\lambda) = \int_0^\infty \mathrm{J}_\mu(at)\,\mathrm{J}_\upsilon(bt)\mathrm{e}^{-ct}t^\lambda \mathrm{d}t, \qquad (2)$$

where $\mathrm{J}_\mu(at)$ and $\mathrm{J}_\upsilon(bt)$ are Bessel functions of the first kind and order μ and ν respectively and λ is a real exponent of the integrand t.

From this definition, the expression for the gravitational potential in Equation (1) may be written as (Singh and Sabina 1978):

$$U(\mathbf{r}) = 2\pi\,\mathrm{G}\rho a I(1,0;-2). \qquad (3)$$

The development by Singh (1977b) was important because it has allowed for the formulation of expressions for the anomalous gravity field vector and its associated gravity gradient tensor. Even more importantly, the expressions for the gravity field vector and gravity gradient tensor may be used to derive expressions for the anomalous magnetic scalar potential $V(\mathbf{r})$ and the anomalous magnetic field vector $\mathbf{b}(\mathbf{r})$ respectively via an application of Poisson's relation. This was recognised by Singh and Sabina (1978) who derived expressions for the total anomalous magnetic field intensity $b_\mathrm{T}(\mathbf{r})$ due to a right circular vertical cylinder with uniform intrinsic total magnetisation **M** where the effect of self-demagnetisation is neglected. Here, it is noted that Poisson's relation may be applied to any uniformly magnetised homogeneous body with magnetisation **M** and density or density contrast ρ (Blakely 1995).

The magnetic scalar potential $V(\mathbf{r})$ due to a semi-infinite right circular vertical cylinder

Expressions for the magnetic scalar potential $V(\mathbf{r})$ and the anomalous magnetic field vector $\mathbf{b}(\mathbf{r}) = (b_x,b_y,b_z)^T$ at a measurement point P(**r**) external to a uniform right circular cylinder with magnetisation $\mathbf{M} = (M_x,M_y,M_z)^T$ and density ρ may be derived from the gravity field vector $\mathbf{g}(\mathbf{r}) = (g_x,g_y,g_z)^T$ and the gravity gradient tensor $\boldsymbol{\Gamma}(\mathbf{r})$ respectively via an application of Poisson's relation (Blakely 1995, 91–93). An expression for the magnetic scalar potential may derived from the following relation:

$$V(\mathbf{r}) = -C_\mathrm{m}\left(\frac{1}{G\rho}\right)\nabla U(\mathbf{r})\cdot\mathbf{M} = -\left(\frac{C_\mathrm{m}}{G\rho}\right)\mathbf{g}^T(\mathbf{r})\cdot\mathbf{M}, \qquad (4)$$

where $\mathbf{g}^T(\mathbf{r})$ denotes the transpose of column vector $\mathbf{g}(\mathbf{r})$ and C_m is a constant which depends on the system of electromagnetic units used [see Blakely 1995, 67–68]. In the International Standard (SI) system of units used here, C_m is a constant which has a value of 100 nH/m or 100 nTm/A for magnetic fields expressed in nanotesla (nT) and magnetisations expressed in ampere per metre (A/m). The magnetic scalar potential is expressed in nWb/m or nTm.

The expressions for the gravitational field vector $\mathbf{g}(\mathbf{r})$ at a measurement point P(x,y,z), a radial distance $r = \sqrt{\mathrm{x}^2+\mathrm{y}^2}$ and axial coordinate $z < 0$ above a semi-infinite right circular vertical cylinder of radius a as shown in Figure 1 are derived by taking directional derivatives of the gravitational potential given by Equation (1), namely,

$$\mathbf{g}(\mathbf{r}) = \nabla\mathrm{U}(\mathbf{r}) = \left(\frac{\partial U}{\partial x}\right)\hat{\mathbf{x}} + \left(\frac{\partial U}{\partial y}\right)\hat{\mathbf{y}} + \left(\frac{\partial U}{\partial z}\right)\hat{\mathbf{z}}, \qquad (5)$$

where $\hat{\mathbf{x}},\hat{\mathbf{y}},\hat{\mathbf{z}}$ are the direction cosines along the x, y, z axes, respectively.

Since $\frac{\partial r}{\partial x} = x/r$ and $\frac{\partial r}{\partial y} = y/r$, then by the chain rule of partial differentiation:

$$g_\mathrm{x}(\mathbf{r}) = \left(\frac{\partial U}{\partial x}\right) = \left(\frac{\partial U}{\partial r}\right)\left(\frac{\partial r}{\partial x}\right) = \left(\frac{x}{r}\right)\left(\frac{\partial U}{\partial r}\right)$$
$$= 2\pi G\rho a\left(\frac{x}{r}\right)\frac{\partial I(1,0;-2)}{\partial r}. \qquad (6.1)$$

$$g_y(\mathbf{r}) = \left(\frac{\partial U}{\partial y}\right) = \left(\frac{\partial U}{\partial r}\right)\left(\frac{\partial r}{\partial y}\right) = \left(\frac{y}{r}\right)\left(\frac{\partial U}{\partial r}\right)$$
$$= 2\pi G\rho a\left(\frac{y}{r}\right)\frac{\partial I(1,0;-2)}{\partial r}. \quad (6.2)$$
$$g_z(\mathbf{r}) = \left(\frac{\partial U}{\partial z}\right) = 2\pi G\rho a\frac{\partial I(1,0;-2)}{\partial z}. \quad (6.3)$$

From Appendix 3, the r and z partial derivatives of $I(1,0;-2)$ are

$$\frac{\partial I(1,0;-2)}{\partial r} = -\int_0^\infty \mathrm{J}_1(ap)\,\mathrm{J}_1(rp)\mathrm{e}^{-p|z|}\,p^{-1}\,\mathrm{d}p$$
$$= -I(1,1;-1). \quad (7)$$
$$\frac{\partial I(1,0;-2)}{\partial z} = \int_0^\infty \mathrm{J}_1(ap)\,\mathrm{J}_0(rp)\mathrm{e}^{-p|z|}\,p^{-1}\,\mathrm{d}p$$
$$= I(1,0;-1). \quad (8)$$

Hence from Equations (6.1)–(6.3) and (7)–(8), the components of the gravitational field due to the semi-infinite right circular vertical cylinder may be expressed in Cartesian or cylindrical coordinates:

$$g_x(\mathbf{r}) = -2\pi G\rho a\left(\frac{x}{r}\right) I(1,1;-1)$$
$$= -2\pi G\rho a\cos\theta\, I(1,1;-1). \quad (9.1)$$
$$g_y(\mathbf{r}) = -2\pi G\rho a\left(\frac{y}{r}\right) I(1,1;-1)$$
$$= -2\pi G\rho a\sin\theta\, I(1,1;-1). \quad (9.2)$$
$$g_z(\mathbf{r}) = 2\pi G\rho a I(1,0;-1). \quad (9.3)$$

The expression for the magnetic scalar potential at an observation point P($\mathbf{r}$) on or above the top surface of a semi-infinite right circular vertical cylinder may be derived by substitution of Equations (9.1)–(9.3) into Equation (4):

$$V(\mathbf{r}) = 2\pi a\mathrm{C_m}\left\{\left[\left(\frac{x}{r}\right)M_x + \left(\frac{y}{r}\right)M_y\right] I(1,1;-1)\right.$$
$$\left. - M_z\, I(1,0;-1)\right\}. \quad (10)$$

This expression for the magnetic scalar potential may be further simplified by defining a radial component of magnetisation M_r:

$$V(\mathbf{r}) = 2\pi a\mathrm{C_m}\{M_r\, I(1,1;-1) - M_z\, I(1,0;-1)\}, \quad (11)$$

where $M_r = M_x\cos\theta + M_y\sin\theta = M_x\left(\frac{x}{r}\right) + M_y\left(\frac{y}{r}\right)$.

These expressions for the magnetic scalar potential are in agreement with those derived by Siew (1990).

The magnetic field vector $\mathbf{b}(\mathbf{r_P})$ and the gravity gradient tensor $\boldsymbol{\Gamma}(\mathbf{r})$

The anomalous magnetic field vector $\mathbf{b}(\mathbf{r}) = (b_x,b_y,b_z)^T$ at a point $\mathbf{r}$ external to a uniformly magnetised body is defined as the gradient of the magnetic scalar potential $V(\mathbf{r})$

$$\mathbf{b}(\mathbf{r}) = -\nabla V(\mathbf{r})$$
$$= -\left[\left(\frac{\partial V}{\partial x}\right)\hat{\mathbf{x}} + \left(\frac{\partial V}{\partial y}\right)\hat{\mathbf{y}} + \left(\frac{\partial V}{\partial z}\right)\hat{\mathbf{z}}\right], \quad (12)$$

where $\hat{\mathbf{x}},\hat{\mathbf{y}},\hat{\mathbf{z}}$ are the direction cosines along the x, y, z axes, respectively. Expressions for the anomalous magnetic field vector may also be derived from its gravity gradient tensor $\boldsymbol{\Gamma}(\mathbf{r})$ via an application of Poisson's relation (Blakely 1995). For example, on taking the gradient of the magnetic scalar potential in Equation (4), then

$$\mathbf{b}(\mathbf{r}) = -\left(\frac{\mathrm{C_m}}{\mathrm{G}\rho}\right)\boldsymbol{\Gamma}(\mathbf{r})\cdot\mathbf{M} = -\mathrm{C_m}\mathbf{T}(\mathbf{r})\cdot\mathbf{M}, \quad (13)$$

where $\boldsymbol{\Gamma}(\mathbf{r}) = \nabla\mathbf{g}(\mathbf{r})$ is the gravity gradient tensor at an external measurement point $\mathbf{r}$. Further on in this section I will show that the matrix $\mathbf{T}(\mathbf{r})$ is a symmetric tensor of Green's functions associated with the gravity gradient tensor. Omitting the $\mathbf{r}$ dependence of elements in the $\mathbf{T}(\mathbf{r})$ and $\boldsymbol{\Gamma}(\mathbf{r})$ tensors which is implicit, then

$$\mathbf{T}(\mathbf{r}) = \left(\frac{1}{\mathrm{G}\rho}\right)\boldsymbol{\Gamma}(\mathbf{r}) = \begin{bmatrix} T_{xx} & T_{xy} & T_{xz} \\ T_{yx} & T_{yy} & T_{yz} \\ T_{zx} & T_{zy} & T_{zz} \end{bmatrix},$$

where

$$\boldsymbol{\Gamma}(\mathbf{r}) = \mathrm{G}\rho\,\mathbf{T}(\mathbf{r}) = \begin{bmatrix} \frac{\partial g_x}{\partial x} & \frac{\partial g_x}{\partial y} & \frac{\partial g_x}{\partial z} \\ \frac{\partial g_y}{\partial x} & \frac{\partial g_y}{\partial y} & \frac{\partial g_y}{\partial z} \\ \frac{\partial g_z}{\partial x} & \frac{\partial g_z}{\partial y} & \frac{\partial g_z}{\partial z} \end{bmatrix}$$
$$= \begin{bmatrix} \frac{\partial^2 U}{\partial x^2} & \frac{\partial^2 U}{\partial x\partial y} & \frac{\partial^2 U}{\partial x\partial z} \\ \frac{\partial^2 U}{\partial y\partial x} & \frac{\partial^2 U}{\partial y^2} & \frac{\partial^2 U}{\partial y\partial z} \\ \frac{\partial^2 U}{\partial z\partial x} & \frac{\partial^2 U}{\partial z\partial y} & \frac{\partial^2 U}{\partial z^2} \end{bmatrix}. \quad (14)$$

Hence in matrix notation the magnetic field vector is

$$\mathbf{b}(\mathbf{r}) = \mathrm{C_m}\begin{bmatrix} T_{xx} & T_{xy} & T_{xz} \\ T_{yx} & T_{yy} & T_{yz} \\ T_{zx} & T_{zy} & T_{zz} \end{bmatrix}\begin{pmatrix} M_x \\ M_y \\ M_z \end{pmatrix}. \quad (15)$$

The expressions for the Green's functions $T_{ij}(\mathbf{r})$; $i,j = x$, y, z at a measurement point P($\mathbf{r}$) which may be on or above or coplanar with the top surface of a semi-infinite right circular vertical cylinder source of radius a as shown in Figure 1 may now be derived by differentiation of Equations (9.1)–(9.3). This involves using the chain rule to obtain expressions for the x, y, and z partial derivatives of the $I(1,1;-1)$ and $I(1,0;-1)$ Lipschitz–Hankel integrals as outlined in Appendix 3. Thus

$$T_{xx}(\mathbf{r}) = \left(\frac{1}{G\rho}\right)\frac{\partial g_x}{\partial x}$$
$$= -2\pi a\left\{\left(\frac{x}{r}\right)^2 I(1,0;0) + \left(1-\frac{2x^2}{r^2}\right)\frac{1}{r}I(1,1;-1)\right\},$$
$$= -\pi a\left\{I(1,0;0) + \cos 2\theta \times\left[I(1,0;0) - \frac{2}{r}I(1,1;-1)\right]\right\}. \quad (16.1.1)$$

$$T_{xy}(\mathbf{r}) = \left(\frac{1}{G\rho}\right)\frac{\partial g_x}{\partial y}$$
$$= -2\pi a\left\{\left(\frac{xy}{r^2}\right)\left[I(1,0;0) - \frac{2}{r}I(1,1;-1)\right]\right\},$$
$$= -\pi a\left\{\sin 2\theta\left[I(1,0;0) - \frac{2}{r}I(1,1;-1)\right]\right\}. \quad (16.1.2)$$

$$T_{xz}(\mathbf{r}) = \left(\frac{1}{G\rho}\right)\frac{\partial g_x}{\partial z} = -2\pi a\left\{\left(\frac{x}{r}\right)I(1,1;0)\right\},$$
$$= -2\pi a\{I(1,1;0)\cos\theta\}. \quad (16.1.3)$$

$$T_{yx}(\mathbf{r}) = \left(\frac{1}{G\rho}\right)\frac{\partial g_y}{\partial x}$$
$$= -2\pi a\left\{\left(\frac{xy}{r^2}\right)\left[I(1,0;0) - \frac{2}{r}I(1,1;-1)\right]\right\},$$
$$= -\pi a\left\{\sin 2\theta\left[I(1,0;0) - \frac{2}{r}I(1,1;-1)\right]\right\}$$
$$= T_{xy}(\mathrm{r}). \quad (16.2.1)$$

$$T_{yy}(\mathbf{r}) = \left(\frac{1}{G\rho}\right)\frac{\partial g_y}{\partial y}$$
$$= -2\pi a\left\{\left(\frac{y}{r}\right)^2 I(1,0;0) + \left(1-\frac{2y^2}{r^2}\right)\frac{1}{r}I(1,1;-1)\right\},$$
$$= -\pi a\left\{I(1,0;0) - \cos 2\theta \times\left[I(1,0;0) - \frac{2}{r}I(1,1;-1)\right]\right\}. \quad (16.2.2)$$

$$T_{yz}(\mathbf{r}) = \left(\frac{1}{G\rho}\right)\frac{\partial g_y}{\partial z} = -2\pi a\left\{\left(\frac{y}{r}\right)I(1,1;0)\right\},$$
$$= -2\pi a\{I(1,1;0)\sin\theta\}. \quad (16.2.3)$$

$$T_{zx}(\mathbf{r}) = \left(\frac{1}{G\rho}\right)\frac{\partial g_z}{\partial x} = -2\pi a\left\{\left(\frac{x}{r}\right)I(1,1;0)\right\},$$
$$= -2\pi a\{I(1,1;0)\cos\theta\} = T_{xz}(\mathbf{r}). \quad (16.3.1)$$

$$T_{zy}(\mathbf{r}) = \left(\frac{1}{G\rho}\right)\frac{\partial g_z}{\partial y} = -2\pi a\left\{\left(\frac{y}{r}\right)I(1,1;0)\right\},$$
$$= -2\pi a\{I(1,1;0)\sin\theta\}, = T_{yz}(\mathbf{r}). \quad (16.3.2)$$

$$T_{zz}(\mathbf{r}) = \left(\frac{1}{G\rho}\right)\frac{\partial g_z}{\partial z} = 2\pi a\, I(1,0;0), \quad (16.3.3)$$

where $I(1,0;0), I(1,1;-1), I(1,1;0)$ are Lipschitz–Hankel integrals (Eason, Noble, and Sneddon 1955),

$$I(1,0;0) = \int_0^\infty \mathrm{J}_1(ap)\,\mathrm{J}_0(rp)\mathrm{e}^{-p|z|}\,\mathrm{d}p. \quad (17)$$

$$I(1,1;-1) = \int_0^\infty \mathrm{J}_1(ap)\,\mathrm{J}_1(rp)\mathrm{e}^{-p|z|}\,p^{-1}\,\mathrm{d}p. \quad (18)$$

$$I(1,1;0) = \int_0^\infty \mathrm{J}_1(ap)\,\mathrm{J}_1(rp)\mathrm{e}^{-p|z|}\,\mathrm{d}p. \quad (19)$$

The equations for the gravity gradient tensor $\Gamma_{ij}(\mathbf{r})$; $i, j = x, y, z$ at a measurement point P($\mathbf{r}$) above a semi-infinite right circular vertical cylinder with uniform density or density contrast ρ may be expressed in radial-axial or cylindrical coordinates (r, θ, z) namely,

$$\Gamma_{xx}(\mathbf{r}) = -\pi \mathrm{G}\rho\, a\left\{I(1,0;0) + \cos 2\theta\left[I(1,0;0) - \frac{2}{r}I(1,1;-1)\right]\right\}. \quad (20.1)$$

$$\Gamma_{xy}(\mathbf{r}) = -\pi \mathrm{G}\rho\, a\left\{\sin 2\theta\left[I(1,0;0) - \frac{2}{r}I(1,1;-1)\right]\right\} = \Gamma_{yx}(\mathbf{r}). \quad (20.2)$$

$$\Gamma_{xz}(\mathbf{r}) = -2\pi \mathrm{G}\rho\, a\,\{I(1,1;0)\cos\theta\} = \Gamma_{zx}(\mathbf{r}). \quad (20.3)$$

$$\Gamma_{yy}(\mathbf{r}) = -\pi \mathrm{G}\rho\, a\left\{I(1,0;0) - \cos 2\theta\left[I(1,0;0) - \frac{2}{r}I(1,1;-1)\right]\right\}. \quad (20.4)$$

$$\Gamma_{yz}(\mathbf{r}) = -2\pi \mathrm{G}\rho\, a\,\{I(1,1;0)\sin\theta\} = \Gamma_{zy}(\mathbf{r}). \quad (20.5)$$

$$\Gamma_{zz}(\mathbf{r}) = 2\pi \mathrm{G}\rho\, a\, I(1,0;0) = -\{\Gamma_{xx}(\mathbf{r}) + \Gamma_{yy}(\mathbf{r})\}. \quad (20.6)$$

By inspection of Equations (20.2), (20.3) and (20.5) it is noted that the gravity gradient tensor is symmetric, and, from Equations (20.1), (20.4) and (20.6), it may be deduced that it is also traceless satisfying Laplace's equation since the sum of its three diagonal elements is zero, i.e. $\Gamma_{xx} + \Gamma_{yy} + \Gamma_{zz} = 0$. The expressions for the gravity gradient tensor in equations (20.1)–(20.6) are in agreement with those given for a right circular plunging cylinder in Rim and Li (2016).

The four Lipschitz–Hankel integrals $I(1,0;-1)$, $I(1,1;-1)$, $I(1,0;0)$ and $I(1,1;0)$ which appear in expressions for the gravity field vector, the gravity gradient tensor, the magnetic scalar potential and the magnetic field vector have been evaluated in closed form by Eason, Noble, and Sneddon (1955, equations (4.6), (4.9) (4.7) and (4.2) respectively). The expressions for these four Lipschitz–Hankel integrals are given as equations (A1.1), (A1.2), (A1.3), and (A1.4) respectively in Appendix 1.

The magnetic field b(r) due to a semi-infinite right circular vertical cylinder

From Equation (13), it is immediately evident that the components of the anomalous magnetic field vector are found as the dot or scalar product of the columns of the

Green's function tensor **T** with the magnetisation vector **M**. Also since the tensor **T** is symmetric as shown in equations (16.1.1)–(16.3.3), the magnetic field components are found as the dot or scalar product of the rows of the Green's function tensor **T** with the magnetisation vector **M**. Hence,

$$b_x(\mathbf{r}) = \mathrm{C_m}(\,T_{xx}\,M_x + \,T_{xy}\,M_y + \,T_{xz}\,M_z). \tag{21.1}$$

$$b_y(\mathbf{r}) = \mathrm{C_m}(\,T_{yx}\,M_x + \,T_{yy}\,M_y + \,T_{yz}\,M_z). \tag{21.2}$$

$$b_z(\mathbf{r}) = \mathrm{C_m}(\,T_{zx}\,M_x + \,T_{zy}\,M_y + \,T_{zz}\,M_z). \tag{21.3}$$

Then, by substitution of expressions for T_{xx}, T_{xy}, T_{xz} in Equations (16.1.1)–(16.1.3) into Equation (21.1), the full expression for the anomalous magnetic field component b_x due to a to a uniformly magnetised, semi-infinite, vertical, right circular cylinder at an observation point P(**r**) is

$$b_x(\mathbf{r}) = -2\pi a\mathrm{C_m}\left\{\begin{array}{c}\left[\left(\frac{x}{r}\right)^2 M_x + \left(\frac{xy}{r^2}\right)M_y\right] I(1,0;0)\\ +\left[\left(1\ -\frac{2x^2}{r^2}\right)M_x - \left(\frac{2xy}{r^2}\right)M_y\right]\\ \frac{1}{r}I(1,1;-1)\\ +\left(\frac{x}{r}\right)M_z\,I(1,1;0)\end{array}\right\},$$

or in cylindrical coordinates,

$$b_x(\mathbf{r}) = -\pi a\mathrm{C_m}\left\{\begin{array}{c}[\,M_x\cos 2\theta + M_y\sin 2\theta]\\ \left[I(1,0;0) - \frac{2}{r}I(1,1;-1)\right]+\\ M_xI(1,0;0) + 2M_z\cos\theta\,I(1,1;0)\end{array}\right\}. \tag{22.1}$$

Similarly, by substitution of expressions for T_{yx}, T_{yy}, T_{yz} in Equations (16.2.1)–(16.2.3) into Equation (21.2), the full expression for the anomalous magnetic field component b_y due to a uniformly magnetised, semi-infinite, vertical, right circular cylinder at an observation point P(**r**) is

$$b_y(\mathbf{r}) = -2\pi a\mathrm{C_m}\left\{\begin{array}{c}\left[\left(\frac{xy}{r^2}\right)M_x + \left(\frac{y}{r}\right)^2 M_y\right] I(1,0;0)\\ +\left[\left(1-\frac{2y^2}{r^2}\right)M_y - \left(\frac{2xy}{r^2}\right)M_x\right]\\ \frac{1}{r}I(1,1;-1)\\ +\left(\frac{y}{r}\right)M_z\,I(1,1;0)\end{array}\right\},$$

or in cylindrical coordinates,

$$b_y(\mathbf{r}) = -\pi a\mathrm{C_m}\left\{\begin{array}{c}[M_x\sin 2\theta - M_y\cos 2\theta\,]\\ \left[I(1,0;0) - \frac{2}{r}I(1,1;-1)\right]+\\ M_yI(1,0;0) + 2M_z\sin\theta\,I(1,1;0)\end{array}\right\}. \tag{22.2}$$

Similarly, by substitution of expressions for T_{yx}, T_{yy}, T_{yz} in Equations (16.3.1)–(16.3.3) into Equation (21.3), the full expression for the anomalous magnetic field component b_z due to a uniformly magnetised, semi-infinite right circular vertical cylinder at an observation point P(r) is

$$b_z(\mathbf{r}) = 2\pi\,\mathrm{aC_m}\left\{M_z\,I(1,0;0) - \left[\frac{x}{r}M_x + \frac{y}{r}M_y\right]I(1,1;0)\right\},$$

or in cylindrical coordinates,

$$b_z(\mathbf{r}) = 2\pi\,a\mathrm{C_m}\,\{\,M_z\,I(1,0;0) - (M_x\cos\theta + M_y\sin\theta)\;I(1,1;0)\}. \tag{22.3}$$

The expressions for the magnetic field components in Cartesian coordinates may be further simplified by defining a pair of radial M_r and transverse M_t components of horizontal magnetisation namely,

$$b_x(\mathbf{r}) = -2\pi\,a\mathrm{C_m}\left\{[M_r\,I(1,0;0)\ + M_z\,I(1,1;0)]\left(\frac{x}{r}\right) - \left[\left(\frac{x}{r}\right)M_r + \left(\frac{y}{r}\right)M_t\right]\left(\frac{1}{r}\right)\,I(1,1;-1)\right\}.$$

$$b_y(\mathbf{r}) = -2\pi\,a\mathrm{C_m}\left\{[M_r\,I(1,0;0)\ + M_z\,I(1,1;0)]\left(\frac{y}{r}\right) - \left[\left(\frac{y}{r}\right)M_r - \left(\frac{x}{r}\right)M_t\right]\left(\frac{1}{r}\right)\,I(1,1;-1)\right\}.$$

$$b_z(\mathbf{r}) = 2\pi\,a\mathrm{C_m}\{M_z\,I(1,0;0) - M_r\,I(1,1;0)\}.$$

((23.1)–(23.3))

where

$$M_r = \mathbf{M}^T\cdot\mathbf{u_r} = M_x\cos\theta + M_y\sin\theta = M_x\left(\frac{x}{r}\right) + M_y\left(\frac{y}{r}\right), \tag{24.1}$$

and

$$M_t = \mathbf{M}^T\cdot\mathbf{u_t} = -M_x\sin\theta + M_y\cos\theta = -M_x\left(\frac{y}{r}\right) + M_y\left(\frac{x}{r}\right), \tag{24.2}$$

and

$$\mathbf{u_r} = (\cos\theta, \sin\theta,\ 0)^T;$$

$$\mathbf{u_t} = (-\sin\,\theta, \cos\theta,\ 0)^T; \mathbf{M}^T = (\,M_x, M_y, M_z). \tag{24.3}$$

and $\mathbf{M}^T$ denotes the transpose of column vector **M**.

The expressions for calculating the magnetic field components in equations (22.1)–(22.3) and (23.1)–(23.3) are generic in that they cover both the general case where the external observation station P(**r**) is located above and away from the axis of the semi-infinite right circular cylinder, i.e. where $r > 0$ and $z < 0$, as well as some particular or special cases. For some of these particular cases, the expressions for the magnetic field components and the magnetic gradient tensor may be simplified and, when a measurement point lies on the rim of the top surface of the cylinder, the expressions become undefined. Broadly the particular cases for calculating the anomalous magnetic potential and magnetic field of a semi-infinite circular cylinder at an observation station P(**r**) may be defined as follows:

Table 1. Some particular cases for the Lipschitz–Hankel integrals which appear in the expressions for the magnetic scalar potential and the magnetic field vector at a measurement point P(*r*,*z*) due to a uniformly magnetised semi-infinite right circular vertical cylinder of radius *a*. The functions $F_0(k) = (2/\pi)\,F(k)$ and $E_0(k) = (2/\pi)E(k)$ are the complete elliptic integrals of the first and second kind with modulus *k* and modular angle α as defined by equations (A1.7), (A1.8) and (A1.9) in Appendix 1.

P(**r**) sub-case	$I(1,0;-1)$	$I(1,1;-1)$	$I(1,0;0)$	$I(1,1;-1)/r$	$I(1,1;0)$
axial $r = 0; z < 0$	$\frac{\sqrt{a^2+z^2}-\lvert z\rvert}{a}$	0	$\frac{1}{a}\left(1-\frac{\lvert z\rvert}{\sqrt{a^2+z^2}}\right)$	$\frac{1}{2a}\left(1-\frac{\lvert z\rvert}{\sqrt{a^2+z^2}}\right)$	0
origin $r = 0, z = 0$	1	0	$\left(\frac{1}{a}\right)$	$\left(\frac{1}{2a}\right)$	0
coplanar-top $0 < r < a, z = 0$	$\left\{\begin{matrix}\frac{(a+r)}{2a}E_0(k)+\\ \frac{(a-r)}{2a}F_0(k)\end{matrix}\right\}$	$\left(\frac{r}{2a}\right)$	$\left(\frac{1}{a}\right)$	$\left(\frac{1}{2a}\right)$	$\frac{1}{k\sqrt{ar}}\left\{\begin{matrix}\left(1-\frac{k^2}{2}\right)F_0(k)\\ -E_0(k)\end{matrix}\right\}$
coplanar-rim $r = a, z = 0$	1	$\frac{1}{2}$	$\left(\frac{1}{2a}\right)$	$\left(\frac{1}{2a}\right)$	∞
coplanar-external $r > a, z = 0$	$\left\{\begin{matrix}\frac{(a+r)}{2a}E_0(k)+\\ \frac{(a-r)}{2a}F_0(k)\end{matrix}\right\}$	$\left(\frac{a}{2r}\right)$	0	$\left(\frac{a}{2r^2}\right)$	$\frac{1}{k\sqrt{ar}}\left\{\begin{matrix}\left(1-\frac{k^2}{2}\right)F_0(k)\\ -E_0(k)\end{matrix}\right\}$

1. general case $r > 0$; $z < 0$ sub-cases: $0 < r < a$; $r = a$; $r > a$.
2. axial cases $r = 0; z \le 0$ sub-cases: $r = 0$ and $z < 0$; $r = 0$ and $z = 0$ (origin).
3. coplanar cases $z = 0$ sub-cases: $0 < r < a$; $r = a$; $r > a$.

Expressions for the five Lipschitz–Hankel integrals $I(1,0;-1)$, $I(1,1;-1)$, $I(1,0;0)$, $I(1,1;-1)/r$ and $I(1,1;0)$ in each of the two axial cases and the three coplanar cases are shown in Table 1. A derivation of these particular cases is outlined in Appendices 3 and 4.

The magnetic gradient tensor due to a semi-infinite right circular vertical cylinder

The magnetic gradient tensor $\mathbf{B}(\mathbf{r})$ is defined as the gradient of the magnetic field vector $\mathbf{b}(\mathbf{r})$ or as the directional derivatives of the magnetic field components b_x, b_y, b_z along each of the three Cartesian directions *x*, *y*, *z* respectively, namely,

$$\mathbf{B}(\mathbf{r}) = \nabla\mathbf{b}(\mathbf{r}) = \left[\left(\frac{\partial\mathbf{b}(\mathbf{r})}{\partial x}\right), \left(\frac{\partial\mathbf{b}(\mathbf{r})}{\partial y}\right), \left(\frac{\partial\mathbf{b}(\mathbf{r})}{\partial z}\right)\right], \tag{25}$$

where $\left(\frac{\partial\mathbf{b}(\mathbf{r})}{\partial x}\right), \left(\frac{\partial\mathbf{b}(\mathbf{r})}{\partial y}\right), \left(\frac{\partial\mathbf{b}(\mathbf{r})}{\partial z}\right)$ are column vectors.

Omitting the **r** dependence of the magnetic field components and tensor elements, which is implicit, then in matrix notation the magnetic gradient tensor is

$$\mathbf{B}(\mathbf{r}) = \begin{bmatrix} B_{xx} & B_{xy} & B_{xz} \\ B_{yx} & B_{yy} & B_{yz} \\ B_{zx} & B_{zy} & B_{zz} \end{bmatrix} = \begin{bmatrix} \frac{\partial b_x}{\partial x} & \frac{\partial b_x}{\partial y} & \frac{\partial b_x}{\partial z} \\ \frac{\partial b_y}{\partial x} & \frac{\partial b_y}{\partial y} & \frac{\partial b_y}{\partial z} \\ \frac{\partial b_z}{\partial x} & \frac{\partial b_z}{\partial y} & \frac{\partial b_z}{\partial z} \end{bmatrix}$$

$$= \begin{bmatrix} \frac{\partial^2 V}{\partial x^2} & \frac{\partial^2 V}{\partial x\partial y} & \frac{\partial^2 V}{\partial x\partial z} \\ \frac{\partial^2 V}{\partial y\partial x} & \frac{\partial^2 V}{\partial y^2} & \frac{\partial^2 V}{\partial y\partial z} \\ \frac{\partial^2 V}{\partial z\partial x} & \frac{\partial^2 V}{\partial z\partial y} & \frac{\partial^2 V}{\partial z^2} \end{bmatrix}. \tag{26}$$

From Equations (23.1) and (26), expressions for the elements in the first row of the gradient tensor are formulated by taking the *x*, *y*, *z* directional derivatives of b_x. Hence for a point $\mathbf{r} = (x, y, z)$ on or above a semi-infinite right circular vertical cylinder

$$B_{xx}(\mathbf{r}) = -2\pi a C_m \frac{\partial}{\partial x}\left\{[M_r\, I(1,0;0) + M_z\, I(1,1;0)]\left(\frac{x}{r}\right) - \left[\left(\frac{x}{r}\right)M_r + \left(\frac{y}{r}\right)M_t\right]\left(\frac{1}{r}\right) I(1,1;-1)\right\}.$$

$$B_{xy}(\mathbf{r}) = -2\pi a C_m \frac{\partial}{\partial y}\left\{[M_r\, I(1,0;0) + M_z\, I(1,1;0)]\left(\frac{x}{r}\right) - \left[\left(\frac{x}{r}\right)M_r + \left(\frac{y}{r}\right)M_t\right]\left(\frac{1}{r}\right) I(1,1;-1)\right\}.$$

$$B_{xz}(\mathbf{r}) = -2\pi a C_m \frac{\partial}{\partial z}\left\{[M_r\, I(1,0;0) + M_z\, I(1,1;0)]\left(\frac{x}{r}\right) - \left[\left(\frac{x}{r}\right)M_r + \left(\frac{y}{r}\right)M_t\right]\left(\frac{1}{r}\right) I(1,1;-1)\right\} \tag{27.1.1–27.1.3}$$

Similarly from Equations (23.2) and (26), expressions for the elements in the second row of the gradient tensor are formulated by taking the *x*, *y*, *z* directional derivatives of b_y. Hence

$$B_{yx}(\mathbf{r}) = -2\pi a C_m \frac{\partial}{\partial x}\left\{[M_r\, I(1,0;0) + M_z\, I(1,1;0)]\left(\frac{y}{r}\right) - \left[\left(\frac{y}{r}\right)M_r - \left(\frac{x}{r}\right)M_t\right]\left(\frac{1}{r}\right) I(1,1;-1)\right\}.$$

$$B_{yy}(\mathbf{r}) = -2\pi a C_m \frac{\partial}{\partial y}\left\{[M_r\, I(1,0;0) + M_z\, I(1,1;0)]\left(\frac{y}{r}\right) - \left[\left(\frac{y}{r}\right)M_r - \left(\frac{x}{r}\right)M_t\right]\left(\frac{1}{r}\right) I(1,1;-1)\right\}.$$

$$B_{yz}(\mathbf{r}) = -2\pi a C_m \frac{\partial}{\partial z}\left\{[M_r\, I(1,0;0) + M_z\, I(1,1;0)]\left(\frac{y}{r}\right) - \left[\left(\frac{y}{r}\right)M_r - \left(\frac{x}{r}\right)M_t\right]\left(\frac{1}{r}\right) I(1,1;-1)\right\}. \tag{27.2.1–27.2.3}$$

Finally from Equations (23.3) and (26), expressions for the elements in the third row of the gradient tensor are formulated by taking the x, y, z directional derivatives of b_z. Hence

$$B_{zx}(\mathbf{r}) = 2\pi a \mathsf{C}_\mathrm{m} \frac{\partial}{\partial x}\left\{M_z\, I(1,0;0) - M_r\, I(1,1;0)\right\}. \tag{27.3.1}$$

$$B_{zy}(\mathbf{r}) = 2\pi a \mathsf{C}_\mathrm{m} \frac{\partial}{\partial y}\left\{M_z\, I(1,0;0) - M_r\, I(1,1;0)\right\}. \tag{27.3.2}$$

$$B_{zz}(\mathbf{r}) = 2\pi a \mathsf{C}_\mathrm{m} \frac{\partial}{\partial z}\left\{M_z\, I(1,0;0) - M_r\, I(1,1;0)\right\}. \tag{27.3.3}$$

Expressions for the r, z spatial derivatives of the $I(1,0;0)$, $I(1,1;-1)$, $I(1,1;0)$ Lipschitz–Hankel integrals are derived in Appendix 3. By the chain rule of differentiation their x, y partial derivatives are as follows:

$$\frac{\partial I(1,0;\,0)}{\partial x} = \frac{\partial I(1,0;0)}{\partial r}\frac{\partial r}{\partial x} = -\left(\frac{x}{r}\right) I(1,1;1), \tag{28.1}$$

$$\frac{\partial I(1,0;0)}{\partial y} = \frac{\partial I(1,0;0)}{\partial r}\frac{\partial r}{\partial y} = -\left(\frac{y}{r}\right) I(1,1;1), \tag{28.2}$$

$$\frac{\partial I(1,1;\,-1)}{\partial x} = \frac{\partial I(1,0;0)}{\partial r}\frac{\partial r}{\partial x} = \left(\frac{x}{r}\right)\left[I(1,0;0) - \frac{1}{r}(1,1;\,-1)\right], \tag{29.1}$$

$$\frac{\partial I(1,1;\,-1)}{\partial y} = \frac{\partial I(1,0;0)}{\partial r}\frac{\partial r}{\partial y} = \left(\frac{y}{r}\right)\left[I(1,0;0) - \frac{1}{r}I(1,1;-1)\right], \tag{29.2}$$

$$\frac{\partial I(1,1;0)}{\partial x} = \frac{\partial I(1,1;0)}{\partial r}\frac{\partial r}{\partial x} = \left(\frac{x}{r}\right)\left[I(1,0;1) - \frac{1}{r}I(1,1;0)\right], \tag{30.1}$$

$$\frac{\partial I(1,1;0)}{\partial y} = \frac{\partial I(1,1;0)}{\partial r}\frac{\partial r}{\partial y} = \left(\frac{y}{r}\right)\left[I(1,0;1) - \frac{1}{r}I(1,1;0)\right], \tag{30.2}$$

$$\frac{\partial I(1,1;-1)}{\partial z} = I(1,1;\,0);\ \frac{\partial I(1,0;\,0)}{\partial z} = I(1,0;\,1);\ \frac{\partial I(1,1;\,0)}{\partial z} = I(1,1;1), \tag{31}$$

where $I(1,0;\,1)$, and $I(1,1;\,0)$ are Lipschitz–Hankel integrals (Eason, Noble, and Sneddon 1955), namely,

$$I(1,0;1) = \int_0^\infty \mathrm{J}_1(ap)\,\mathrm{J}_0(rp)\mathrm{e}^{-p|z|}\,p\,\mathrm{d}p, \tag{32}$$

$$I(1,1;1) = \int_0^\infty \mathrm{J}_1(ap)\,\mathrm{J}_1(rp)\mathrm{e}^{-p|z|}\,p\,\mathrm{d}p, \tag{33}$$

and

$$\frac{\partial M_r}{\partial x} = -\frac{y}{r^2}M_t\,;\ \frac{\partial M_t}{\partial x} = \frac{y}{r^2}M_r\,;\ \frac{\partial}{\partial x}\left(\frac{x}{r}\right) = \frac{y^2}{r^3}\,;\ \frac{\partial}{\partial x}\left(\frac{y}{r}\right) = -\left(\frac{xy}{r^3}\right), \tag{34}$$

$$\frac{\partial M_r}{\partial y} = \frac{x}{r^2}M_t;\ \frac{\partial M_t}{\partial y} = -\frac{x}{r^2}M_t;\ \frac{\partial}{\partial y}\left(\frac{y}{r}\right) = \frac{x^2}{r^3};\ \frac{\partial}{\partial y}\left(\frac{x}{r}\right) = -\left(\frac{xy}{r^3}\right). \tag{35}$$

The formulae for the x partial derivatives in Equations (28.1)–(30.1) and (34) may now be used to derive expressions for the three elements in the first column of the magnetic gradient tensor. Then from Equation (27.1.1), the expression for $B_{xx} = \partial b_x/\partial x$ is:

$$B_{xx}(\mathbf{r}) = 2\pi a\,\mathsf{C}_\mathrm{m}\left\{\begin{array}{l}\left[\left(\frac{x^2-y^2}{r^2}\right)M_r + \left(\frac{2xy}{r^2}\right)M_t\right]\\ \left[\frac{1}{r}\,I(1,0;0) - \frac{2}{r^2}I(1,1;\,-1)\right]\\ +M_z\left[\left(\frac{x^2-y^2}{r^2}\right)\frac{1}{r}\,I(1,1;0)\right.\\ \left.-\left(\frac{x^2}{r^2}\right)I(1,0;1)\right]\\ +\left(\frac{x^2}{r^2}\right)M_r\,I(1,1;1)\end{array}\right\}.$$

Similarly, from Equation (27.2.1), the expression for $B_{yx} = \partial b_y/\partial x$ is:

$$B_{yx}(\mathbf{r}) = 2\pi a\,\mathsf{C}_\mathrm{m}\left\{\begin{array}{l}\left[\left(\frac{2xy}{r^2}\right)M_r - \left(\frac{x^2-y^2}{r^2}\right)M_t\right]\\ \left[\frac{1}{r}\,I(1,0;0) - \frac{2}{r^2}I(1,1;-1)\right]\\ +M_z\left(\frac{xy}{r^2}\right)\left[\frac{2}{r}\,I(1,1;0)\right.\\ \quad\left.-I(1,0;1)\right]\\ +\left(\frac{xy}{r^2}\right)M_r\,I(1,1;1)\end{array}\right\}.$$

Similarly, from Equation (27.3.1), the expression for $B_{zx} = \partial b_z/\partial x$ is:

$$B_{zx}(\mathbf{r}) = 2\pi a\,\mathsf{C}_\mathrm{m}\left\{\left[\left(\frac{x}{r}\right)M_r + \left(\frac{y}{r}\right)M_t\right]\frac{1}{r}\,I(1,1;0) - \left(\frac{x}{r}\right)\left[M_r\,I(1,0;1) + M_z\,I(1,1;1)\right]\right\}. \tag{36.1.1)–(36.1.3}$$

The formulae for the y partial derivatives in Equations (28.2), (29.2), (30.2) and (35) may now be used to derive expressions for the three elements in the second column of the magnetic gradient tensor. Then from Equation (27.2.1), the expression for $B_{xy} = \partial b_x/\partial y$ is:

$$B_{xy}(\mathbf{r}) = 2\pi a\,\mathsf{C}_\mathrm{m}\left\{\begin{array}{l}\left[\left(\frac{2xy}{r^2}\right)M_r - \left(\frac{x^2-y^2}{r^2}\right)M_t\right]\\ \left[\frac{1}{r}\,I(1,0;0) - \frac{2}{r^2}I(1,1;-1)\right]\\ +M_z\left(\frac{xy}{r^2}\right)\left[\frac{2}{r}\,I(1,1;0) - I(1,0;1)\right]\\ +\left(\frac{xy}{r^2}\right)M_r\,I(1,1;1)\end{array}\right\},$$

$$= B_{yx}(\mathbf{r}). \tag{36.2.1}$$

Similarly, from Equation (27.2.2), the expression for $B_{yy} = \partial b_y/\partial y$ is:

$$B_{yy}(\mathbf{r}) = 2\pi a\,\mathrm{C_m}\left\{\begin{array}{l} -\left[\left(\frac{x^2-y^2}{r^2}\right)M_r + \left(\frac{2xy}{r^2}\right)M_t\right] \\ \left[\frac{1}{r}\,I(1,0;0) - \frac{2}{r^2}I(1,1;-1)\right] \\ -M_z\left[\left(\frac{x^2-y^2}{r^2}\right)\frac{1}{r}\,I(1,1;0)\right. \\ \left. + \left(\frac{y^2}{r^2}\right)I(1,0;1)\right] \\ +\left(\frac{y^2}{r^2}\right)M_r\,I(1,1;1) \end{array}\right\}. \quad (36.2.2)$$

Similarly, from Equation (27.3.2), the expression for $B_{zy} = \partial b_z/\partial y$ is:

$$B_{zy}(\mathbf{r}) = 2\pi a\,\mathrm{C_m}\left\{\left[\left(\frac{y}{r}\right)M_r - \left(\frac{x}{r}\right)M_t\right]\frac{1}{r}\,I(1,1;0) - \left(\frac{y}{r}\right)[M_r\,I(1,0;1) + M_z\,I(1,1;1)]\right\}. \quad (36.2.3)$$

The formulae for the z partial derivatives of the $I(1,1;-1)$, $I(1,0;0)$, $I(1,1;0)$ Lipschitz–Hankel integrals are shown in Equation (31). These formulae may be used to derive expressions for elements in the third column of the magnetic gradient tensor. Then from Equation (27.1.3), the expression for $B_{xz} = \partial b_x/\partial z$ is:

$$\begin{aligned} B_{xz}(\mathbf{r}) &= 2\pi a\,\mathrm{C_m}\left\{\left[\left(\frac{x}{r}\right)M_r + \left(\frac{y}{r}\right)M_t\right]\frac{1}{r}I(1,1;0) - \left(\frac{x}{r}\right)[M_r\,I(1,0;1) + M_z\,I(1,1;1)]\right\}, \\ &= B_{zx}(\mathbf{r}). \end{aligned} \quad (36.3.1)$$

Similarly from Equation (27.2.3), the expression for $B_{yz} = \partial b_y/\partial z$ is:

$$\begin{aligned} B_{yz}(\mathbf{r}) &= 2\pi\,\mathrm{a\,C_m}\left\{\left[\left(\frac{y}{r}\right)M_r - \left(\frac{x}{r}\right)M_t\right]\frac{1}{r}\,I(1,1;0) - \left(\frac{y}{r}\right)[M_r\,I(1,0;1) + M_z\,I(1,1;1)]\right\}, \\ &= B_{zy}(\mathbf{r}). \end{aligned} \quad (36.3.2)$$

Similarly from Equation (27.3.3), the expression for $B_{zz} = \partial b_z/\partial z$ is:

$$B_{zz}(\mathbf{r}) = 2\pi\,\mathrm{a\,C_m}\{M_z\,I(1,0;1) - M_r\,I(1,1;1)\}. \quad (36.3.3)$$

Inspection of pairs of Equations (36.1.2) and (36.2.1); (36.1.3) and (36.3.1); and (36.2.3) and (36.3.2) respectively, confirms that the magnetic gradient tensor is symmetric for all observation points above the top surface of a semi-infinite, right circular vertical cylinder, i.e. $B_{xy} = B_{yx}$; $B_{xz} = B_{zx}$; $B_{yz} = B_{zy}$ and $\mathbf{B} = \mathbf{B^T}$.

Furthermore by inspection of equations (36.1.1) and (36.2.2), it is immediately evident that terms involving the $I(1,1;-1)$, $I(1,0;0)$, $I(1,1;0)$ integrals in expressions for elements B_{xx} and B_{yy} of the magnetic gradient tensor have opposite signs and therefore cancel upon addition. Thus

$$\begin{aligned} B_{xx} + B_{yy} &= 2\pi a\,\mathrm{C_m}\left\{-\left(\frac{x^2+y^2}{r^2}\right)[M_z\,I(1,0;1) - M_r\,I(1,1;1)]\right\}, \\ &= -2\pi a\,\mathrm{C_m}\{M_z\,I(1,0;1) - M_r\,I(1,1;1)\}, = -B_{zz}, \end{aligned}$$

and therefore, I am able to demonstrate that the magnetic gradient tensor is traceless, i.e. $B_{xx} + B_{yy} + B_{zz} = 0$.

The tracelessness and symmetry properties of the magnetic gradient tensor confirm that the magnetic scalar potential $V(\mathbf{r})$ due to a uniformly magnetised, semi-infinite right circular vertical cylinder source is a harmonic potential field function satisfying Maxwell's magnetostatic equations in the absence of electric currents, i.e. div $\mathbf{b}(\mathbf{r}) = 0$ and curl $\mathbf{b}(\mathbf{r}) = 0$, and therefore, Laplace's equation for all external points $P(\mathbf{r})$ above the top of the cylinder. This harmonic property of the magnetic scalar potential due to the semi-infinite cylinder means that its gradient tensor is completely specified by only five of the nine tensor elements, namely, by its three upper triangular or three lower triangular elements and by two of its three diagonal elements.

The two Lipschitz–Hankel integrals $I(1,0;1)$ and $I(1,1;1)$ in equations (36.1.1)-(36.3.3) have been evaluated in closed form by Eason, Noble, and Sneddon (1955). These expressions for $I(1,0;1)$ and $I(1,1;1)$ are given as equations (A1.5) and (A1.6) in Appendix 1 respectively.

General expressions for the gradient tensor in radial-axial or cylindrical coordinates

The expressions for magnetic gradient tensor elements in Equations (36.1.1)–(36.3.3) which are written in Cartesian coordinates may also be expressed in radial-axial or cylindrical coordinates, i.e. (r,θ,z) using the following trigonometric identities,

$$\cos 2\theta = \cos^2\theta - \sin^2\theta = \left(\frac{x^2-y^2}{r^2}\right)$$
$$\text{and } \sin 2\theta = 2\sin\theta\cos\theta = \left(\frac{2xy}{r^2}\right).$$

This leads to expressions for a plunging semi-infinite right circular cylinder as detailed in the next section where the radial, azimuthal and axial coordinates of the observation station $\mathrm{P}(r,\theta,z)$ are defined in the body axis coordinate system of the plunging right circular cylinder (see Figure 2).

From Equation (36.1.1), the expression for the B_{xx} magnetic gradient tensor element is:

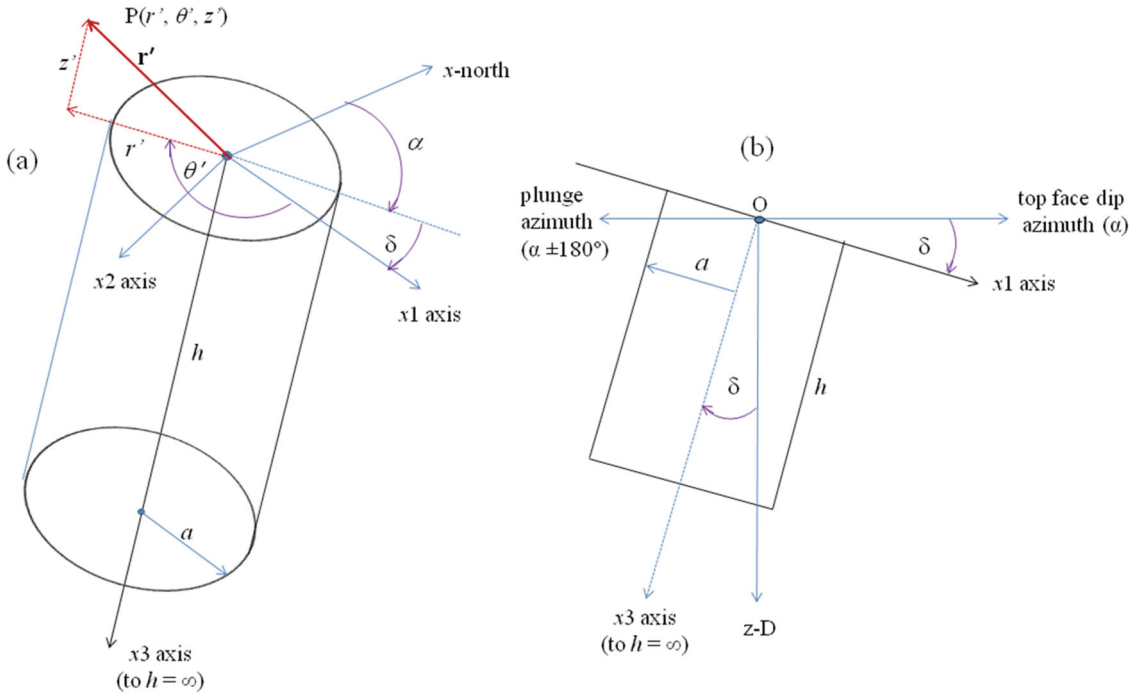

Figure 2. The three-dimensional schematic in (a) shows the body axis coordinate system with direction cosines $\hat{\mathbf{x}}_1, \hat{\mathbf{x}}_2, \hat{\mathbf{x}}_3$ along the x_1, x_2, x_3. axes respectively for a plunging right circular cylinder of radius a, axial length h, plunge $(90° - \delta)$ and plunge azimuth $(\alpha \pm 180°)$. The external measurement station relative to the origin O at the centre of the top face of the cylinder is shown as $P(x_1, x_2, x_3)$ or $P(r', \theta', z')$. (b) shows a vertical $x_1 - x_3$ section through the cylinder in the direction of downward dip of the top face. The body axis coordinate system is defined with respect to the top face of the cylinder, i.e. the x_1 axis is in the direction of downward dip δ of the top face of the cylinder with azimuth α; the x_3 axis is along the downward pointing central axis of the cylinder with plunge $(90° - \delta)$ and azimuth $(\alpha \pm 180°)$; and the x_3 axis is along the direction of strike of the cylinder given by $\hat{\mathbf{x}}_2 = \hat{\mathbf{x}}_3 \times \hat{\mathbf{x}}_1$. The radial distance of P from the origin is $r' = \sqrt{(x_1^2 + x_2^2)}$ and θ' is the azimuth of P measured positive clockwise from the $\hat{\mathbf{x}}_1$ body axis in the plane of the top surface of the cylinder.

$$B_{xx}(\mathbf{r}) = 2\pi\, a\, C_m \left\{ \begin{array}{l} [M_r \cos 2\theta + M_t \sin 2\theta] \\ \left[\frac{1}{r} I(1,0;0) - \frac{2}{r^2} I(1,1;-1)\right] \\ + \frac{M_z}{2}\left[\cos 2\theta \left(\frac{2}{r} I(1,1;0) - I(1,0;1)\right)\right. \\ \left. - I(1,0;1)\right] + M_r \cos^2\theta\, I(1,1;1) \end{array} \right\}. \quad (37.1)$$

Similarly, from Equation (36.2.1), the expression for gradient tensor elements B_{xy} and B_{yx} is:

$$B_{xy}(\mathbf{r}) = 2\pi\, a\, C_m \left\{ \begin{array}{l} [M_r \sin 2\theta - M_t \cos 2\theta] \\ \left[\frac{1}{r} I(1,0;0) - \frac{2}{r^2} I(1,1;-1)\right] \\ + \frac{M_z}{2} \sin 2\theta \left[\frac{2}{r} I(1,1;0) - I(1,0;1)\right] \\ + \frac{1}{2} M_r \sin 2\theta\, I(1,1;1) \end{array} \right\},$$

$$= B_{yx}(\mathbf{r}). \quad (37.2)$$

Similarly, from Equation (36.3.1), the expression for gradient tensor elements B_{xz} and B_{zx} is:

$$B_{xz}(\mathbf{r}) = 2\pi\, a\, C_m \left\{ \begin{array}{l} [M_x \cos 2\theta + M_y \sin 2\theta] \\ \left[\frac{1}{r} I(1,1;0) - \frac{1}{2} I(1,0;1)\right] \\ - \frac{1}{2} M_x I(1,0;1) - M_z \cos\theta\, I(1,1;1) \end{array} \right\},$$

$$= B_{zx}(\mathbf{r}). \quad (37.3)$$

Similarly, from Equation (36.2.2), the expression for gradient tensor elements B_{yy} is:

$$B_{yy}(\mathbf{r}) = 2\pi\, a\, C_m \left\{ \begin{array}{l} -[M_r \cos 2\theta + M_t \sin 2\theta] \\ \left[\frac{1}{r} I(1,0;0) - \frac{2}{r^2} I(1,1;-1)\right] - \\ \frac{M_z}{2}\left[\cos 2\theta \left(\frac{2}{r} I(1,1;0) - I(1,0;1)\right)\right. \\ \left. + I(1,0;1)\right] + M_r \sin^2\theta\, I(1,1;1) \end{array} \right\}. \quad (37.4)$$

Similarly, from Equation (36.3.2), the expression for gradient tensor elements B_{yz} and B_{zy} is:

$$B_{yz}(\mathbf{r}) = 2\pi\, a\, C_m \left\{ \begin{array}{l} [M_x \sin 2\theta - M_y \cos 2\theta] \\ \left[\frac{1}{r} I(1,1;0) - \frac{1}{2} I(1,0;1)\right] \\ - \frac{1}{2} M_y I(1,0;1) - M_z \sin\theta\, I(1,1;1) \end{array} \right\},$$

$$= B_{zy}(\mathbf{r}). \quad (37.5)$$

Similarly, from Equation (36.3.3), the expression for gradient tensor elements B_{zz} is:

$$B_{zz}(\mathbf{r}) = 2\pi\, a\, C_m \{M_z\, I(1,0;1) - (M_x \cos\theta + M_y \sin\theta)\, I(1,1;1)\}. \quad (37.6)$$

The magnetic gradient tensor due to a finite length right circular vertical cylinder

In the case of a finite length circular cylinder, the magnetic field and gradient tensor are calculated using the superposition theorem or principle of superposition. I will also invoke the principle of reciprocity since I will be shifting the position of the origin located at the top surface of a semi-infinite pair of cylinders. More specifically for a finite length right circular vertical cylinder of radius a total magnetisation $\mathbf{M}$ and axial length h, any harmonic component of its magnetic field or gradient tensor $b_c(x,y,z;a,h,\mathbf{M})$ at an observation point $\mathbf{r} = (x,y,z)^T$ is calculated as the difference between the field component or tensor element due to a pair of semi-infinite cylinders of identical radii and magnetisations separated by a vertical or axial length h. Therefore

$$b_c(x,y,z;a,h,\mathbf{M}) = b_c(x,y,z;a,\infty,\mathbf{M}) - b_c(x,y,z-h;a,\infty,\mathbf{M}), \quad (38)$$

where $b_c(x,y,z;a,\infty,\mathbf{M})$ is any harmonic magnetic field component or tensor element due to a semi-infinite, right circular vertical cylinder at a measurement point $\mathbf{r} = (x,y,z)^T$ defined with respect to an origin on the top surface of the finite length cylinder and $b_c(x,y,z-h;a,\infty,\mathbf{M})$ is the magnetic field component or tensor element due to a second semi-infinite right circular vertical cylinder, coaxial with the first, and at the same measurement point whose vertical coordinate is $z-h$ relative to a new origin on the top surface of the second cylinder. In this instance the top surface of the second cylinder is coincident with the base of the first so that the separation distance between top surfaces of the pair of coaxial cylinders is h. This follows the reciprocity principle where source and sensor are interchangeable or in this case, the measurement point is fixed but the source position rather than the sensor position is shifted downwards a distance h.

Computation of the magnetic field and gradient tensor for a plunging right circular cylinder

The generalisation of theory to the plunging right circular cylinder is straightforward for both the magnetic and gravity cases. The expressions for both the fields and the gradient tensors of the right circular vertical cylinder may be used to calculate the field components and gradient tensor elements for a plunging right circular cylinder. In this instance however the equations for the field components and gradient tensor elements must be expressed in the body axis coordinate system of the plunging circular cylinder. This is shown in Figure 2. Previously the equations for the magnetic field and gradient tensor were defined within the survey coordinate system $\mathbf{r}_s = (x,y,z)^T$ (i.e. north, south, down) which is coincident with the body axis coordinate system of the right circular vertical cylinder, i.e. $\mathbf{r}_b = (x_1,x_2,x_3)^T$.

The orientation of a plunging right circular cylinder may be defined by the orientation of its top planar surface. The orientation of this surface is defined by two angles, first by an azimuth of downward dip α measured clockwise from north ($0 \leq \alpha < 360°$), and second, by a dip angle δ measured positive from the horizontal in the downward pointing dip direction ($0° \leq \delta \leq 90°$). The transformation matrix $\mathbf{U}$ from the survey coordinate system $\mathbf{r_s} = (x,y,z)^T$ to the new body coordinate system $\mathbf{r_b} = (x_1,x_2,x_3)^T$ of the plunging cylinder is given by

$$\mathbf{U} = \begin{bmatrix} \cos\alpha\cos\delta & \sin\alpha\cos\delta & \sin\delta \\ -\sin\alpha & \cos\alpha & 0 \\ -\cos\alpha\sin\delta & -\sin\alpha\sin\delta & \cos\delta \end{bmatrix} = \begin{pmatrix} \hat{\mathbf{x}}_1^{\mathbf{T}} \\ \hat{\mathbf{x}}_2^{\mathbf{T}} \\ \hat{\mathbf{x}}_3^{\mathbf{T}} \end{pmatrix}, \quad (39)$$

where $\hat{\mathbf{x}}_1, \hat{\mathbf{x}}_2, \hat{\mathbf{x}}_3$ (shown above as row vectors) are the direction cosines along the x_1, x_2, x_3 body axes of the plunging right circular cylinder respectively (see Figure 2).

I note that the x_1 body axis points in the down dip direction of the top face; the x_3 body axis is directed along the plunge axis of the cylinder and the x_2 body axis is horizontal forming a right hand clockwise triad such that $\hat{\mathbf{x}}_2 = \hat{\mathbf{x}}_3 \times \hat{\mathbf{x}}_1$. The choice of a body axis system based on the orientation of the top surface means that when the cylinder is vertical the orientation angles of the top planar surface are $\alpha = 0°$ and $\delta = 0°$ respectively, and therefore, the transformation matrix $\mathbf{U}$ is equal to the identity matrix $\mathbf{I}$ and $\mathbf{r_b}$ reverts to $\mathbf{r_s}$.

Computation of the magnetic field and the magnetic gradient tensor due to a plunging right circular cylinder is accomplished by the following steps:

1. Determine the total magnetisation vector $\mathbf{M}(\mathbf{r_s})$ in the survey coordinate system. The total magnetisation vector is defined as the vector sum of the induced $\mathbf{M_{ind}}$ and remanent $\mathbf{M_{rem}}$ magnetisations. The phenomenon of self-demagnetisation is not considered in this paper. The induced magnetisation vector $\mathbf{M_{ind}}$, which includes the unusual case of intrinsic anisotropy of magnetic susceptibility, is discussed in Emerson, Clark, and Saul (1985) and McKenzie (2020).
2. Calculate the orthogonal matrix $\mathbf{U}$ for transformations from the survey coordinate system $\mathbf{r_s} = (x,y,z)^T$ to the body axis coordinate system $\mathbf{r_b} = (x_1,x_2,x_3)^T$.
3. Transformation of the total magnetisation vector $\mathbf{M}(\mathbf{r_s}) = (\mathrm{M_x},\mathrm{M_y},\mathrm{M_z})^T$ to the body axis coordinate system $\mathbf{M}(\mathbf{r_b}) = (\mathrm{M_1},\mathrm{M_2},\mathrm{M_3})^T$ and then compute M_r' and M_t', $\mathbf{M}(\mathbf{r_b}) = \mathbf{UM}(\mathbf{r_s})$; $M_r' = M_1\cos\theta' + M_2\sin\theta'$; $M_t' = -M_1\sin\theta' + M_2\cos\theta'$.
4. Transformation of each observation point $\mathbf{r_s} = (x,y,z)^T$ to the body axis coordinate system $\mathbf{r_b} =$

$(x_1, x_2, x_3)^T$ using $\mathbf{r_b} = \mathbf{U}\mathbf{r_s}$, and then reset the cylindrical coordinates $\mathbf{r_b} = (r', \theta', z')^T$ as:

$$r' = \sqrt{x_1^2 + x_2^2};\ \theta' = \arctan\left(\frac{x_2}{x_1}\right);\ z' = x_3$$

5. Computation of the magnetic field vector $\mathbf{b}(\mathbf{r_b})$ and the magnetic gradient tensor $\mathbf{B}(\mathbf{r_b})$ at each observation point $\mathbf{r_b}$ in the body axis coordinate system using Equations (23.1)–(23.3) and (37.1–37.6) respectively with the x_1 body axis replacing x; x_2 replacing y x_3 replacing z, r' replacing r and θ' replacing θ. Importantly the magnetisation $\mathbf{M}(\mathbf{r_b})$ replaces $\mathbf{M}(\mathbf{r_s})$. These computations depend upon the case type for each observation point relative to the origin at the centre of the top surface of the cylinder (see Table 3) and secondly, whether the circular cylinder is finite or semi-infinite.
6. Transformation of the magnetic field vector $\mathbf{b}(\mathbf{r_b})$ and the magnetic gradient tensor $\mathbf{B}(\mathbf{r_b})$ from the body axis coordinate system to the survey axis coordinate system $\mathbf{r_s}$. Since $\mathbf{U}$ is an orthogonal matrix, i.e. $\mathbf{U^{-1}} = \mathbf{U^T}$, then the magnetic field vector and the magnetic gradient tensor $\mathbf{B}(\mathbf{r_s})$ at each observation point in the survey axis coordinate system are computed as $\mathbf{b}(\mathbf{r_s}) = \mathbf{U^T b}(\mathbf{r_b})$ and $\mathbf{B}(\mathbf{r_s}) = \mathbf{U^T B}(\mathbf{r_b})\,\mathbf{U}$ respectively.

For a right circular vertical cylinder the computation of the magnetic field and the gradient tensor involve steps (1) and (5) only.

Computational accuracies for the Lipschitz–Hankel integrals

The calculation of the magnetic scalar potential, the magnetic field components and the magnetic gradient tensor at a measurement point P($\mathbf{r}$) involves the numerical computation of six Lipschitz–Hankel integrals, namely, $I(1,0;-1)$, $I(1,1;-1)$, $I(1,0;0)$, $I(1,1;0)$, $I(1,0;1)$ and $I(1,1;1)$. The first two integrals $I(1,0;-1)$, $I(1,1;-1)$ appear in expressions for the gravitational field and the magnetic scalar potential while the last five integrals appear in expressions for the magnetic field vector and the magnetic gradient tensor. Eason, Noble, and Sneddon (1955) have derived closed form expressions for these six integrals which are shown in Appendix 1 as equations (A1.1), (A1.2), (A1.3), (A1.4), (A1.5) and (A1.6), respectively. The closed form expressions for the Lipschitz–Hankel integrals involve computing the complete and incomplete elliptic integrals of the first and second kind (see Appendix 1). These elliptic integrals have been computed in double precision using an algorithm based on Landen's transformation (Abramowitz and Stegun 1964 and Press et al. 1992). The accuracy of these computations has been tested against tables of $I(1,0;-1)$, $I(1,1;-1)$ $I(1,1;-1)$, $aI(1,0;0)$, $aI(1,1;0)$,$a^2I(1,0;1)$, and $a^2I(1,1;1)$ (where a is the radius of the circular cylinder) for values of r/a and $|z|/a$ ranging from 0.0 to 3.0 in steps of 0.2 in Eason, Noble, and Sneddon (1955) (see Figure 3). The tables in Eason, Noble, and Sneddon (1955) only show accuracies to four significant figures. However these tables are in complete agreement with my algorithm which computes the Lipschitz–Hankel integrals in full double precision. The first and second complete elliptic integrals $F_0(k)$ and $E_0(k)$ have been successfully tested to at least 12 significant figures or more by comparison with tables in Abramowitz and Stegun (1964, Tables 17.1 and 17.2) while the pair of incomplete elliptic integrals $F_0(k,\beta)$ and $E_0(k,\beta)$ and Heuman's lambda function $\Lambda_0(k,\beta)$ have been successfully tested to eight and six significant figures respectively by comparison with tables in Abramowitz and Stegun (1964, Tables 17.5, 17.6 and 17.8 respectively; Byrd and Friedman 1971, Appendix).

Importantly, the Lipschitz–Hankel integrals $I(1,0;-1)$, $I(1,1;-1)$, $aI(1,0;0)$, $aI(1,1;0)$ and $a^2I(1,0;1)$, $a^2I(1,1;1)$ shown in Figure 3 are radially symmetric functions of the horizontal distance parameter r for a particular observation height $|z|$. This is because the elliptic integral functions $F_0(k,\beta)$ and $E_0(k,\beta)$ are also radially symmetric functions for a particular value of $|z|/a$ in the expressions for the modulus k and the amplitude angle β [see Equations (A1.9) and (A1.10)].

Numerical verification of results

For purposes of the numerical verification of the theoretical equations for the magnetic field and magnetic gradient tensor, I have calculated the magnetic field and gradient tensor components due to a right circular vertical cylinder of radius $a = 100$ m and finite length $h = 1000$ m possessing a high total magnetisation of 23.077 A/m (Pipe Model 1a). The results for b_z and B_{zz} have been compared with those derived from a facetted quasi-circular vertical pipe in which the number of sides in transverse section n_s is 18, 36, 72 and 144. The magnetic field components and gradient tensor elements for the facetted quasi-circular cylinder were calculated in ModelVision Pro 15.1 (Pratt et al. 2005) based on theory for computing the gravity and magnetic response due to a triangular facet (Barnett 1976). The absolute value of relative departures between the reference right circular vertical cylinder model and the facetted quasi-circular cylinders for both b_z and B_{zz} have been calculated over a 1 km square horizontal grid for an observation height of 50 m. Statistics for the absolute relative departures are shown in Table 2. This includes an estimate of the departures due to volume differences $|V_{\mathrm{fp}} - V_{\mathrm{cp}}|/V_{\mathrm{cp}}$ between the true circular cylinder model and its facetted equivalent. Quantile plots of the relative departures $|(B_{zz}^{\mathrm{fp}} - B_{zz})/B_{zz}|$ from the theoretically computed gradient tensor element B_{zz} for a series of facetted quasi-circular cylinder models with $n_s = 18$,

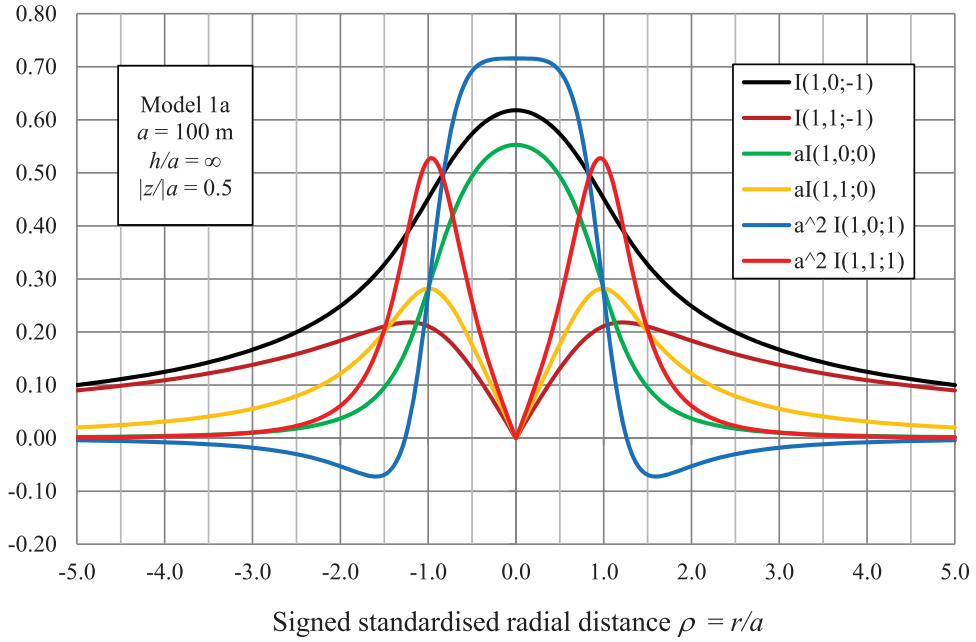

Figure 3. Lipschitz–Hankel integrals at a standardised observation height $|z|/a = 0.5$ for the magnetic scalar potential, magnetic field and gradient tensor due to a semi-infinite right circular cylinder Note that the Lipschitz–Hankel integrals $I(1,0;-1)$, $I(1,1;-1)$, $aI(1,0;0)$, $aI(1,0;0)$, $a^2I(1,0;1)$ and $a^2I(1,1;1)$ are dimensionless.

Table 2. Absolute value of relative departures (rel_dep) in percent from the theoretical model for B_{zz} and b_z calculated using a equivalent facetted model in which the number of sides in polygonal section n_s is 18, 36, 72 and 144. The sample size is 2121 points for the mean statistic. The trimmed mean is calculated for all percentiles from 0 to 95 (2150 points). All quantities are in percent.

Statistic	rel_dep{$\|B_{zz}\|$} $n_s = 18$	rel_dep{$\|B_{zz}\|$} $n_s = 36$	rel_dep{$\|B_{zz}\|$} $n_s = 72$	rel_dep{$\|B_{zz}\|$} $n_s = 144$
$\|V_{fp} - V_{cp}\|/V_{cp}$	2.018446	0.506923	0.126876	0.031728
Trimmed_Mean	2.028800	0.509785	0.127597	0.031896
Median (md)	2.074641	0.521188	0.130351	0.032437
V_{diff}/Median	95.84442	95.76759	95.74819	95.74321
Percentile q95	2.421054	0.612045	0.153317	0.038348
(q95 – md/md)	14.9619	15.6272	15.7027	15.7213
Statistic	rel_dep{$\|b_z\|$} $n_s = 18$	rel_dep{$\|b_z\|$} $n_s = 36$	rel_dep{$\|b_z\|$} $n_s = 72$	rel_dep{$\|b_z\|$} $n_s = 144$
$\|V_{fp} - V_{cp}\|/V_{cp}$	2.018446	0.506923	0.126876	0.031728
Trimmed_Mean	2.065267	0.519028	0.129927	0.032492
Median (md)	2.105961	0.529326	0.132510	0.033139
V_{diff}/Median	97.29134	97.26293	97.33389	97.81474
Percentile q95	2.739717	0.692217	0.173505	0.043393
(q95 – md/md)	32.0574	32.8152	33.1058	33.7781

36 and 72 are shown in Figure 4(a). The distribution of the relative departures with standardised radial distance r/a from the axis of the cylinder are shown for B_{zz} ($n_s = 18$) in Figure 4(b).

From Table 2, I note that the bulk of relative departures from the theoretical model are due to volume differences between the true right circular cylinder and its equivalent facetted model. For example, the relative departures from the theoretical model for b_z and B_{zz} are $95.8 \pm 0.05\%$ and $97.5 \pm 0.3\%$, respectively. Furthermore the relative differences do not change greatly as n_s increases and the slight increase in the relative error for B_{zz} is expected since the tensor calculations have higher computational overheads. The quantile plots in Figure 4(a) for B_{zz} show that the 5 and 95 percentiles lie within $\pm 15\%$ of the median. The rapid increase in relative departures beyond the 95 percentile is attributable to near zero values for B_{zz} (i.e. near the zero cross-over points) near the edges of the right circular vertical pipes.

This is confirmed in Figure 4(b) which shows that the highest relative departures for B_{zz} ($n_s = 18$), i.e. those > 2.60 which lie beyond the 95 percentile, occur at standardised radial distances $r/a \approx 1$. Figure 5 shows the absolute values of relative departures from the theoretically computed gradient tensor elements $B_{xy}, B_{xz}, B_{yz}, B_{zz}$ for the facetted quasi-circular cylinder model with $n_s = 144$ for a west–east principal profile 50 m above Pipe Model 1a.

In summary I note the following points. First, the magnetic field components and gradient tensor elements for the reference model have been correctly calculated. Second, the discrepancies between the reference right circular vertical cylinder and the facetted quasi-circular, vertical cylinder models decline rapidly as the number of sides n_s in transverse section increases. Third, the magnetic fields and the magnetic gradient

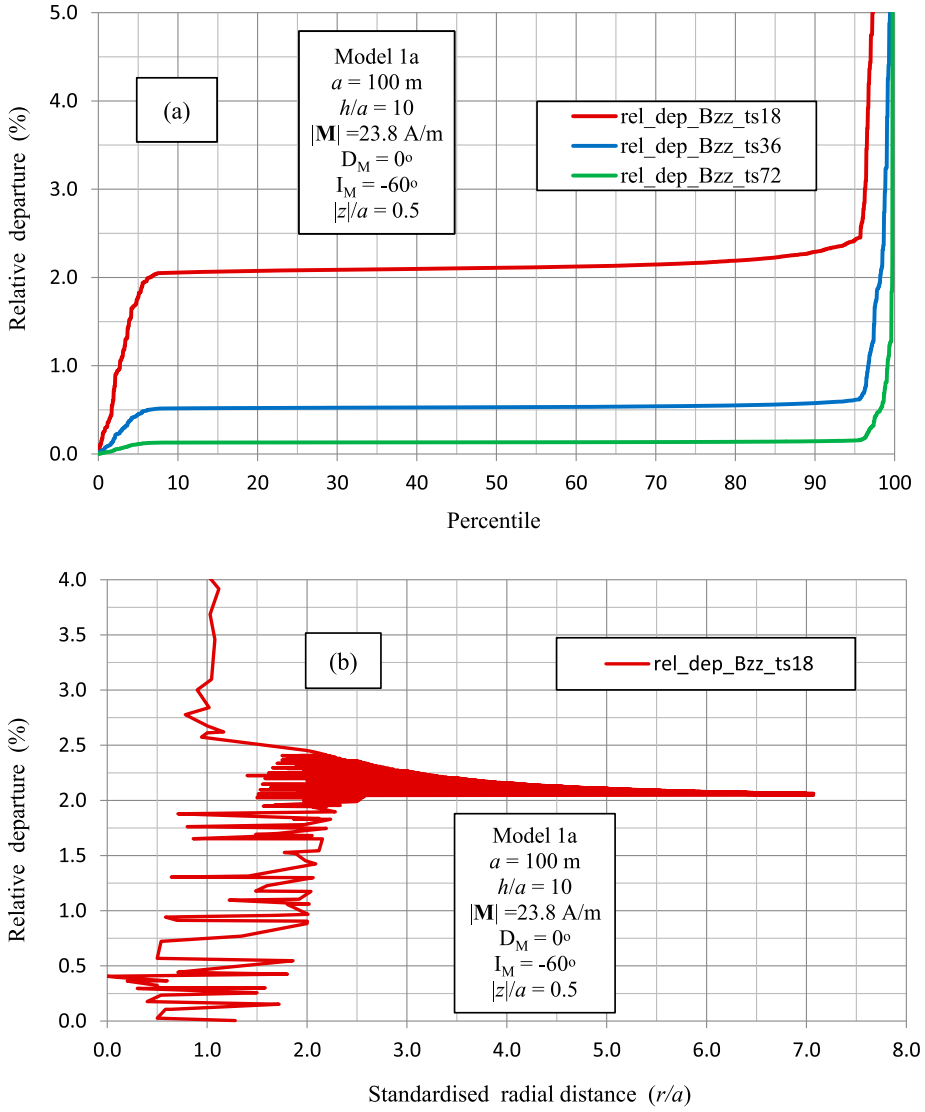

Figure 4. (a) shows quantile plots of the relative departures between the theoretically computed B_{zz} for a finite length right circular vertical cylinder of radius $a = 100$ m and axial length $h = 1000$ m (Pipe Model 1a) and B_{zz} computed for a series of equivalent facetted vertical cylinders in which the number of sides n_s in polygonal section is 18, 36 and 72. (b) displays plots of the relative departures in B_{zz} (sorted into ascending order for $n_s = 18$) versus standardised radial distance.

tensor are modelled more accurately as the observation height $|z|$ is increased. Fourth, the errors in the computed magnetic field components and gradient tensor elements are generally larger for near-surface stations above the rim of the cylinder (at $r/a = 1$) where there is a singularity. This is especially the case for the B_{xz} and B_{yz} tensor elements at stations close to the rim of each vertical, right circular cylinder. This is not unexpected, since as previously noted, the B_{xz} and B_{yz} tensor elements are undefined for stations located on the rim of the top surface of the cylinder.

Symmetry relations and some important special cases for the magnetic field

For a general magnetisation direction both the magnetic scalar potential and the components of the magnetic field vector are asymmetrical for a particular observation height $|z|$ above the top surface of a semi-infinite (and finite length) right circular vertical cylinder source. However some interesting symmetries exist for particular cases of the magnetisation direction, for example, when the magnetisation direction in the cylinder is directed along each one of the three orthogonal directions (x-north, y-east and z-vertically down). These symmetries may be deduced from the expressions for the magnetic scalar potential and the magnetic field vector when these are expressed in radial axial coordinates. Figure 6 shows contoured grid images of the magnetic field components for a series of semi-infinite right circular vertical cylinders of radius $a = 100$ m and possessing uniform 1 Am^{-1} magnetisations $\mathbf{M}$ in the north $\mathbf{M} = |\mathbf{M}|\,\hat{\mathbf{x}}$, east $\mathbf{M} = |\mathbf{M}|\,\hat{\mathbf{y}}$, and downward vertical $\mathbf{M} = |\mathbf{M}|\,\hat{\mathbf{z}}$ directions respectively. The plane of observation is 50 m above the top surface of the cylinder.

For a series of uniform magnetisations of equal magnitude $\mathbf{M} = M\hat{\mathbf{x}}$; $\mathbf{M} = M\hat{\mathbf{y}}$; $\mathbf{M} = M\hat{\mathbf{z}}$ M_r along the north, east and vertically down directions respectively, the

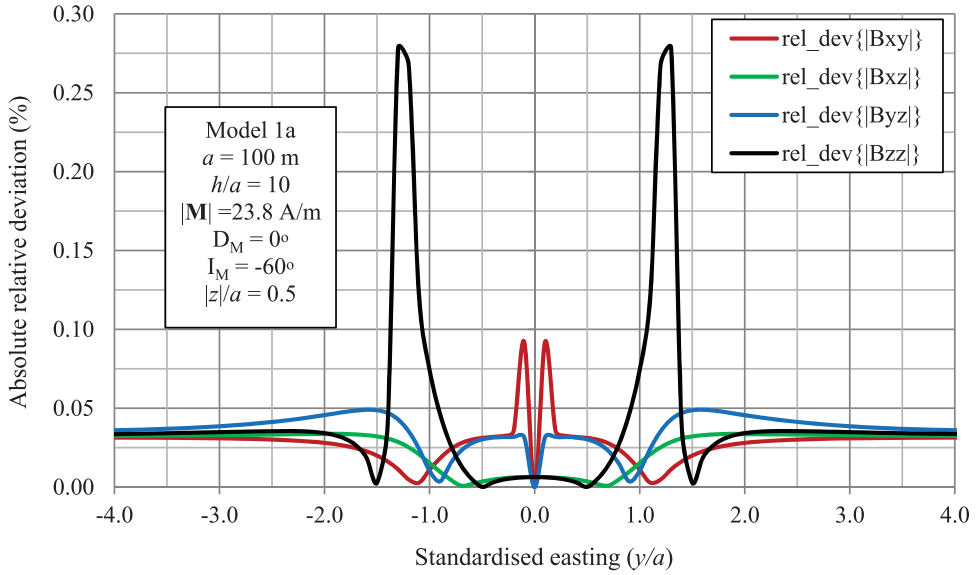

Figure 5. Absolute relative departures between the theoretically computed gradient tensor elements $B_{xy}, B_{xz}, B_{yz}, B_{zz}$ for a finite length, right circular vertical cylinder of radius $a = 100$ m and axial length $h = 1000$ m and those computed for an equivalent facetted vertical cylinder in which the number of sides n_s in polygonal section is 144. The magnetisation in both models is $|\mathbf{M}| = 23.8$ A/m with declination $D_M = 0°$ and inclination $I_M = -60°$ and the observation height is $|z| = 50$ m.

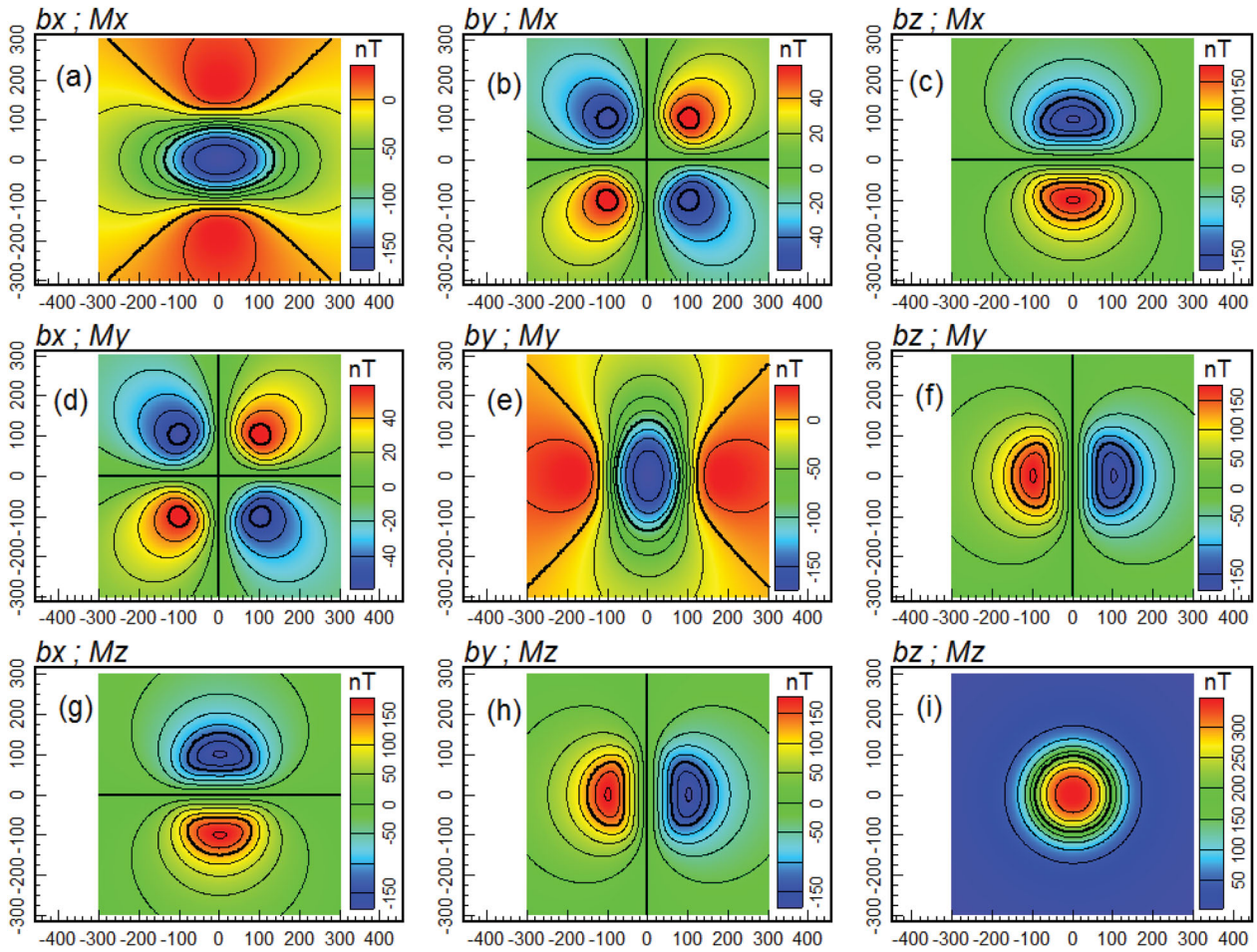

Figure 6. Contoured grid images (north is up the page) of the magnetic field components b_x, b_y, b_z for a series of uniform magnetisations of equal magnitude $|\mathbf{M}| = 1$A/m. (a–c) in the top row show b_x, b_y, b_x respectively for $\mathbf{M} = M\hat{\mathbf{x}}$; (d–f) in the second row show b_x, b_y, b_x for $\mathbf{M} = M\hat{\mathbf{y}}$; (g–i) in the bottom row show b_x, b_y, b_x respectively for $\mathbf{M} = M\hat{\mathbf{z}}$. The notation $b_x; M_x$ is short for field component $b_x(\mathbf{r}; \mathbf{M} = M\hat{\mathbf{x}})$ and so on.

following relations may be deduced:

$$b_x(\mathbf{r};\mathbf{M} = M\hat{\mathbf{x}}) = -\pi a\,\mathrm{C_m}\,M\left\{I(1,0;0) + \cos 2\theta\left[I(1,0;0) - \frac{2}{r}I(1,1;-1)\right]\right\}, \quad (40.1)$$

$$b_x(\mathbf{r};\mathbf{M} = M\hat{\mathbf{y}}) = -\pi a\,\mathrm{C_m}\,M \times \left\{\sin 2\theta\left[I(1,0;0) - \frac{2}{r}I(1,1;-1)\right]\right\} = b_y(\mathbf{r};\mathbf{M} = M\hat{\mathbf{x}}), \quad (40.2)$$

$$b_x(\mathbf{r};\mathbf{M} = M\hat{\mathbf{z}}) = -2\pi a\,\mathrm{C_m}\,M\cos\theta\, I(1,1;0) = b_z(\mathbf{r};\mathbf{M} = M\hat{\mathbf{x}}), \quad (40.3)$$

$$b_y(\mathbf{r};\mathbf{M} = M\hat{\mathbf{y}}) = -\pi a\,\mathrm{C_m}\,M\left\{I(1,0;0) - \cos 2\theta\left[I(1,0;0) - \frac{2}{r}I(1,1;-1)\right]\right\}, \quad (40.4)$$

$$b_y(\mathbf{r};\mathbf{M} = M\hat{\mathbf{z}}) = -2\pi a\,\mathrm{C_m}\,M\sin\theta\, I(1,1;0) = b_z(\mathbf{r};\mathbf{M} = M\hat{\mathbf{y}}), \quad (40.5)$$

$$b_z(\mathbf{r};\mathbf{M} = M\hat{\mathbf{z}}) = 2\pi a\,\mathrm{C_m}\,MI(1,0;0) = \mathrm{C_m}M\,\Omega\,, \quad (40.6)$$

where Ω is the solid angle subtended at the upper surface of the right circular cylinder (Singh and Sabina 1978). Hence for observation stations at the origin on the top surface of the cylinder ($r = 0$), the vertical field component $b_z(0,0,0;\mathbf{M} = M\hat{\mathbf{z}}) = 2\pi\mathrm{C_m}M = 2\pi\mathrm{C_m}M_z$. This is confirmed by the limit for $I(1,0;0)$ in Table 1 which is $1/a$.

Furthermore the expressions for the three magnetic field components in equations (40.1)–(40.6) may be expressed in matrix form, namely,

$$\mathbf{B_M}(\mathbf{r}) = \begin{pmatrix} b_x^{Mx} & b_y^{Mx} & b_z^{Mx} \\ b_x^{My} & b_y^{My} & b_z^{My} \\ b_x^{Mz} & b_y^{Mz} & b_z^{Mz} \end{pmatrix} = \mathrm{C_m}M\begin{pmatrix} T_{xx} & T_{xy} & T_{xz} \\ T_{yx} & T_{yy} & T_{yz} \\ T_{zx} & T_{zy} & T_{zz} \end{pmatrix} = \mathrm{C_m}M\,\mathbf{T}(\mathbf{r}), \quad (41)$$

where $\mathbf{T}(\mathbf{r})$ is the symmetric matrix of Green's functions given in Equations (16.1.1)–(16.3.3) and where $b_x^{Mx} = b_x(\mathbf{r};\mathbf{M} = M\hat{\mathbf{x}})$ represents the magnetic field component b_x due to a magnetisation $\mathbf{M} = M\hat{\mathbf{x}}$. Since $\mathbf{T}(\mathbf{r})$ is related to the gravity gradient tensor of a semi-infinite right circular vertical cylinder by the relation $\mathbf{\Gamma}(\mathbf{r}) = G\rho\mathbf{T}(\mathbf{r})$ as shown in Equation (14), then Equation (41) may be expressed as follows:

$$\mathbf{B_M}(\mathbf{r}) = \left(\frac{\mathrm{C_m}M}{G\rho}\right)\,\mathbf{\Gamma}(\mathbf{r}). \quad (42)$$

Hence there is equivalence between the gravity gradient tensor $\mathbf{\Gamma}(\mathbf{r})$ and the (3×3) matrix $\mathbf{B_M}(\mathbf{r})$ of magnetic field components for the three orthogonal magnetisation directions with the constant of the proportionality between $\mathbf{B_M}(\mathbf{r})$ and $\mathbf{\Gamma}(\mathbf{r})$ being $\left(\frac{\mathrm{C_m}M}{G\rho}\right)$. This equivalence is reflected in the symmetry patterns shown for $\mathbf{B_M}(\mathbf{r})$ in Figure 6 and also in the elements of the gravity gradient tensor $\mathbf{\Gamma}(\mathbf{r})$. The results shown here are in agreement with Pedersen and Bastani (2016).

The expressions in Equations (40.1)–(40.3) and in row 1 of Equation (41) represent the magnetic field reduced to the equator as shown in Figure 6(a–c) while Equations (40.3), (40.5) and (40.6) and row 3 of Equation (48) represent the magnetic field reduced to the north magnetic pole (see Figure 6(g–i)). From Table 1, expressions for $\left[I(1,0;0) - \frac{2}{r}I(1,1;-1)\right]$ and $I(1,1;0)$ are identically zero on the axis of a right circular vertical cylinder. Therefore the expressions for the magnetic field components on the axis $\mathbf{r} = (0,0,z)^T$ of a semi-infinite right circular vertical cylinder are:

$$b_x(\mathbf{r})_{r=0} = -\pi a\,\mathrm{C_m}M_x I(1,0;0)_{r=0} = -\pi\,\mathrm{C_m}M_x\left\{1 - \frac{|z|}{\sqrt{a^2+z^2}}\right\}. \quad (43.1)$$

$$b_y(\mathbf{r})_{r=0} = -\pi a\,\mathrm{C_m}M_y I(1,0;0)_{r=0} = -\pi\,\mathrm{C_m}M_y\left\{1 - \frac{|z|}{\sqrt{a^2+z^2}}\right\}. \quad (43.2)$$

$$b_z(\mathbf{r})_{r=0} = 2\pi a\,\mathrm{C_m}M_z\, I(1,0;0)_{r=0} = 2\pi\,\mathrm{C_m}M_z\left\{1 - \frac{|z|}{\sqrt{a^2+z^2}}\right\}. \quad (43.3)$$

By inspection of Equations (43.1)–(43.3), it is immediately evident that expressions for the declination and inclination of magnetisation for a uniformly magnetised right circular vertical cylinder or pipe may be derived by taking ratios of the b_x, b_y, and b_z field components at points on its vertical axis. The declination of magnetisation D_M which is defined from the ratio of the horizontal components of magnetisation, i.e. M_x and M_y, is given as

$$D_M = \arctan\left(\frac{M_y}{M_x}\right) = \arctan\left(\frac{-b_y}{-b_x}\right)\ (\text{for } 0 \le D_M < 2\pi\ ). \quad (44)$$

The inclination of magnetisation I_M which is defined from the ratio of the horizontal and vertical components of magnetisation, i.e. $M_h = \sqrt{M_x^2 + M_y^2}$ and M_z, is given as

$$I_M = \arctan\left(\frac{M_z}{\sqrt{M_x^2+M_y^2}}\right) = \arctan\left(\frac{b_z}{2\sqrt{b_x^2+b_y^2}}\right)\ \left(\text{for } -\frac{\pi}{2} \le I_M \le \frac{\pi}{2}\ \right). \quad (45)$$

These expressions are identical to those derived for a point magnetic dipole with moment $\mathbf{m}$ or a uniformly magnetised sphere with magnetisation $\mathbf{M}$ (McKenzie 2020).

Table 3. Particular cases for the Lipschitz–Hankel integrals appearing in expressions for the magnetic gradient tensor at an observation height $|z|$ above the top surface of a uniformly magnetised, semi-infinite right circular vertical cylinder source of radius a where $F_0(k)$ and $E_0(k)$ are the complete elliptic integrals of the first and second kind with modulus k and modular angle α as defined by Equations (A1.8), (A1.9) and (A1.10) in Appendix 1.

$P(r,z)$ sub-case	$I(1,0;0)$	$I(1,1;-1)/r$	$I(1,1;0)$	$I(1,0;1)$	$I(1,1;1)$
axial $r=0; z<0$	$\frac{1}{a}\left(1-\frac{\lvert z\rvert}{\sqrt{a^2+z^2}}\right)$	$\frac{1}{2a}\left(1-\frac{\lvert z\rvert}{\sqrt{a^2+z^2}}\right)$	0	$\frac{a}{(a^2+z^2)^{3/2}}$	0
Origin $r=0, z=0$	$\left(\frac{1}{a}\right)$	$\left(\frac{1}{2a}\right)$	0	$\left(\frac{1}{a^2}\right)$	0
coplanar-top $0<r<a, z=0$	$\left(\frac{1}{a}\right)$	$\left(\frac{1}{2a}\right)$	$\frac{1}{k\sqrt{ar}}\left\{\begin{matrix}\left(1-\frac{k^2}{2}\right)F_0(k)\\ -E_0(k)\end{matrix}\right\}$	$\frac{1}{a}\left\{\begin{matrix}\frac{E_0(k)}{(a-r)}+\\ \frac{F_0(k)}{(a+r)}\end{matrix}\right\}$	0
coplanar-rim $r=a, z=0$	$\left(\frac{1}{2a}\right)$	$\left(\frac{1}{2a}\right)$	∞	$\pm\infty$	∞
coplanar-external $r>a, z=0$	0	$\left(\frac{a}{2r^2}\right)$	$\frac{1}{k\sqrt{ar}}\left\{\begin{matrix}\left(1-\frac{k^2}{2}\right)F_0(k)\\ -E_0(k)\end{matrix}\right\}$	$\frac{1}{a}\left\{\begin{matrix}\frac{E_0(k)}{(a-r)}+\\ \frac{F_0(k)}{(a+r)}\end{matrix}\right\}$	0

Particular cases for the magnetic gradient tensor

Some particular cases for the magnetic gradient tensor arise due to the position of the observation station P(**r**) relative to the centre of the top face of the cylinder or when the total resultant magnetisation direction of the circular cylinder is aligned along the north, east or vertical directions. In the former, the relative observation position determines the Lipschitz–Hankel integral functions in the expressions for the gradient tensor in Equations (37.1)–(37.6). The nature of these integral functions is summarised in Table 3 for various axial and coplanar cases. In particular for observation stations located on the axis of the cylinder, it may be shown that in the limit as the radial distance r approaches zero, the pair of terms $\left[\frac{1}{r}I(1,0;0)-\frac{2}{r^2}I(1,1;-1)\right]$ and $\left[\frac{1}{r}I(1,1;0)-\frac{1}{2}I(1,0;1)\right]$ in Equations (37.1)–(37.5) are both identically zero [see Appendix 4, equations (A4.9.7) and (A4.9.11) respectively]. Furthermore from Table 3, the axial limits for the $I(1,0;1)$ and $I(1,1;1)$ integrals are $a/(a^2+z^2)^{3/2}$ and 0 respectively. Hence the magnetic gradient tensor for an axial observation station $\mathbf{r}=(0,0,z)$ including the origin at (0,0,0) is

$$\mathbf{B}(\mathbf{r})_{r=0}=\begin{bmatrix}B_{xx}&B_{xy}&B_{xz}\\B_{yx}&B_{yy}&B_{yz}\\B_{zx}&B_{zy}&B_{zz}\end{bmatrix}=\frac{\pi a^2\,\mathsf{C_m}}{(a^2+z^2)^{3/2}}\begin{bmatrix}-M_z&0&-M_x\\0&-M_z&-M_y\\-M_x&-M_y&2M_z\end{bmatrix}. \tag{46}$$

An application to the determination of magnetisation direction from the gradient tensor

From Equation (46), it is immediately evident that expressions for the declination and inclination of magnetisation for a uniformly magnetised pipe may be derived by taking ratios of the B_{xz},B_{xz}, and B_{zz} tensor elements at points on the vertical axis of a right circular vertical cylinder. First for the declination of magnetisation D_M which is defined from the ratio of the horizontal components M_x and M_y of magnetisation, namely,

$$D_M=\arctan\left(\frac{M_y}{M_x}\right)=\arctan\left(\frac{-B_{yz}}{-B_{xz}}\right)\quad(\text{for } 0\le D_M<2\pi\,). \tag{47}$$

The inclination of magnetisation I_M is defined from the ratio of the horizontal and vertical components of magnetisation, namely,

$$I_M=\arctan\left(\frac{M_z}{\sqrt{M_x^2+M_y^2}}\right)=\arctan\left(\frac{B_{zz}}{2\sqrt{B_{xz}^2+B_{yz}^2}}\right)\quad(\text{for } -\frac{\pi}{2}\le I_M\le\frac{\pi}{2}\,). \tag{48}$$

These expressions are identical to those derived for a point magnetic dipole with moment **m** or a uniformly magnetised sphere (McKenzie 2020).

The effect of plunge on field and gradient tensor computations

As I noted earlier, the theory presented here for the gravity and magnetic fields and gradient tensors due to a right circular vertical pipe only allows for potential field calculations level with or above the top face of the pipe. For this reason, the theory presented here for the modelling of plunging right circular pipes should be used with caution at low sensor heights when plunge angles are significantly non-vertical. This is illustrated in Figure 7 which shows the region of coverage at a height of 50 m above a series of plunging right circular pipes with radius $a=100$ m and plunge angles of 75°, 80° and 85°, respectively. In this example, the coverage region is significantly reduced for plunge angles below 75°. The regions of unrestricted coverage are shown in blue while regions where coverage is invalid are shown in red.

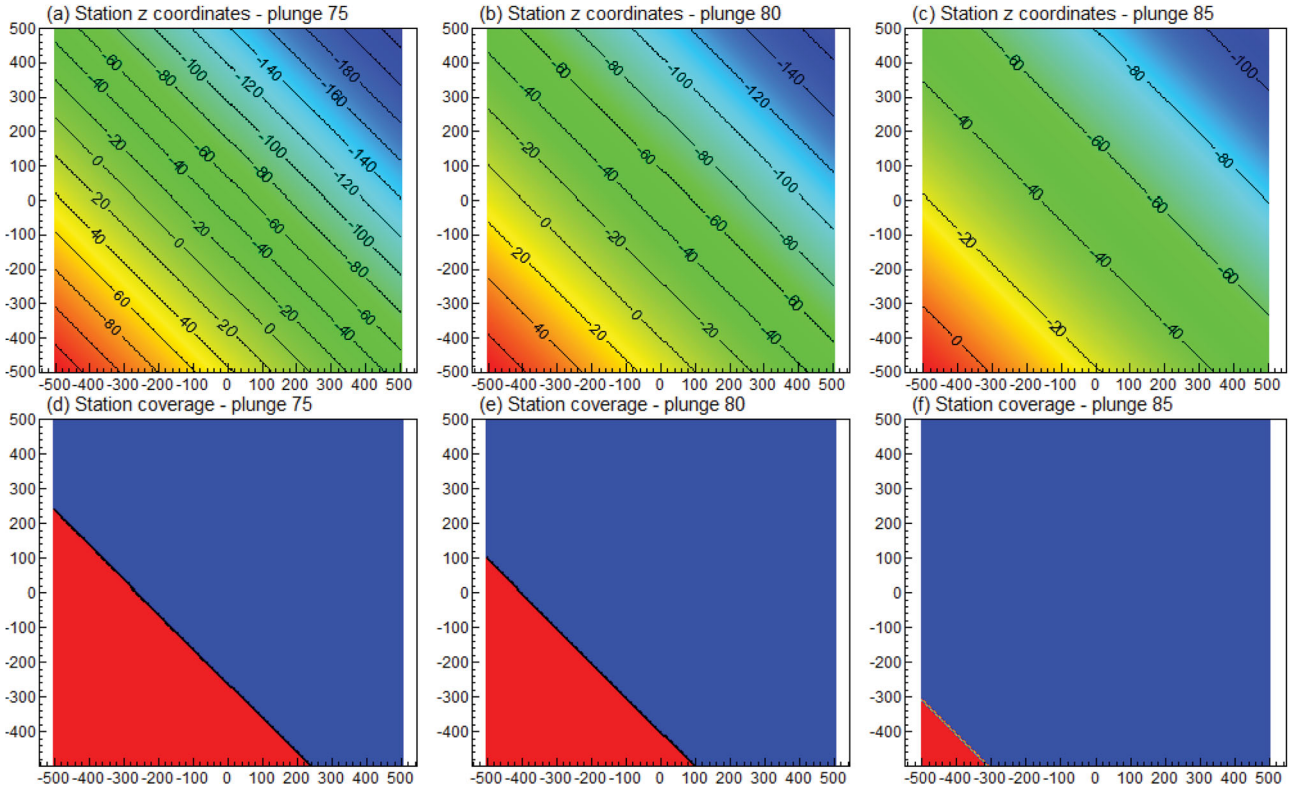

Figure 7. East-north grid images showing the region of coverage at a height of 50 m above a series of plunging right circular pipes with radius $a = 100$ m, plunge azimuth 45° and plunge angles of 75°, 80° and 85°. (a–c) show the vertical coordinates z of the observation stations relative to the plane of the top surface for each of the plunging pipe models. (d–f) display the region of valid coverage (shown in blue) for each of the plunging pipe models.

In addition to the theoretical restriction on observation points, there is another possible pitfall associated with the use of the plunging circular pipe model in certain geological situations. Most importantly the plunging right circular cylinder model should only be used in the investigation of plunging pipes which are approximately right circular. Geological situations where a plunging pipe may not be right circular may occur when the top surface of the plunging pipe has been removed by erosion or effectively demagnetised by weathering.

Symmetry properties of the magnetic gradient tensor for special magnetisation directions

The elements of the magnetic gradient tensor exhibit reflective and rotational symmetries for particular cases of the magnetisation direction, for example, when the magnetisation direction in a right circular vertical cylinder is directed along each one of the three orthogonal directions (x-north, y-east and z-vertically down). These symmetries may be deduced from expressions for the $B_{xx}, B_{xy}, B_{xz}, B_{yy}, B_{yz}, B_{zz}$ gradient tensor elements due to a semi-infinite right circular vertical cylinder as given in Equations (37.1) to (37.6) respectively.

Figures 8–10 show contoured grid images of the six main elements of the magnetic gradient tensor for a series of semi-infinite right circular vertical cylinders of radius $a = 100$ m and possessing uniform 1 Am^{-1} magnetisations $\mathbf{M}$ in the north $\mathbf{M} = |\mathbf{M}|\,\hat{\mathbf{x}}$, east $\mathbf{M} = |\mathbf{M}|\,\hat{\mathbf{y}}$, and downward vertical $\mathbf{M} = |\mathbf{M}|\,\hat{\mathbf{z}}$ directions, respectively. The plane of observation is 50 m above the top surface of the cylinder. The expressions for the B_{xx}, B_{xy}, B_{xz}, B_{yy}, B_{yz}, B_{zz} gradient tensor elements for these three magnetisation directions are given in Appendix 5. The grid images for $\mathbf{B}(\mathbf{r}; \mathbf{M} = M\,\hat{\mathbf{x}})$ in Figure 8(a–f) and also Equations (A5.1.1)–(A5.1.6) in Appendix 5 represent those for the magnetic gradient tensor $\mathbf{B}(\mathbf{r})$ reduced to the equator (RTE) while the grid images for $\mathbf{B}(\mathbf{r}; \mathbf{M} = M\,\hat{\mathbf{z}})$ in Figure 10(a–f) and also Equations (A5.3.1)–(A5.3.6) in Appendix 5 represent those for the magnetic gradient tensor $\mathbf{B}(\mathbf{r})$ reduced to the north magnetic pole (RTP).

By inspection of Figures 8–10 and also from Equations (A5.1.1)–(A5.3.6) in Appendix 5, I note the following symmetries when the intensity of magnetisation $|\mathbf{M}|$ is set to a constant in each of the north, east and downward vertical directions, i.e. when $|\mathbf{M}| = M = M_x = M_y = M_z$.

These symmetries are as follows:

$$B_{xy}(\mathbf{r}; \mathbf{M} = M\,\hat{\mathbf{x}}) = B_{xx}(\mathbf{r}; \mathbf{M} = M\,\hat{\mathbf{y}}).$$

(see Figures 8(b) and 9(a))

$$B_{yy}(\mathbf{r}; \mathbf{M} = M\,\hat{\mathbf{x}}) = B_{xy}(\mathbf{r}; \mathbf{M} = M\,\hat{\mathbf{y}}).$$

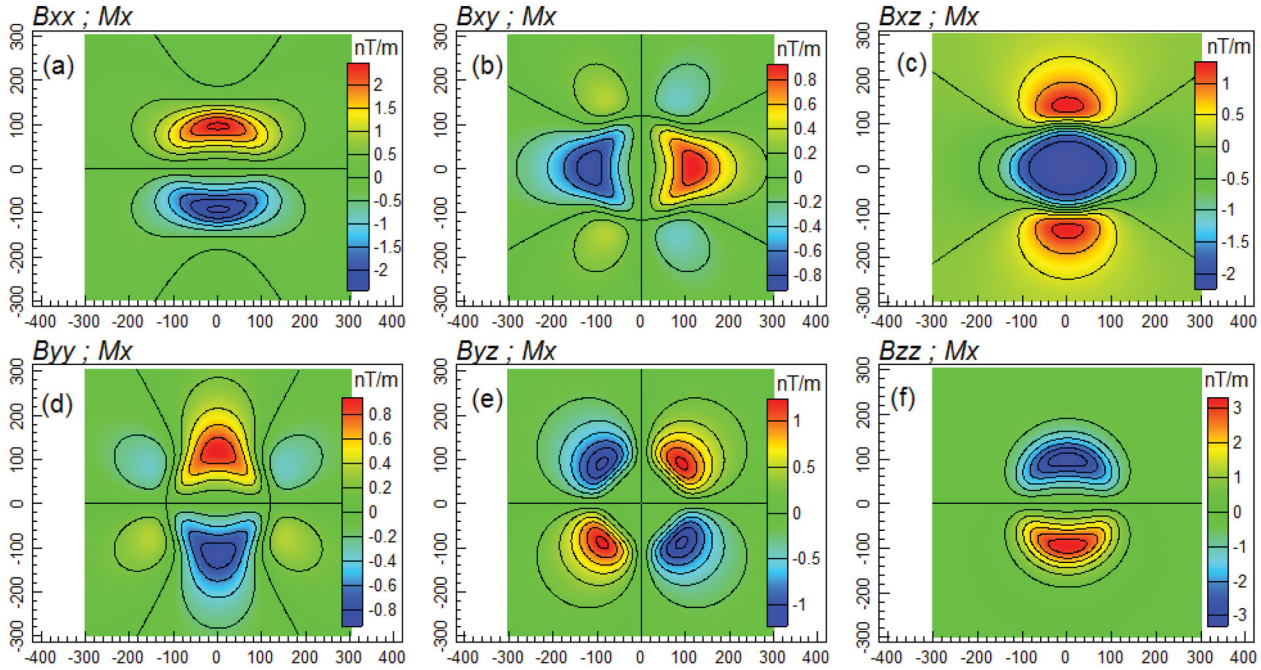

Figure 8. Contoured grid images (north is up the page) of the magnetic gradient tensor elements due to a semi-infinite right circular vertical pipe of radius $a = 100$ m, uniform magnetisation $\mathbf{M} = M\hat{\mathbf{x}}$ and intensity $M = 1\ \mathrm{Am}^{-1}$. (a–c) in the top row show tensor elements B_{xx},B_{xy},B_{xz} respectively. (d–f) in the bottom row show tensor elements B_{yy}, B_{yz}, B_{zz} respectively.

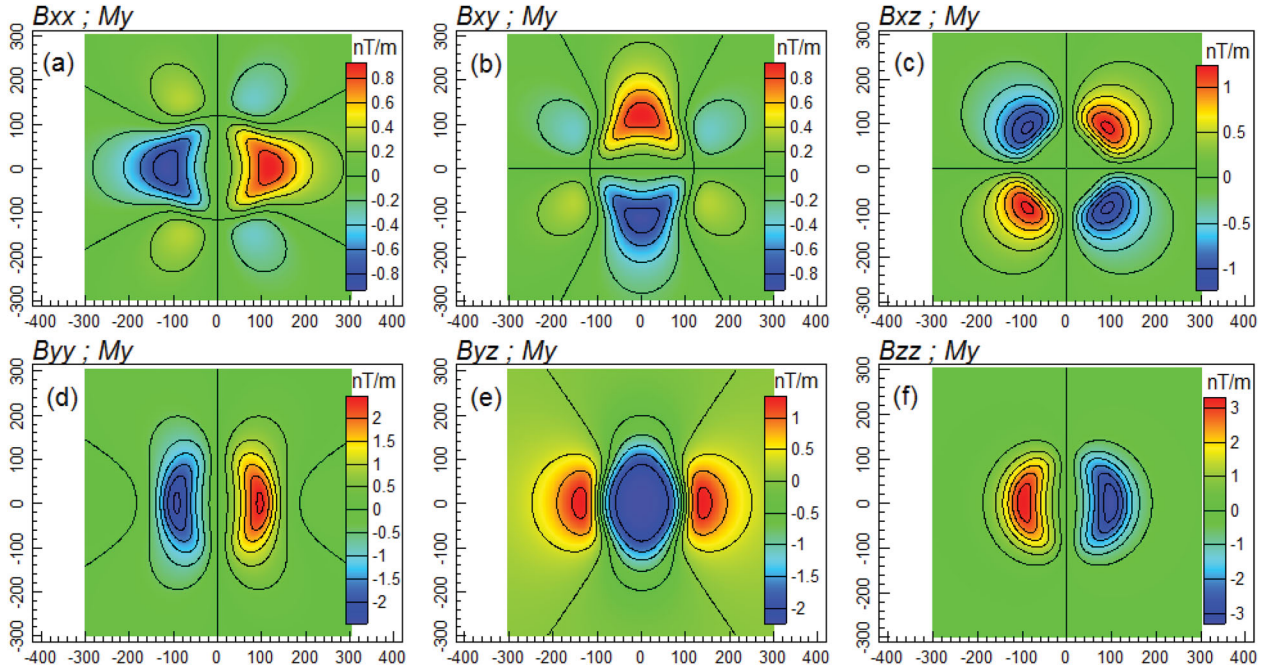

Figure 9. Contoured grid images (north is up the page) of the magnetic gradient tensor elements due to a semi-infinite right circular vertical pipe of radius $a = 100$m, uniform magnetisation $\mathbf{M} = M\hat{\mathbf{y}}$ and intensity $M = 1\ \mathrm{Am}^{-1}$. (a–c) in the top row show tensor elements B_{xx}, B_{xy}, B_{xz} respectively. (d–f) in the bottom row show tensor elements B_{yy}, B_{yz}, B_{zz} respectively.

(see Figures 8(d) and 9(b))

$$B_{xz}(\mathbf{r};\mathbf{M} = M\hat{\mathbf{x}}) = B_{xx}(\mathbf{r};\mathbf{M} = M\hat{\mathbf{z}}).$$

(see Figures 8(c) and 10(a))

$$B_{yz}(\mathbf{r};\mathbf{M} = M\hat{\mathbf{y}}) = B_{yy}(\mathbf{r};\mathbf{M} = M\hat{\mathbf{z}}).$$

(see Figures 9(e) and 10(d))

$$B_{yz}(\mathbf{r};\mathbf{M} = M\hat{\mathbf{x}}) = B_{xz}(\mathbf{r};\mathbf{M} = M\hat{\mathbf{y}}).$$

(see Figures 8(e) and 9(c))

$$B_{yz}(\mathbf{r};\mathbf{M} = M\hat{\mathbf{x}}) = B_{xy}(\mathbf{r};\mathbf{M} = M\hat{\mathbf{z}}).$$

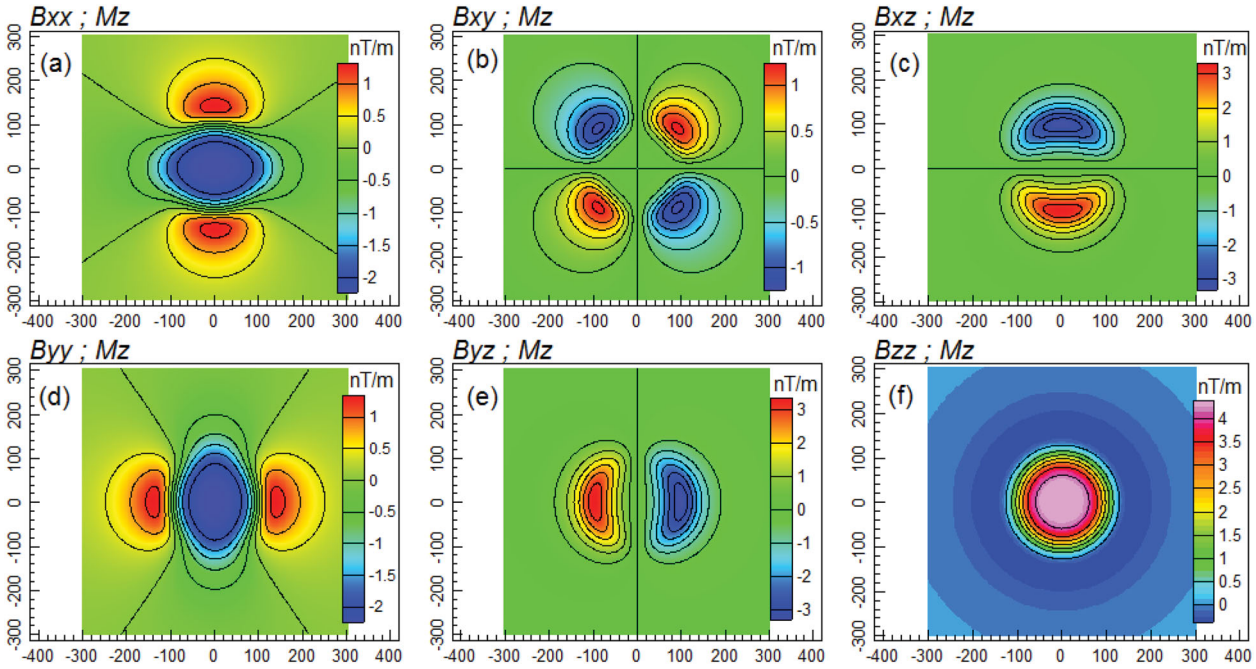

Figure 10. Contoured grid images (north is up the page) of the magnetic gradient tensor elements due to a semi-infinite right circular vertical pipe of radius $a = 100$ m, uniform magnetisation $\mathbf{M} = M\hat{\mathbf{z}}$ and intensity $M = 1$ Am^{-1}. (a–c) in the top row show tensor elements B_{xx}, B_{xy}, B_{xz} respectively. (d–f) in the bottom row show tensor elements B_{yy}, B_{yz}, B_{zz} respectively.

(see Figures 8(e) and 10(b))

$$B_{xz}(\mathbf{r};\mathbf{M}=M\hat{\mathbf{y}}) = B_{xy}(\mathbf{r};\mathbf{M}=M\hat{\mathbf{z}}).$$

(see Figures 9(c) and 10(b))

$$B_{zz}(\mathbf{r};\mathbf{M}=M\hat{\mathbf{x}}) = B_{xz}(\mathbf{r};\mathbf{M}=M\hat{\mathbf{z}}).$$

(see Figures 8(f) and 10(c))

$$B_{zz}(\mathbf{r};\mathbf{M}=M\hat{\mathbf{y}}) = B_{yz}(\mathbf{r};\mathbf{M}=M\hat{\mathbf{z}}).$$

(see Figures 9(f) and 10(e))

Rotational symmetries also exist between some of the magnetic gradient tensor elements for the three independent magnetisations of equal intensity $|\mathbf{M}| = M = M_x = M_y = M_z$. as shown in Figures 8–10. For example,

$$B_{yy}(r,\theta+\frac{\pi}{2},z;\mathbf{M}=M\hat{\mathbf{y}}) = B_{xx}(r,\theta,z;\mathbf{M}=M\hat{\mathbf{x}}).$$

(see Figures 9(d) and 8(a))

$$B_{xy}(r,\theta+\frac{\pi}{2},z;\mathbf{M}=M\hat{\mathbf{x}}) = B_{yy}(r,\theta,z;\mathbf{M}=M\hat{\mathbf{x}}).$$

(see Figure 8(b,d))

$$B_{xy}(r,\theta+\frac{\pi}{2},z;\mathbf{M}=M\hat{\mathbf{x}}) = B_{xy}(r,\theta,z;\mathbf{M}=M\hat{\mathbf{y}}).$$

(see Figures 8(b) and 9(b))

$$B_{xx}(r,\theta+\frac{\pi}{2},z;\mathbf{M}=M\hat{\mathbf{y}}) = B_{xy}(r,\theta,z;\mathbf{M}=M\hat{\mathbf{y}}).$$

(see Figure 9(a,b))

$$B_{xx}(r,\theta+\frac{\pi}{2},z;\mathbf{M}=M\hat{\mathbf{y}}) = B_{yy}(r,\theta,z;\mathbf{M}=M\hat{\mathbf{x}}).$$

(see Figures 9(a) and 8(d))

$$B_{yz}(r,\theta\pm\frac{\pi}{2},z;\mathbf{M}=M\hat{\mathbf{y}}) = B_{xz}(r,\theta,z;\mathbf{M}=M\hat{\mathbf{x}}).$$

(see Figures 9(e) and 8(c))

$$B_{yz}(r,\theta\pm\frac{\pi}{2},z;\mathbf{M}=M\hat{\mathbf{y}}) = B_{xx}(r,\theta,z;\mathbf{M}=M\hat{\mathbf{z}}).$$

(see Figures 9(e) and 10(a))

$$B_{yy}(r,\theta\pm\frac{\pi}{2},z;\mathbf{M}=M\hat{\mathbf{z}}) = B_{xz}(r,\theta,z;\mathbf{M}=M\hat{\mathbf{x}}).$$

(see Figures 10(d) and 8(c))

$$B_{yy}(r,\theta\pm\frac{\pi}{2},z;\mathbf{M}=M\hat{\mathbf{z}}) = B_{xx}(r,\theta,z;\mathbf{M}=M\hat{\mathbf{z}}).$$

(see Figures 10(d) and 10(a))

$$B_{zz}(r,\theta+\frac{\pi}{2},z;\mathbf{M}=M\hat{\mathbf{y}}) = B_{zz}(r,\theta,z;\mathbf{M}=M\hat{\mathbf{x}}).$$

(see Figures 9(f) and 8(f))

$$B_{zz}(r,\theta+\frac{\pi}{2},z;\mathbf{M}=M\hat{\mathbf{y}}) = B_{xz}(r,\theta,z;\mathbf{M}=M\hat{\mathbf{z}}).$$

(see Figures 9(f) and 10(c))

$$B_{yz}(r,\theta+\frac{\pi}{2},z;\mathbf{M}=M\hat{\mathbf{z}}) = B_{zz}(r,\theta,z;\mathbf{M}=M\hat{\mathbf{x}}).$$

(see Figures 10(e) and 8(f))

$$B_{yz}(r,\theta+\frac{\pi}{2},z;\mathbf{M}=M\hat{\mathbf{z}}) = B_{xz}(r,\theta,z;\mathbf{M}=M\hat{\mathbf{z}}).$$

(see Figures 10(e) and 10(c))

From the above symmetries it is possible to construct the elements of the magnetic gradient tensor $\mathbf{B}(\mathbf{r};\mathbf{M}=M\hat{\mathbf{y}})$ from the RTE and RTP gradient tensors $\mathbf{B}(\mathbf{r};\mathbf{M}=M\hat{\mathbf{x}})$ and $\mathbf{B}(\mathbf{r};\mathbf{M}=M\hat{\mathbf{z}})$ respectively.

A note on model scaling with respect to the radius *a*

For a pair of uniformly magnetised semi-infinite right circular vertical pipes with radii a_1 and a_2 and magnetisation **M**, and for a pair of measurement points $\mathrm{P}(r_1,\theta,z_1)$ and $\mathrm{P}(r_2,\theta,z_2)$ in which the standardised distances r/a and z/a are identical, the ratio $B_{ij;2}/B_{ij;1}$ of any tensor element B_{ij} for this pair of pipes is inversely proportional to the ratio of their respective radii, namely,

$$B_{ij;2}(r_2,\theta,z_2;a_2,\mathbf{M}) = \left(\frac{a_1}{a_2}\right) B_{ij;1}(r_1,\theta,z_1;a_1,\mathbf{M}) \quad \text{for } i,j=x,y,z \text{ and } r_1=(a_1/a_2)r_2. \tag{49}$$

This follows from the fact that when the standardised distances r/a and z/a are identical, then it may be shown that the Green's functions f_1 and f_2 for gradient tensor elements $B_{ij;1}$ and $B_{ij;2}$ in pipes 1 and 2 respectively are related as $f_2 = \left(\frac{a_1}{a_2}\right)^2 f_1$ (see Eason, Noble, and Sneddon 1955, Part II, 542–546). Since the gradient tensor elements $B_{ij;1}$ and $B_{ij;2}$ can be expressed as $B_{ij;1}(r_1,\theta,z_1;a_1,\mathbf{M}) = 2\pi\, a_1\, \mathrm{C_m}\,|\mathbf{M}|f_1$ and $B_{ij;2}(r_2,\theta,z_2;a_2,\mathbf{M}) = 2\pi\, a_2\, \mathrm{C_m}\,|\mathbf{M}|f_2 = 2\pi\ \mathrm{C_m}|\mathbf{M}|(a_1^2/a_2)f_1$, then the ratio $B_{ij;2}\,/\,B_{ij;1}$ is $(a_1\,/\,a_2)$. For example, if $a_1 = 100\,\mathrm{m}$ and $z_1 = -50\,\mathrm{m}$ in pipe 1 (Model 1a) and $a_2 = 10\,\mathrm{m}$ and $z_2 = -5\,\mathrm{m}$ in pipe 2 (Model 1b), then $B_{ij;2} = 10\,B_{ij;1}$ for all standardised observation points $(r_2/a_2, z_2/a_2)$ and $(r_1/a_1, z_1/a_1)$ respectively. Importantly, I also note that the pair of right circular vertical pipe models can be made scalable cylinder sources by choosing a magnetisation intensity $|\mathbf{M}_2|$ for pipe 2 in Equation (49) that is $|\mathbf{M}_2| = (a_2/a_1)|\mathbf{M}_1|$. This scalability property of right circular vertical cylinders relates to the equivalence between confocal ellipsoids or magnetic spheres with the same magnetic moment $\mathbf{m} = \mathbf{M}\,\mathrm{v}$ as noted in Medeiros and Silva (1995) and illustrated in Clark (2014).

For the magnetic field components b_i and the gravity gradient tensor elements Γ_{ij}, the pair of Green's functions f_1 and f_2 for $b_{i;1}$ and $b_{i;2}$ (and $\Gamma_{ij;1}$ and $\Gamma_{ij;2}$), are related as $f_2 = \left(\frac{a_1}{a_2}\right) f_1$ so that ratio $b_{i;2}\,/\,b_{i;1}$ (and $\Gamma_{ij;2}\,/\,\Gamma_{ij;1}$) is 1 when the standardised distances r/a and z/a are identical, i.e.

$$b_{i;2}(r_2,\theta,z_2;a_2,\mathbf{M}) = b_{i;1}(r_1,\theta,z_1;a_1,\mathbf{M}) \quad \text{for } i=x,y,z \text{ and } r_1=(a_1/a_2)r_2. \tag{50}$$

Finally for the magnetic scalar potential and the gravity field components, the pair of Green's functions f_1 and f_2 for V_1 and V_2 are identical, i.e. $f_2 = f_1$, so that the ratio $V_2\,/\,V_1$ (and also $g_{i;2}\,/\,g_{i;1}$ for $i=x,y,z$) is a_2/a_1 when standardised distances r/a and z/a are identical, i.e.

$$V_2(r_2,\theta,z_2;a_2,\mathbf{M}) = \left(\frac{a_2}{a_1}\right) V_1(r_1,\theta,z_1;a_1,\mathbf{M}) \quad \text{for } r_1=(a_1/a_2)r_2. \tag{51}$$

Thus the dimensionality of the Green's functions are L^0, L^{-1}, L^{-2} yielding scaling factors of a_2/a_1, 1 and a_1/a_2 for the magnetic scalar potential, the magnetic field and the magnetic gradient tensor respectively.

The superposition of magnetic field components and gradient tensor elements

The superposition principle applies to harmonic potential fields which satisfy Laplace's Equation (Blakely 1995). It is used to calculate the gravity and magnetic field components in source free regions. In the absence of significant demagnetisation effects, the superposition principle may be used to calculate the magnetic field and gradient tensor due to the following right circular cylinder models:

1. a finite length, vertical or plunging right circular cylinder
2. a concentrically zoned, semi-infinite or finite length, right circular vertical cylinder with a specific magnetisation **M** and outer radius a in each zone
3. a vertical stack of coaxial finite length vertical cylinders each with a specific magnetisation **M,** radius a and axial length h in each cylinder
4. a distributed multitude of finite-length and/or semi-infinite, right circular vertical pipes each with a specific diameter $2a$, axial length h and magnetisation **M**

The finite length right circular vertical cylinder has been discussed previously but for a plunging right circular cylinder of radius a_1, magnetisation $\mathbf{M}_1$ and axial length h_1, the magnetic field or gradient tensor response for a particular harmonic component b_c of its magnetic field or gradient tensor $b_c(x_1,x_2,x_3;a_1,h_1,\mathbf{M}_1)$ at an observation point $\mathbf{r}' = (x_1,x_2,x_3)^T$ in the body axis coordinate system is

$$b_c(x_1,x_2,x_3;a_1,h_1,\mathbf{M}_1) = b_c(x_1,x_2,x_3;a_1,\infty,\mathbf{M}_1) - b_c(x_1,x_2,x_3-h_1;a_1,\infty,\mathbf{M}_1), \tag{52}$$

where $b_c(x_1,x_2,x_3;\ a_1,\infty,\mathbf{M}_1)$ is any harmonic magnetic field component or tensor element due to a semi-infinite, right circular plunging cylinder at a measurement point $\mathbf{r}'$ defined with respect to an origin on the top surface of the finite length cylinder and $b_c(x,y,z-h;a,\infty,\mathbf{M})$, is the magnetic field component or tensor element due to a second semi-infinite right circular vertical cylinder, coaxial with the first, and at the same measurement point whose axial coordinate is $x_3 - h_1$ relative to a new origin on the top surface of the second cylinder. In this instance the top surface of the second cylinder is coincident with the base of the first so that

the separation distance between top surfaces of the pair of coaxial cylinders is h_1.

For a concentrically zoned, semi-infinite or finite length, vertical, right circular cylinder of vertical depth extent h_1, which is comprised of an inner core or annulus with radius a_1 and magnetisation $\mathbf{M}_1$ and $(n-1)$ outer rings with radius a_i and magnetisation $\mathbf{M}_i$ as in model case type 2 above, the calculated component b_c for both the semi-infinite and finite depth extent models is

$$\begin{aligned} b_c(x,y,z_1) = {} & b_c(x,y,z_1;a_1,h_1,\mathbf{M}_1) \\ & + \sum_{i=2}^{n} b_c(x,y,z_1;a_i,h_1,\mathbf{M}_i) \\ & - b_c(x,y,z_1;a_{i-1},h_1,\mathbf{M}_i) \text{ for } n \geq 2. \end{aligned} \quad (53)$$

For a coaxial stack of n cylinders in case model 3 above, the calculated component b_c for the finite depth extent model is

$$\begin{aligned} b_c(x,y,z_1) = {} & \sum_{i=1}^{n} b_c(x,y,z_i;a_i,\infty,\mathbf{M}_i) \\ & - b_c(x,y,z_i-h_i;a_i,\infty,\mathbf{M}_i) \quad (h_n < \infty), \end{aligned} \quad (54)$$

where $z_k = z_1 - \sum_{i=1}^{k-1} h_i \; (2 \leq k \leq n)$.

And for the semi-infinite depth extent model in case 3 in which $h_n = \infty$

$$\begin{aligned} b_c(x,y,z_1) = {} & \sum_{i=1}^{n-1} \{ b_c(x,y,z_i;a_i,\infty,\mathbf{M}_i) \\ & - b_c(x,y,z_i-h_i;a_i,\infty,\mathbf{M}_i) \} \\ & + b_c(x,y,z_n;a_n,\infty,\mathbf{M}_n), \end{aligned} \quad (55)$$

$$\text{where } z_k = z_1 - \sum_{i=1}^{k-1} h_i \; (2 \leq k \leq n).$$

I also note that the superposition principle may be used to calculate the gravity fields and gradient tensors in each of the above composite models except that the magnetisation $\mathbf{M}$ is replaced by the density or density contrast ρ in each of the above models.

Conclusions – Final overview

This paper has presented a set of closed form expressions for the direct calculation of the magnetic gradient tensor due to a uniformly magnetised right circular cylinder or pipe. My formulation is based on Poisson's relation beginning with an expression for the magnetic scalar potential for a semi-infinite right circular vertical cylinder or pipe. The expressions for all magnetic fields and gradient tensors are applicable to either a vertical or plunging right circular pipe provided that observation points lie above or are coplanar with the top surface of the pipe. I also provide expressions for calculating both the gravity and magnetic gradient tensors for various particular cases including measurement stations on the axis of the circular cylinder or stations coplanar with its top surface. The expressions for the magnetic field and its gradient tensor on the axis of the cylinder are derived from Taylor's series expansions of the Lipschitz–Hankel integrals near its central axis. At least six Lipschitz–Hankel integrals are required to formulate the magnetic scalar potential, the magnetic field components and the magnetic gradient tensor for a uniform magnetic pipe. The expressions for the gradient tensor shown in my paper have passed the following tests, namely,

1. The expressions for the magnetic gradient tensor (shown here in both Cartesian and cylindrical coordinates) satisfy the trace and symmetry relations for all observation points outside the pipe, i.e. satisfying Laplace's equations.
2. Singularities in the equations for magnetic field and magnetic gradient tensor have been confirmed for all points on the rim of the top surface of the cylinder.
3. Gradient tensors calculated for a facetted quasi-circular pipe are in close agreement with those computed from the closed form theoretical expressions shown in this paper. Hence the theory presented here is correct.
4. The scalability of magnetic sources which is well known for magnetic spheres possessing identical magnetisations (but not moments) is shown to apply to right circular vertical pipes.
5. The superposition principle allows for the computation of the magnetic and gravity potential fields for a finite length or concentrically zoned circular pipe.

The expressions for the magnetic field and gradient tensor on the axis of a vertical pipe are particularly important because they lead to equations for determining the magnetisation direction in a uniform pipe.

Acknowledgements

This paper represents a partial contribution towards a Ph.D. in the Department of Earth and Environmental Sciences at Macquarie University under the supervision of Mark Lackie and Craig O'Neill. I should like to thank Clive Foss, David Pratt and David Clark for encouraging me to write this paper.

Disclosure statement

No potential conflict of interest was reported by the author(s).

Data availability statement

Data sharing is not applicable to this article as no new data were created or analysed in this study.

References

Abramowitz, M., and I.A. Stegun. 1964. *Handbook of mathematical functions, Applied Mathematical Series*, vol. 58: National Bureau of Standards, reprinted 1968, Dover Publications.

Barnett, C.T. 1976. Theoretical modelling of the magnetic and gravitational fields of an arbitrarily shaped three-dimensional body. *Geophysics* 41: 1353–1364. doi:10.1190/1.1440685.

Blakely, R.J. 1995. *Potential theory in gravity and magnetic applications*. Cambridge: Cambridge University Press.

Byrd, P.F., and M.D. Friedman. 1995 [1971]. *Handbook of elliptic integrals for engineers and physicists*. 2nd ed. Berlin: Sprenger-Verlag.

Clark, D.A. 2012. New methods for interpretation of magnetic vector and gradient tensor data I: eigenvector analysis and the normalised source. *Exploration Geophysics* 43: 267–282. doi:10.1071/EG12020.

Clark, D. A., 2013. New methods for interpretation of magnetic vector and gradient tensor data II: Application to the Mount Leyshon anomaly, Queensland. *Exploration Geophysics* 44: 114–127. doi:10.1071/EG12066

Clark, D.A. 2014. Methods for determining remanent and total magnetisations of magnetic sources – a review. *Exploration Geophysics* 45: 271–304. doi:10.1071/EG14013.

Damiata, B.D., and T.-C. Lee. 2002a. Gravitational attraction of solids of revolution Part 1: Vertical circular with radial variation of density. *Journal of Applied Geophysics* 50: 333–349. doi:10.1016/S0926-9851(02)00151-9.

Damiata, B.D., and T.-C. Lee. 2002b. Gravitational attraction of solids of revolution Part 2: General expressions. *Journal of Applied Geophysics* 50: 351–373. doi:10.1016/S0926-9851(02)00152-0.

Eason, G., B. Noble, and I.N. Sneddon. 1955. On certain integrals of Lipschitz-Hankel type involving products of Bessel functions. *Philosophical Transactions of the Royal Society of London, Series A* 247: 529–551. doi:10.1098/rsta.1955.0005.

Emerson, D.W., D.A. Clark, and S.J. Saul. 1985. Magnetic exploration models incorporating remanence, demagnetisation and anisotropy: HP 41C handheld computer algorithms. *Exploration Geophysics* 16: 1–122. doi:10.1071/EG985001.

Gradshteyn, I.S., and I.W. Ryzhik. 1965. *Table of integrals, series and products*. New York: Academic Press.

Heuman, C. 1941. Tables of complete elliptic integrals. *Journal of Mathematics and Physics* 20: 127–206.

McKenzie, K.B. 2020. The magnetic gradient tensor of a triaxial ellipsoid, its derivation and its application to the determination of magnetisation direction. *Exploration Geophysics* 51: 609–641. doi:10.1080/08123985.2020.1726176.

Medeiros, W.E., and J.B.C. Silva. 1995. Simultaneous estimation of total magnetisation direction and spatial orientation. *Geophysics* 60: 1365–1377. doi:10.1190/1.1443872.

Nabighian, M. 1962. The gravitational attraction of a right circular cylinder at points external to it. *Geofisica Pura e Applicata* 53: 45–51. doi: 10.1007/BF02007/108.

Nagy, D. 1965. The evaluation of Heuman's Lambda function and its application to calculate the gravitational effect of a right circular cylinder. *Geofisica Pura e Applicata* 62: 5–12.

Pedersen, L.B., and M. Bastani. 2016. Estimating rock vector magnetization from coincident measurements of magnetic field and gravity gradient tensor. *Geophysics* 81: B55–B64. doi:10.1190/GEO2015-0100.1.

Pratt, D.A., C.A. Foss, Z. Shi, S. Mann, A.S. White, P.R. Gidley, and K.B. McKenzie. 2005. Model Vision Pro, AutoMag Reference Manual Version 7.00, Encom Technology Pty Ltd.

Pratt, D.A., K.B. McKenzie, and T.S. White. 2014. Remote remanence estimation (RRE). *Exploration Geophysics* 45: 314–323. doi:10.1071/EG14031.

Press, W.H., S.A. Teukolsky, W.T. Vetterling, and B.P. Flannery. 1992. *Numerical recipes in Fortran the art of scientific computing*, 2nd ed. Cambridge: Cambridge University Press.

Reilly, W.J. 1969. Gravitational and magnetic effects of a right circular cylinder. *New Zealand Journal of Geology and Geophysics* 12: 497–506. doi:10.1080/00288306.1969.1042029.

Rim, H., and Y. Li. 2016. Gravity gradient tensor due to a cylinder. *Geophysics* 81: G59–G66. doi:10.1190/GEO2015-0699.1.

Siew, P.F. 1990. Magnetic anomalies of cylinders. *The Quarterly Journal of Mechanics and Applied Mathematics* 43: 373–385.

Siew, P.F. 1997. On the differentiation between the magnetic anomalies of cylinders and disks. *IMA Journal of Applied Mathematics* 59: 149–164.

Singh, S.K. 1977a. The gravitational attraction of a circular disc. *Geophysics* 42: 111–113.

Singh, S.K. 1977b. The gravitational attraction of a vertical right circular cylinder. *Geophysical Journal of the Royal Astronomical Society* 50: 243–246. doi:10.1111/j.1365-246X.1977.tb01332.x.

Singh, S.K., and F.J. Sabina. 1978. Magnetic anomaly due to a vertical right circular cylinder with arbitrary polarization. *Geophysics* 43: 173–178. doi:10.1190/1.1440818.

Watson, G.N. 1943. *The theory of Bessel functions*. 2nd ed. Cambridge: Cambridge University Press.

Woodward, D.J. 1973. Gravitational and magnetic effects of a solid of revolution (note). *New Zealand Journal of Geology and Geophysics* 16: 170–171. doi:/10.1080/00288306.1973.10425390.

Appendix 1: Closed form expressions for the Lipschitz–Hankel integrals

The six Lipschitz–Hankel integrals $I(1,0;-1)$, $I(1,1;-1)$, $I(1,0;0)$, $I(1,1;0)$, $I(1,0;1)$ and $I(1,1;1)$ which appear in expressions for the gravity field vector, the gravity gradient tensor, the scalar magnetic potential, the magnetic field vector and the magnetic gradient tensor have been evaluated in closed form by Eason, Noble, and Sneddon (1955), equations (4.6), (4.9), (4.7), (4.2), (4.8), and (4.4) respectively.

For the $I(1,0;-1)$, $I(1,1;-1)$ and $I(1,0;0)$ integrals there are three particular general cases, namely, $0 < r < a, r = a, r > a$.

The closed form expression for the $I(1,0;-1)$ integral is (Eason, Noble, and Sneddon 1955, equation 4.6):

$$I(1,0;-1) = \begin{cases} \dfrac{\sqrt{ar}}{ka}E_0(k) + \dfrac{k\,(a^2-r^2)}{4a\sqrt{ar}}F_0(k) + \dfrac{|z|}{2a}\Lambda_0(k,\beta) & \\ \qquad -\dfrac{|z|}{a} & (r<a) \\ \dfrac{E_0(k)}{k} - \dfrac{|z|}{2a} & (r=a) \\ \dfrac{\sqrt{ar}}{ka}E_0(k) + \dfrac{k(a^2-r^2)}{4a\sqrt{ar}}F_0(k) - \dfrac{|z|}{2a}\Lambda_0(k,\beta) & (r>a) \end{cases}. \tag{A1.1}$$

The closed form expression for the $I(1,1;-1)$ integral is (Eason, Noble, and Sneddon 1955, equation 4.9):

$$I(1,1;-1) = \left\{ \begin{array}{ll} \frac{|z|}{2k\sqrt{ar}}E_0(k) - \frac{k|z|(a^2+r^2+z^2/2)}{4ar\sqrt{ar}}F_0(k) & \\ \quad + \frac{(a^2-r^2)}{4ar}\Lambda_0(k,\beta) + \frac{r}{2a} & (r<a) \\ \frac{|z|}{2ka}E_0(k) - \frac{k|z|\ (2a^2+z^2/2)}{4a^3}F_0(k) + \frac{1}{2} & (r=a) \\ \frac{|z|}{2k\sqrt{ar}}E_0(k) - \frac{k|z|\ (a^2+r^2+z^2/2)}{4ar\sqrt{ar}}F_0(k) & \\ \quad + \frac{(r^2-a^2)}{4ar}\Lambda_0(k,\beta) + \frac{a}{2r} & (r>a) \end{array} \right\}. \quad \text{(A1.2)}$$

The closed form expression for the $I(1,0;0)$ integral is (Eason, Noble, and Sneddon 1955, equation 4.7):

$$I(1,0;0) = \left\{ \begin{array}{ll} -\frac{k|z|}{4a\sqrt{ar}}F_0(k) - \frac{1}{2a}\Lambda_0(k,\beta) + \frac{1}{a} & (r<a) \\ -\frac{k|z|}{4a^2}F_0(k) + \frac{1}{2a} & (r=a) \\ -\frac{k|z|}{4a\sqrt{ar}}F_0(k) + \frac{1}{2a}\Lambda_0(k,\beta) & (r>a) \end{array} \right\}. \quad \text{(A1.3)}$$

The closed form expression for the $I(1,1;0)$ integral is (Eason, Noble, and Sneddon 1955, equation 4.2):

$$I(1,1;0) = \frac{1}{k\sqrt{ar}}\left\{\left(1-\frac{k^2}{2}\right)F_0(k) - E_0(k)\right\} \quad (\text{for } r > 0). \quad \text{(A1.4)}$$

The closed form expression for the $I(1,0;1)$ integral is (Eason, Noble, and Sneddon 1955, equation 4.8)

$$I(1,0;1) = \frac{k^3(a^2-r^2-z^2)}{16\,a\,k'^2(ar)^{3/2}}E_0(k) + \frac{k}{4a\sqrt{ar}}F_0(k) \quad (\text{for } r > 0). \quad \text{(A1.5)}$$

The closed form expression for the $I(1,1;1)$ integral is (Eason, Noble, and Sneddon 1955, equation 4.4)

$$I(1,1;1) = \frac{k|z|}{4(ar)^{3/2}}\left[\left(1-\frac{k^2}{2}\right)\left(\frac{1}{k'^2}\right)E_0(k) - F_0(k)\right] \quad (\text{for } r > 0). \quad \text{(A1.6)}$$

where $F_0(k) = (2/\pi)\,F(k)$ and $E_0(k) = (2/\pi)E(k)$ are the complete elliptic integrals of the first and second kind with modulus k, namely,

$$F(k) = \int_0^{\pi/2} \frac{1}{\sqrt{1-k^2\sin^2\theta}}\,\mathrm{d}\theta \quad \text{(A1.7)}$$

and

$$E(k) = \int_0^{\pi/2} \sqrt{1-k^2\sin^2\theta}\,\mathrm{d}\theta \quad \text{(A1.8)}$$

The modulus k and the modular angle α are defined as

$$k^2 = \sin^2\alpha = \frac{4ar}{(a+r)^2+z^2} \quad \text{(A1.9)}$$

Also $\Lambda_0(k,\beta)$ is Heuman's lambda function with modulus k and angular amplitude β (Heuman 1941; Eason, Noble, and Sneddon 1955; Abramowitz and Stegun 1964; Byrd and Friedman 1971; Singh and Sabina 1978). Heuman's Lambda function is defined in terms of the following elliptic integrals, namely,

$$\Lambda_0(k,\beta) = F_0(k)E(k',\beta) - [F_0(k) - E_0(k)]\,F(k',\beta), \quad \text{(A1.10)}$$

where $F(k',\beta)$ and $E(k',\beta)$ are the incomplete elliptic integrals of the first and second kind respectively with modular angle $(\pi/2-\alpha)$, co-modulus $k' = \sqrt{1-k^2}'$ and angular amplitude β which is defined as $\sin^2\beta = \frac{z^2}{(a-r)^2+z^2}$. The incomplete elliptic integrals of the first and second kind respectively with modulus $k = \sin\alpha$ and angular amplitude β are defined as follows:

$$F(k,\beta) = \int_0^{\beta} \frac{1}{\sqrt{1-k^2\sin^2\theta}}\,\mathrm{d}\theta \quad \text{(A1.11)}$$

and

$$E(k,\beta) = \int_0^{\beta} \sqrt{1-\mathrm{k}^2\sin^2\theta}\,\mathrm{d}\theta \quad \text{(A1.12)}$$

Appendix 2: Particular limiting cases for the Lipschitz–Hankel integrals

In this Appendix I shall examine some important particular cases for the Lipschitz–Hankel integrals which occur in the generic expressions for the magnetic scalar potential, the magnetic field vector and the magnetic gradient tensor of the semi-infinite right circular vertical cylinder. Expressions for the magnetic scalar potential require the following pair of Lipschitz–Hankel integrals, namely, $I(1,0;-1)$ and $I(1,1;-1)$, while expressions for the magnetic field components require $I(1,0;0)$, $I(1,1;-1)/r$ and $I(1,1;0)$, and expressions for the magnetic gradient tensor also require $I(1,0;0)/\mathrm{r}$, $I(1,1;-1)/r^2$, $I(1,1;0)/r$, $I(1,0;1)$ and $I(1,1;1)$. The particular cases to be considered are as follows:

(1) Any axial measurement point P(0,0,z) which is above the top of the cylinder, i.e. where $r = \sqrt{x^2+y^2} = 0$ and $z < 0$.
(2) The axial measurement point P(0,0,0) which lies at the origin on the top surface of the cylinder, i.e. where $r = \sqrt{x^2+y^2} = 0$ and $z = 0$.
(3) The coplanar measurement point P(r,θ, 0) or P(x,y,0) which lies on the top surface of the cylinder or is coplanar with it, i.e. where $r = \sqrt{x^2+y^2}$; $\theta = \arctan(\mathrm{y/x})$; $z = 0$ and the three sub-cases $0 < r < a$; $r = a$; $r > a$.

1. Axial cases

The expressions for the axial measurement cases in the six Lipschitz–Hankel integrals $I(1,0;-1)$, $I(1,1;-1)$, $I(1,0;0)$, $I(1,1;0)$, $I(1,0;1)$ and $I(1,1;1)$ are derived by setting $r = 0$ in the integral forms of these functions. However the integrals $I(1,1;-1)/r$, $I(1,0;0)/r$, $I(1,1;-1)/r^2$ and $I(1,1;0)/r$ which have factors of $1/r$ or $1/r^2$ require a different treatment involving expansions of the Lipschitz–Hankel integrals for small r/a (see Appendix 4). For the axial cases in which $r = 0$, the $\mathrm{J}_0(rp)$ and $\mathrm{J}_1(rp)$ Bessel functions are $\mathrm{J}_0(rp) = 1$ and $\mathrm{J}_1(rp) = 0$ (Abramowitz and Stegun 1964, Table 9.1, p.390). Then for the $I(1,1;-1)$ Lipschitz–Hankel integral in Equation (A1.1)

$$I(1,1;-1) = \int_0^{\infty} \mathrm{J}_1(ap)\,\mathrm{J}_1(rp)\mathrm{e}^{-p|z|}\,p^{-1}\mathrm{d}p = \int_0^{\infty} \mathrm{J}_1(ap)\,\mathrm{J}_1(0)\mathrm{e}^{-p|z|}\,p^{-1}\,\mathrm{d}p = 0. \quad \text{(A2.1.1)}$$

Similarly for the $I(1,1;0)$ Lipschitz–Hankel integral in Equation (A1.4)

$$I(1,1;\,0) = \int_0^\infty \mathrm{J}_1(ap)\,\mathrm{J}_1(rp)\mathrm{e}^{-p|z|}\,\mathrm{d}p = \int_0^\infty \mathrm{J}_1(ap)\,\mathrm{J}_1(0)\mathrm{e}^{-p|z|}\,\mathrm{d}p = 0. \qquad \text{(A2.1.2)}$$

Similarly for the $I(1,1;1)$ Lipschitz–Hankel integral in Equation (A1.6)

$$I(1,1;1) = \int_0^\infty \mathrm{J}_1(ap)\,\mathrm{J}_1(rp)\mathrm{e}^{-p|z|}\,p\,\mathrm{d}p = 0. \qquad \text{(A2.1.3)}$$

For the $I(1,0;-1)$ Lipschitz–Hankel integral in Equation (A1.1) setting $\mathrm{J}_0(rp) = 1$ for $r = 0$,

$$I(1,0;-1) = \int_0^\infty \mathrm{J}_1(ap)\,\mathrm{J}_0(0)\mathrm{e}^{-p|z|}\,p^{-1}\,\mathrm{d}p = \int_0^\infty \mathrm{J}_1(ap)\,\mathrm{e}^{-p|z|}\,p^{-1}\,\mathrm{d}p.$$

Integrals of this form have been evaluated by Gradshteyn and Ryzhik (1965, equation 6.623.3) namely,

$$\int_0^\infty \mathrm{e}^{-\alpha x}\mathrm{J}_\nu(\beta x)\,x^{-1}\,\mathrm{d}x = \frac{\left(\sqrt{\alpha^2+\beta^2}-\alpha\right)^\nu}{\nu\beta^\nu}.$$

Hence for $\nu = 1, \alpha = |z|\,, \beta = a$, then

$$I(1,0;-1) = \int_0^\infty \mathrm{J}_1(ap)\,\mathrm{e}^{-p|z|}\,p^{-1}\,\mathrm{d}p = \frac{\sqrt{z^2+a^2}-|z|}{a} \quad (r=0, z<0). \qquad \text{(A2.1.4)}$$

For the $I(1,0;0)$ Lipschitz–Hankel integral in Equation (A1.3) on setting $\mathrm{J}_0(rp) = 1$ for $r = 0$,

$$I(1,0;0) = \int_0^\infty \mathrm{J}_1(ap)\,\mathrm{J}_0(0)\mathrm{e}^{-p|z|}\,\mathrm{d}p = \int_0^\infty \mathrm{J}_1(ap)\,\mathrm{e}^{-p|z|}\,\mathrm{d}p.$$

Integrals of this form have been evaluated by Gradshteyn and Ryzhik (1965, equation 6.621.4) namely,

$$\int_0^\infty \mathrm{e}^{-\alpha x}\mathrm{J}_\nu(\beta x)\,\mathrm{d}x = \frac{\left(\sqrt{\alpha^2+\beta^2}-\alpha\right)^\nu}{\beta^\nu\sqrt{\alpha^2+\beta^2}}.$$

Thus for $\nu = 1, \alpha = |z|\,, \beta = a$,

$$I(1,0;0) = \int_0^\infty \mathrm{J}_1(ap)\,\mathrm{e}^{-p|z|}\,\mathrm{d}p = \frac{\sqrt{z^2+a^2}-|z|}{a\sqrt{z^2+a^2}} = \frac{1}{a}\left\{1 - \frac{|z|}{\sqrt{z^2+a^2}}\right\} (r=0, z<0). \qquad \text{(A2.1.5)}$$

Finally to determine the limit for the integral $I(1,1;-1)/r$ in the axial case, it is necessary to find a series expansion of the integral $I(1,1;-1)$ for small values of (r/a). Following Eason, Noble, and Sneddon (1955, 535), it may be shown that for $\zeta = |z|/a$

$$I(1,1;-1) = \frac{\sqrt{1+\zeta^2}-\zeta}{2\sqrt{1+\zeta^2}}\left(\frac{r}{a}\right) + \mathrm{O}\left(\frac{r}{a}\right)^3 = \frac{1}{2}\left[1 - \frac{\zeta}{\sqrt{1+\zeta^2}}\right]\left(\frac{r}{a}\right) + \mathrm{O}\left(\frac{r}{a}\right)^3.$$

$$\text{Hence } I(1,1;-1)/r = \frac{1}{2a}\left[1 - \frac{\zeta}{\sqrt{1+\zeta^2}}\right] + \mathrm{O}\left(\frac{r}{a}\right)^2 = \frac{1}{2a}\left[1 - \frac{|z|}{\sqrt{a^2+z^2}}\right] + \mathrm{O}\left(\frac{r}{a}\right)^2,$$

$$\text{so that } I(1,1;-1)/r = \frac{1}{2a}\left[1 - \frac{|z|}{\sqrt{a^2+z^2}}\right] = \frac{1}{2}\,I(1,0;0) \quad (\text{for } r=0). \qquad \text{(A2.1.6)}$$

2. Origin cases

For an observation station at the origin or centre of the top face of the semi-infinite right circular vertical cylinder, the expressions for the three Lipschitz–Hankel integrals $I(1,0;-1)$, $I(1,0;0)$ and $I(1,1;-1)/r$ respectively are derived by setting $z = 0$ in the expressions for these functions in equations (A2.1.4)–(A2.1.6) above. Thus from Equation (A2.1.4), the $I(1,0;-1)$ Lipschitz–Hankel integral at the origin is

$$I(1,0;-1) = \frac{\sqrt{z^2+a^2}-|z|}{a} = 1 \quad (\text{for } r=0, z=0). \qquad \text{(A2.2.1)}$$

Similarly from Equation (A2.1.5), the $I(1,0;0)$ Lipschitz–Hankel integral is

$$I(1,0;0) = \frac{1}{a}\left\{1 - \frac{|z|}{\sqrt{z^2+a^2}}\right\} = \frac{1}{a} \quad (r=0, z=0)\,, \qquad \text{(A2.2.2)}$$

and from Equation (A2.1.6), the $I(1,1;-1)/r$ Lipschitz–Hankel integral is

$$I(1,1;-1)/r = \frac{1}{2a}\left[1 - \frac{|z|}{\sqrt{z^2+a^2}}\right] = \frac{1}{2}I(1,0;0) = \frac{1}{2a} \quad (\text{for } r=0, z=0). \qquad \text{(A2.2.3)}$$

The $I(1,1;-1)$, $I(1,1;0)$ and $I(1,1;1)$ Lipschitz–Hankel integrals are identically zero at the origin as in the axial cases above,

$$I(1,1;-1) = 0; \quad I(1,1;0) = 0\,; \quad I(1,1;1) = 0\,(r=0, z\le 0). \qquad \text{(A2.2.4)}$$

3. Coplanar cases

The $I(1,0;-1)$, $I(1,1;-1)$ and $I(1,0;0)$ Lipschitz–Hankel integrals contain terms involving Heuman's Lambda function $\Lambda_0(k,\beta)$ where $\sin^2\beta = z^2/\{(a-r)^2+z^2\}$ [see Equation (A1.10)]. In each of the three coplanar cases $|z| = 0$ so that $\sin^2\beta = 0$. Therefore Heuman's Lambda function $\Lambda_0(k,\beta)$ and the incomplete elliptic integrals $F_0(k,\beta)$ and $E_0(k,\beta)$ are all identically zero in equations (A1.1), (A1.2), and (A1.3) respectively (Abramowitz and Stegun 1964, Tables 17.5 and 17.6).

The expressions for the $I(1,0;-1)$ integral in the three particular coplanar cases above are derived by setting $|z| = 0$ in Equation (A1.1), namely,

$$I(1,0;-1) = \begin{Bmatrix} \dfrac{(a+r)}{2a}E_0(k) + \dfrac{(a-r)}{2a}F_0(k) & (r<a) \\ 1 & (r=a) \\ \dfrac{(a+r)}{2a}E_0(k) + \dfrac{(a-r)}{2a}F_0(k) & (r>a) \end{Bmatrix}, \qquad \text{(A2.3.1)}$$

$$k^2 = \sin^2\alpha = \frac{4ar}{(a+r)^2}\,;\, \sin^2\beta = 0\,;\, \Lambda_0(k,0) = 0. \qquad \text{(A2.3.2)}$$

Similarly, the expressions for the three particular coplanar cases belonging to the $I(1,1;-1)$ and $I(1,1;-1)/r$ integrals are

derived by setting $|z| = 0$ in Equation (A1.2), namely,

$$I(1,1;-1) = \begin{Bmatrix} \dfrac{r}{2a} & (r < a) \\ \dfrac{1}{2} & (r = a) \\ \dfrac{a}{2r} & (r > a) \end{Bmatrix},$$

and

$$I(1,1;-1)/r = \begin{Bmatrix} \dfrac{1}{2a} & (r < a) \\ \dfrac{1}{2a} & (r = a) \\ \dfrac{a}{2r^2} & (r > a) \end{Bmatrix}. \quad \text{(A2.3.3)}$$

Similarly, the expressions for the $I(1,0;0)$ and $I(1,0;0)/r$ integrals in the three coplanar cases above are derived by setting $|z| = 0$ in Equation (A1.3). Hence

$$I(1,0;0) = \begin{Bmatrix} \dfrac{1}{a} & (r < a) \\ \dfrac{1}{2a} & (r = a) \\ 0 & (r > a) \end{Bmatrix},$$

and

$$I(1,0;0)/r = \begin{Bmatrix} \dfrac{1}{ar} & (r < a) \\ \dfrac{1}{2a^2} & (r = a) \\ 0 & (r > a) \end{Bmatrix}. \quad \text{(A2.3.4)}$$

It is noted that the limit for $r = a$ is exactly the Dirichlet limit for the $(r < a)$ and $(r > a)$ particular cases as r approaches a, i.e.

$$I(1,0;0)|_{r=a} = \frac{1}{2}\left\{\lim_{r\to a}[I(1,0;0)|_{r<a} + I(1,0;0)|_{r>a}]\right\},$$
$$= \frac{1}{2}\left(\frac{1}{a} + 0\right) = \frac{1}{2a}.$$

The expressions for the $I(1,1;0)$ and $I(1,1;0)$/r integrals for the $(0 < r < a)$ and $(r > a)$ particular coplanar cases remain unchanged from Equation (A1.4) except at a measurement point P(a, θ, 0) on the rim of the top surface where it is undefined. Hence

$$I(1,1;\,0) = \begin{Bmatrix} \dfrac{1}{k\sqrt{ar}}\left[\left(1 - \dfrac{k^2}{2}\right)F_0(k) - E_0(k)\right] & (r \neq a) \\ \infty & (r = a) \end{Bmatrix}, \quad \text{(A2.3.5)}$$

and

$$I(1,1;\,0)/\mathrm{r} = \begin{Bmatrix} \dfrac{1}{kr\sqrt{ar}}\left[\left(1 - \dfrac{k^2}{2}\right)F_0(k) - E_0(k)\right] & (r \neq a) \\ \infty & (r = a) \end{Bmatrix}. \quad \text{(A2.3.6)}$$

The expression for the $I(1,0;\,1)$ integral for the $(0 < r < a)$ and $(r > a)$ coplanar cases remains unchanged from Equation (A1.5) except at measurement points P(a, θ, 0) on the rim of the top surface of the right circular cylinder where it is undefined. Since the $I(1,0;\,1)$ integral changes sign from positive to negative for measurement points where $r > a$ then

$$I(1,0;\,1) = \begin{Bmatrix} \dfrac{1}{2a}\left[\dfrac{E_0(k)}{(a-r)} + \dfrac{F_0(k)}{(a+r)}\right] & (r \neq a) \\ \pm\infty & (r = a) \end{Bmatrix}. \quad \text{(A2.3.7)}$$

Appendix 3: Derivatives of the Lipschitz–Hankel integrals $I(1,0;-2)$, $I(1,0;-1)$, $I(1,1;-1)$, $I(1,0;0)$, $I(1,1;0)$

Expressions for the gravity field, gravity gradient tensor, magnetic field and magnetic gradient tensor for a semi-infinite right circular vertical cylinder involve finding the partial derivatives of the Lipschitz–Hankel integrals $I(1,0;-2)$, $I(1,0;-1)$, $I(1,1;-1)$, $I(1,0;0)$, and $I(1,1;0)$ with respect to the x, y, z Cartesian coordinates. These integrals take the following general form:

$$I(m,n;l) = \int_0^\infty \mathrm{J}_m(ap)\,\mathrm{J}_n(rp)\mathrm{e}^{-p|z|}\,p^l\,\mathrm{d}p. \quad \text{(A3.1)}$$

where $\mathrm{J}_m(ap)$ and $\mathrm{J}_n(rp)$ are Bessel functions of the first kind and of integer order m and n respectively and where $m = 1$; $n = 0, 1$; $l = -2, -1, 0$ for the five Lipschitz Hankel integrals shown above.

By inspection, it is evident that only the Bessel function $\mathrm{J}_n(rp)$ in Equation (A3.1) is dependent on the radial coordinate r. Furthermore, since $r = \sqrt{x^2 + y^2}$ then $\frac{\partial r}{\partial x} = x/r$ and $\frac{\partial r}{\partial y} = y/r$, and by the chain rule of partial differentiation:

$$\frac{\partial}{\partial x}I(m,n;l) = \frac{\partial}{\partial r}I(m,n;l)\left(\frac{\partial r}{\partial x}\right) = \left(\frac{x}{r}\right)\frac{\partial}{\partial r}I(m,n;l). \quad \text{(A3.2.1)}$$

$$\frac{\partial}{\partial y}I(m,n;l) = \frac{\partial}{\partial r}I(m,n;l)\left(\frac{\partial r}{\partial y}\right) = \left(\frac{y}{r}\right)\frac{\partial}{\partial r}I(m,n;l). \quad \text{(A3.2.2)}$$

Hence expressions for the x, y partial derivatives of $I(m,n;l)$ may be derived from expressions for its radial or r partial derivative. By inspection, it is evident that only the $\mathrm{J}_0(rp)$ and $\mathrm{J}_1(rp)$ Bessel functions for $n = 0, 1$ respectively in Equation (A3.1) are dependent on r. From Abramowitz and Stegun (1964, equation 9.1.28), the r partial derivative of the Bessel function $\mathrm{J}_0(rp)$ is

$$\frac{\partial}{\partial r}\mathrm{J}_0(rp) = -p\,\mathrm{J}_1(rp), \quad \text{(A3.3.1)}$$

while the r partial derivative of the Bessel function $\mathrm{J}_1(rp)$ is (Abramowitz and Stegun, 1964, Equation 9.1.30),

$$\frac{\partial}{\partial r}\mathrm{J}_1(rp) = p\,\mathrm{J}_0(rp) - \frac{1}{r}\mathrm{J}_1(rp). \quad \text{(A3.3.2)}$$

Hence from Equation (A3.3.1) the r partial derivative of the $I(1,0;l)$ integral is given by

$$\frac{\partial}{\partial r}I(1,0;\,l) = \int_0^\infty \mathrm{J}_1(ap)\,\frac{\partial}{\partial r}\mathrm{J}_0(rp)\mathrm{e}^{-p|z|}\,p^l\,\mathrm{d}p$$
$$= \int_0^\infty \mathrm{J}_1(ap)\,-p\,\mathrm{J}_1(rp)\mathrm{e}^{-p|z|}\,p^l\,\mathrm{d}p$$
$$= -\int_0^\infty \mathrm{J}_1(ap)\,\mathrm{J}_1(rp)\mathrm{e}^{-p|z|}\,p^{l+1}\,\mathrm{d}p$$
$$= -I(1,1;l+1). \quad \text{(A3.4.1)}$$

And from Equation (A3.3.2) the r partial derivative of the $I(1,1;l)$ integral is given by

$$\frac{\partial}{\partial r}I(1,1;l) = \int_0^\infty \mathrm{J}_1(ap)\,\frac{\partial}{\partial r}\mathrm{J}_1(rp)\mathrm{e}^{-p|z|}\,p^l\,\mathrm{d}p$$
$$= \int_0^\infty \mathrm{J}_1(ap)\left\{p\,\mathrm{J}_0(rp) - \frac{1}{r}\mathrm{J}_1(rp)\right\}\mathrm{e}^{-p|z|}\,p^l\,\mathrm{d}p$$
$$= \int_0^\infty \mathrm{J}_1(ap)p\,\mathrm{J}_0(rp)\mathrm{e}^{-p|z|}\,p^l\,\mathrm{d}p$$
$$-\int_0^\infty \mathrm{J}_1(ap)\frac{1}{r}\mathrm{J}_1(rp)\mathrm{e}^{-p|z|}\,p^l\,\mathrm{d}p,$$

and therefore,

$$\frac{\partial}{\partial r}I(1,1;l) = \int_0^\infty \mathrm{J}_1(ap)\mathrm{J}_0(rp)\mathrm{e}^{-p|z|}\,p^{l+1}\,\mathrm{d}p - \frac{1}{r}\int_0^\infty \mathrm{J}_1(ap)\,\mathrm{J}_1(rp)\mathrm{e}^{-p|z|}\,p^{l}\,\mathrm{d}p, \text{ or}$$

$$\frac{\partial}{\partial r}I(1,1;l) = I(1,0;l+1) - \frac{1}{r}I(1,1;l) \text{ for } l = -2,\ -1,\ 0. \tag{A3.4.2}$$

The expressions for the r partial derivatives of Lipschitz–Hankel integrals $I(1,0;-2)$, $I(1,0;-1)$, $I(1,1;-1)$, $I(1,0;0)$ and $I(1,0;0)$ may now be written from equations (A3.4.1) and (A3.4.2). First for the three Lipschitz–Hankel integrals involving Equation (A3.4.1) where $n = 0$ and $l = -2,\ -1,\ 0$ respectively,

$$\frac{\partial}{\partial r}I(1,0;-2) = -I(1,1;-1). \tag{A3.5.1}$$

$$\frac{\partial}{\partial r}I(1,0;-1) = -I(1,1;0). \tag{A3.5.2}$$

$$\frac{\partial}{\partial r}I(1,0;0) = -I(1,1;1). \tag{A3.5.3}$$

And second for the pair of Lipschitz–Hankel integrals involving Equation (A3.4.2) where $n = 1$ and $l = -1, 0$

$$\frac{\partial}{\partial r}I(1,1;-1) = I(1,0;0) - \frac{1}{r}I(1,1;-1). \tag{A3.5.4}$$

$$\frac{\partial}{\partial r}I(1,1;0) = I(1,0;1) - \frac{1}{r}I(1,1;0). \tag{A3.5.5}$$

The expressions for the z partial derivatives are straightforward since only the exponential term $\exp(-p|z|)$ in the $I(m,n;l)$ Lipschitz–Hankel integral is dependent on z. Since $\frac{\partial|z|}{\partial z} = -1$ for $z < 0$, the expression for the z partial derivative of $\exp(-p|z|)$ is $p\exp(-p|z|)$. Therefore,

$$\frac{\partial}{\partial z}I(m,n;l) = \int_0^\infty \mathrm{J}_m(ap)\,\frac{\partial}{\partial r}\mathrm{J}_n(rp)p^l\,\frac{\partial}{\partial z}\mathrm{e}^{-p|z|}\,\mathrm{d}p = \int_0^\infty \mathrm{J}_m(ap)\mathrm{J}_n(rp)p^{l+1}\mathrm{e}^{-p|z|}\,\mathrm{d}p, = I(m,n;l+1)\,; m = 1; n = 0,\ 1\,; l = -2,-1,\ 0, \ldots \tag{A3.6}$$

Hence from Equation (A3.6)

$$\frac{\partial}{\partial z}I(1,0;-2) = I(1,0;-1) \text{ for } m = 1,\ n = 0;\ l = -2. \tag{A3.7.1}$$

$$\frac{\partial}{\partial z}I(1,0;-1) = I(1,0;0) \text{ for } m = 1,\ n = 0;\ l = -1. \tag{A3.7.2}$$

$$\frac{\partial}{\partial z}I(1,1;-1) = I(1,1;0) \text{ for } m = 1,\ n = 1;\ l = -1. \tag{A3.7.3}$$

$$\frac{\partial}{\partial z}I(1,0;0) = I(1,0;1) \text{ for } m = 1,\ n = 0;\ l = 0. \tag{A3.7.4}$$

$$\frac{\partial}{\partial z}I(1,1;0) = I(1,1;1) \text{ for } m = 1,\ n = 1;\ l = 0. \tag{A3.7.5}$$

Appendix 4: Evaluation of the Lipschitz–Hankel integrals for small *r/a* including *r* = 0.

The general form of the Lipschitz–Hankel integral $I(\mu,\nu;\lambda)$ is defined by Eason, Noble, and Sneddon (1955) as:

$$I(\mu,\nu;\lambda) = \int_0^\infty \mathrm{J}_\mu(at)\,\mathrm{J}_\nu(bt)\mathrm{e}^{-ct}\,t^\lambda\,\mathrm{d}t, \tag{A4.1}$$

where $\mathrm{J}_\mu(at)$ and $\mathrm{J}_\nu(bt)$ are Bessel functions of the first kind with order μ and ν respectively. A necessary condition for the convergence of the $I(\mu,\nu;\lambda)$ integral is that $\mu - \nu + \lambda > -1$ (Eason, Noble, and Sneddon 1955). An alternative form of Equation (A4.1) is (Eason *et al.*, 1955, equation 1.2)

$$J(\mu,\nu;\lambda) = \int_0^\infty \mathrm{J}_\mu(\xi)\mathrm{J}_\nu(\rho\xi)\mathrm{e}^{-\zeta\xi}\xi^\lambda\,\mathrm{d}\xi, \tag{A4.2}$$

where $\rho = b/a, \zeta = c/a, \xi = at$, and therefore,

$$I(\mu,\nu;\lambda) = a^{-\lambda-1}J(\mu,\nu;\lambda). \tag{A4.3}$$

The parameters b and c in Equation (A4.2) are equivalent to r and $|z|$ respectively in Equation (1) of this paper so that $\rho = r/a$ and $\zeta = |z|/a$.

The Lipschitz–Hankel integrals which appear in the expressions for the magnetic scalar potential, the magnetic field vector and the magnetic gradient tensor have integer values for $\mu,\ \nu;\ \lambda$. Therefore, I shall adopt the notation of Eason, Noble, and Sneddon (1955) where $m,n;l$ replace $\mu,\nu;\lambda$ respectively in equations (A4.1)−(A4.3). Hence

$$I(m,n;l) = a^{-l-1}J(m,n;l) \quad (\text{for } m - n + l > -1). \tag{A4.4}$$

When the parameter $\rho = r/a$ is small, then the $\mathrm{J}_\nu(\rho\xi)$ Bessel function in Equation (A4.2) may be replaced by its series expansion (Eason, Noble, and Sneddon 1955, 535), namely,

$$J(m,n;l) = \frac{\rho^n}{2^n n!}\left\{j(m;l+n) - \frac{\rho^2}{4(n+1)}j(m;l+n+2) + \ldots\right\}, \tag{A4.5}$$

$$\text{where } j(m;q) = \int_0^\infty \mathrm{J}_m(\xi)\xi^q\,\mathrm{e}^{-\zeta\xi}\,\mathrm{d}\xi. \tag{A4.6}$$

The integrals $j(m;q)$ have been evaluated by Watson (1943, 386) for various integer values of m and q. Eason, Noble, and Sneddon (1955, 535) have listed formulae for calculating many of these integrals. These formulae are used to derive approximate expressions for the Lipschitz–Hankel integrals which appear in the equations for the magnetic scalar potential, the magnetic field vector and the magnetic gradient tensor. In particular for small $\rho = r/a$ and $\zeta = |z|/a$,

$$J(m,n;-n) = \frac{\left\{\sqrt{1+\zeta^2} - \zeta\right\}^m}{2^n\,n!\sqrt{1+\zeta^2}}\rho^n + \mathrm{O}(\rho^{n+2}). \tag{A4.7.1}$$

$$J(m,n;-n-1) = \frac{\left\{\sqrt{1+\zeta^2} - \zeta\right\}^m}{2^n\,n!m}\rho^n + \mathrm{O}(\rho^{n+2}). \tag{A4.7.2}$$

$$J(m,n;m-n) = \frac{1.3\ \ldots\ (2m-1)}{2^n\,n!\,(1+\zeta^2)^{m+\frac{1}{2}}}\rho^n + \mathrm{O}(\rho^{n+2}). \tag{A4.7.3}$$

$$J(m,n;m-n+1) = \frac{1.3\ \ldots\ (2m+1)\,\zeta}{2^n\,n!\,(1+\zeta^2)^{m+\frac{3}{2}}}\rho^n + \mathrm{O}(\rho^{n+2}), \tag{A4.7.4}$$

$$\text{where } \mathrm{O}(\rho^{n+2}) = -\frac{\rho^{n+2}}{2^{n+2}\,(n+1)!}j(m;l+n+2). \tag{A4.7.5}$$

Substitution of $m = 1$, $n = 0$ and $l = -n-1$ in Equations (A4.4) and (A4.7.2), yields the following expression for $I(1,0;-1)$ when ρ is small

$$I(1,0;-1) = J(1,0;-1) = \left\{\sqrt{1+\zeta^2} - \zeta\right\} + \mathrm{O}(\rho^2).$$

The first higher order $\mathrm{O}(\rho^2)$ term is found from Equation (A4.7.5), so that

$$I(1,0;-1) = J(1,0;-1) \cong \left\{\sqrt{1+\zeta^2} - \zeta\right\} - \frac{\rho^2}{4}j(1;1). \tag{A4.8.1}$$

Substitution of $m = 1$, $n = 1$ and $l = -n = -1$ in Equations (A4.4) and (A4.7.1), yields the following expression for $I(1,1;-1)$ when ρ is small

$$I(1,1;-1) = J(1,1;-1) = \frac{\left\{\sqrt{1+\zeta^2}-\zeta\right\}}{2\sqrt{1+\zeta^2}}\rho + O(\rho^3).$$

The first higher order $O(\rho^3)$ term is found from Equation (4.7.5), so that

$$I(1,1;-1) = J(1,1;-1) \cong \frac{\left\{\sqrt{1+\zeta^2}-\zeta\right\}}{2\sqrt{1+\zeta^2}}\rho - \frac{\rho^3}{16}j(1;2). \tag{A4.8.2}$$

Also for $I(1,1;-1)/r$

$$I(1,1;-1)/r = J(1,1;-1)/r \cong \frac{1}{2a}\left[\frac{\left\{\sqrt{1+\zeta^2}-\zeta\right\}}{\sqrt{1+\zeta^2}} - \frac{\rho^2}{8}j(1;2)\right]. \tag{A4.8.3}$$

Substitution of $m = 1$, $n = 0$ and $l = -n = 0$ in Equations (A4.4) and (A4.7.1), yields the following expression for $I(1,0;0)$ when ρ is small

$$I(1,0;0) = \frac{1}{a}J(1,0;0) = \frac{1}{a}\left[\frac{\left\{\sqrt{1+\zeta^2}-\zeta\right\}}{\sqrt{1+\zeta^2}} + O(\rho^2)\right].$$

The first higher order $O(\rho^2)$ term is found from Equation (4.7.5), so that

$$I(1,0;0) = \frac{1}{a}J(1,0;0) \cong \frac{1}{a}\left[\frac{\left\{\sqrt{1+\zeta^2}-\zeta\right\}}{\sqrt{1+\zeta^2}} - \frac{\rho^2}{4}j(1;2)\right]. \tag{A4.8.4}$$

Substitution of $m = 1, n = 1$ and $l = m - n = 0$ in equations (A4.4) and (A4.7.3), yields the following expression for $I(1,1;0)$ when ρ is small

$$I(1,1;0) = \frac{1}{a}J(1,1;0) = \frac{1}{a}\left[\frac{1}{2(1+\zeta^2)^{3/2}}\rho + O(\rho^3)\right].$$

The first higher order $O(\rho^3)$ term is found from Equation (4.7.5), so that

$$I(1,1;0) = \frac{1}{a}J(1,1;0) \cong \frac{1}{2a}\left[\frac{1}{(1+\zeta^2)^{3/2}}\rho - \frac{\rho^3}{8}j(1;3)\right]. \tag{A4.8.5}$$

Also for $I(1,1;0)/r$

$$I(1,1;0)/r = \frac{1}{a}J(1,1;0)/r \cong \frac{1}{2a^2}\left[\frac{1}{(1+\zeta^2)^{3/2}} - \frac{\rho^2}{8}j(1;3)\right]. \tag{A4.8.6}$$

Substitution of $m = 1, n = 0$ and $l = m - n = 1$ in equations (A4.4) and (A4.7.3), yields the following expression for $I(1,0;1)$ when ρ is small

$$I(1,0;1) = \frac{1}{a^2}J(1,0;1) = \frac{1}{a^2}\left[\frac{1}{(1+\zeta^2)^{3/2}} + O(\rho^2)\right].$$

The first higher order $O(\rho^2)$ term is found from Equation (4.7.5), so that

$$I(1,0;1) = \frac{1}{a^2}J(1,0;1) \cong \frac{1}{a^2}\left[\frac{1}{(1+\zeta^2)^{3/2}} - \frac{\rho^2}{4}j(1;3)\right]. \tag{A4.8.7}$$

Substitution of $m = 1$, $n = 1$ and $l = m - n + 1 = 1$ in Equations (A4.4) and (A4.7.4), yields the following expression for $I(1,1;1)$ when ρ is small

$$I(1,1;1) = \frac{1}{a^2}J(1,1;1) = \frac{1}{a^2}\left[\frac{3\zeta}{2(1+\zeta^2)^{5/2}}\rho + O(\rho^3)\right].$$

The first higher order $O(\rho^3)$ term is found from Equation (4.7.5), so that

$$I(1,1;1) = \frac{1}{a^2}J(1,1;1) \cong \frac{1}{2a^2}\left[\frac{3\zeta}{(1+\zeta^2)^{5/2}}\rho - \frac{\rho^3}{8}j(1;4)\right]. \tag{A4.8.8}$$

Lipschitz–Hankel integrals at axial measurement points on and above a vertical cylinder

The series expansions for the Lipschitz–Hankel integrals developed in Equations (A4.8.1)–(A4.8.8) may now be used to derive expressions for the Lipschitz–Hankel integrals at axial measurement points by setting $\rho = r/a = 0$ and $\zeta = |z|/a$. From Equation (A4.8.1), the expression for the $I(1,0;-1)$ Lipschitz–Hankel integral at an axial station P(0,0,z) is

$$I(1,0;-1) = \left[\sqrt{1+\zeta^2}-\zeta\right] = \frac{1}{a}\left[\sqrt{z^2+a^2}-|z|\right] \text{ (for } r = 0). \tag{A4.9.1}$$

and at the origin on the top surface of the cylinder

$$I(1,0;-1) = 1 \quad (\text{for } r = 0, z = 0). \tag{A4.9.2}$$

From Equation (A4.8.2), the expression for the $I(1;1;-1)$ Lipschitz–Hankel integral at an axial station P(0,0,z) including the origin is

$$I(1,1;-1) = 0 \quad (\text{for } r = 0, z \le 0). \tag{A4.9.3}$$

From Equation (A4.8.4), the expression for the $I(1,0;0)$ Lipschitz–Hankel integral at an axial station P(0,0,z) is

$$I(1,0;0) = \frac{1}{a}\left[1 - \frac{\zeta}{\sqrt{1+\zeta^2}}\right] = \frac{1}{a}\left[1 - \frac{z}{\sqrt{z^2+a^2}}\right]. \tag{A4.9.4}$$

And at the origin on the top surface of the cylinder

$$I(1,0;0) = \frac{1}{a} \quad (\text{for } r = 0, z = 0). \tag{A4.9.5}$$

Also from Equation (A4.8.3) the expression for $I(1,1;-1)/r$ at an axial station P(0,0,z) is

$$I(1,1;-1)/r = \frac{1}{2a}\left[1 - \frac{\zeta}{\sqrt{1+\zeta^2}}\right] = \frac{1}{2a}\left[1 - \frac{z}{\sqrt{z^2+a^2}}\right], = \frac{1}{2}I(1,0;0). \tag{A4.9.6}$$

And at the origin on the top surface of the cylinder

$$I(1,1;-1)/r = \frac{1}{2a} = \frac{1}{2}I(1,0;0) \quad (\text{for } r = 0, z = 0). \tag{A4.9.7}$$

From Equation (A4.8.5), the expression for the Lipschitz–Hankel integral $I(1;1;0)$ at an axial station P(0,0,z) including the origin is

$$I(1;1;0) = 0 \quad (\text{for } r = 0, z \le 0). \tag{A4.9.8}$$

And from Equation (A4.8.6), the expression for $I(1,1;0)/r$ at an axial station P(0,0,z) is

$$I(1,1;0)/r = \frac{1}{2a^2}\left[\frac{1}{(1+\zeta^2)^{3/2}}\right] = \left[\frac{a}{2(z^2+a^2)^{3/2}}\right]. \tag{A4.9.9}$$

And at the origin on the top surface of the cylinder

$$I(1,1;\,0)/r = \frac{1}{2a^2} \quad (\text{for } r=0, z=0). \tag{A4.9.10}$$

From Equation (A4.8.7), the expression for $I(1,0;\,1)$ at an axial station P(0,0,*z*) is

$$I(1,0;\,1) = \frac{1}{a^2}\left[\frac{1}{(1+\zeta^2)^{3/2}}\right] = \left[\frac{a}{(z^2+a^2)^{3/2}}\right],$$
$$= \frac{2}{r} I(1,1;\,0)\,. \tag{A4.9.11}$$

And at the origin on the top surface of the cylinder

$$I(1,0;\,1) = \frac{1}{a^2} = \frac{2}{r} I(1,1;\,0) \quad (\text{for } r=0, z=0). \tag{A4.9.12}$$

From Equation (A4.8.8), the expression for $I(1,1;\,1)$ at an axial station P(0,0,*z*) including the origin is

$$I(1,1;\,1) = 0 \quad (\text{for } r=0, z \le 0). \tag{A4.9.13}$$

Appendix 5: Symmetry properties of the magnetic gradient tensor for three for special magnetisation directions

For a magnetisation $\mathbf{M} = |\mathbf{M}|\,\hat{\mathbf{x}} = M\hat{\mathbf{x}}$; $M = M_x$ in the north or *x* direction, the magnetic gradient tensor elements at an observation point $\mathbf{r} = (r,\theta,z)$ are as follows:

$$B_{xx}(\mathbf{r};\mathbf{M}=M\hat{\mathbf{x}})$$
$$= 2\pi a\,\mathrm{C_m}\,M\left\{\cos 3\theta\left[\frac{1}{r}I(1,0;\,0) - \frac{2}{r^2}I(1,1;\,-1)\right]\right.$$
$$\left. +\ \cos^3\theta\, I(1,1;1)\right\}. \tag{A5.1.1}$$

$$B_{xy}(\mathbf{r};\mathbf{M}=M\hat{\mathbf{x}})$$
$$= 2\pi a\,\mathrm{C_m}\,M\left\{\sin 3\theta\left[\frac{1}{r}I(1,0;\,0) - \frac{2}{r^2}I(1,1;\,-1)\right]\right.$$
$$\left. +\ \sin\theta\cos^2\theta\, I(1,1;\,1)\right\},$$
$$= B_{yx}(\mathbf{r};\mathbf{M}=M\hat{\mathbf{x}}). \tag{A5.1.2}$$

$$B_{xz}(\mathbf{r};\mathbf{M}=M\hat{\mathbf{x}})$$
$$= \pi a\,\mathrm{C_m}\,M\left\{\cos 2\theta\left[\frac{2}{r}I(1,1;\,0) - I(1,0;\,1)\right] - I(1,0;\,1)\right\},$$
$$= B_{zx}(\mathbf{r};\mathbf{M}=M\hat{\mathbf{x}}). \tag{A5.1.3}$$

$$B_{yy}(\mathbf{r};\mathbf{M}=M\hat{\mathbf{x}})$$
$$= 2\pi a\,\mathrm{C_m}\,M\left\{-\cos 3\theta\left[\frac{1}{r}I(1,0;\,0) - \frac{2}{r^2}I(1,1;\,-1)\right]\right.$$
$$\left. +\ \cos\theta\sin^2\theta\, I(1,1;\,1)\right\}. \tag{A5.1.4}$$

$$B_{yz}(\mathbf{r};\mathbf{M}=M\hat{\mathbf{x}})$$
$$= \pi a\,\mathrm{C_m}\,M\left\{\sin 2\theta\left[\frac{2}{r}I(1,1;\,0) - I(1,0;\,1)\right]\right\},$$
$$= B_{zy}(\mathbf{r};\mathbf{M}=M\hat{\mathbf{x}}). \tag{A5.1.5}$$

$$B_{zz}(\mathbf{r};\mathbf{M}=M\hat{\mathbf{x}}) = -2\pi a\,\mathrm{C_m}\,M\cos\theta\, I(1,1;\,1). \tag{A5.1.6}$$

For a magnetisation $\mathbf{M} = |\mathbf{M}|\,\hat{\mathbf{y}} = M\hat{\mathbf{y}}$; $M = M_y$ in the east or y direction, the magnetic gradient tensor elements at an observation point $\mathbf{r} = (r,\theta,z)$ are as follows:

$$B_{xx}(\mathbf{r};\mathbf{M}=M\hat{\mathbf{y}})$$
$$= 2\pi a\,\mathrm{C_m}M\left\{\sin 3\theta\left[\frac{1}{r}I(1,0;0) - \frac{2}{r^2}I(1,1;\,-1)\right]\right.$$
$$\left. +\ \sin\theta\cos^2\theta\, I(1,1;1)\right\},$$
$$= B_{xy}(\mathbf{r};\mathbf{M}=M\hat{\mathbf{x}}). \tag{A5.2.1}$$

$$B_{xy}(\mathbf{r};\mathbf{M}=M\hat{\mathbf{y}})$$
$$= 2\pi a\,\mathrm{C_m}M\left\{-\cos 3\theta\left[\frac{1}{r}I(1,0;0) - \frac{2}{r^2}I(1,1;\,-1)\right]\right.$$
$$\left. +\ \cos\theta\sin^2\theta\, I(1,1;1)\right\},$$
$$= B_{yy}(\mathbf{r};\mathbf{M}=M\hat{\mathbf{x}}). \tag{A5.2.2}$$

$$B_{xz}(\mathbf{r};\mathbf{M}=M\hat{\mathbf{y}})$$
$$= \pi a\mathrm{C_m}M\left\{\sin 2\theta\left[\frac{2}{r}I(1,1;0) - I(1,0;1)\right]\right\},$$
$$= B_{yz}(\mathbf{r};\mathbf{M}=M\hat{\mathbf{x}}). \tag{A5.2.3}$$

$$B_{yy}(\mathbf{r};\mathbf{M}=M\hat{\mathbf{y}})$$
$$= 2\pi a\,\mathrm{C_m}\,M\left\{-\sin 3\theta\left[\frac{1}{r}I(1,0;0) - \frac{2}{r^2}I(1,1;\,-1)\right]\right.$$
$$\left. +\ \sin^3\theta\, I(1,1;1)\right\}. \tag{A5.2.4}$$

$$B_{yz}(\mathbf{r};\mathbf{M}=M\hat{\mathbf{y}})$$
$$= \pi a\,\mathrm{C_m}\,M\left\{-\cos 2\theta\left[\frac{2}{r}I(1,1;0) - I(1,0;1)\right] - I(1,0;1)\right\}. \tag{A5.2.5}$$

$$B_{zz}(\mathbf{r};\mathbf{M}=M\hat{\mathbf{y}}) = -2\pi a\,\mathrm{C_m}\,M\sin\theta\, I(1,1;\,1). \tag{A5.2.6}$$

For a magnetisation $\mathbf{M} = |\mathbf{M}|\hat{\mathbf{z}} = M\hat{\mathbf{z}}$; $M = M_z$ in the downward vertical or z direction, the magnetic gradient tensor elements at an observation point $\mathbf{r} = (r,\theta,z)$ are as follows:

$$B_{xx}(\mathbf{r};\mathbf{M}=M\hat{\mathbf{z}})$$
$$= \pi a\,\mathrm{C_m}\,M\left\{\cos 2\theta\left[\frac{2}{r}I(1,1;0) - I(1,0;1)\right] - I(1,0;1)\right\},$$
$$= B_{xz}(r;\mathbf{M}=M\hat{\mathbf{x}}). \tag{A5.3.1}$$

$$B_{xy}(\mathbf{r};\mathbf{M}=M\hat{\mathbf{z}})$$
$$= \pi a\,\mathrm{C_m}\,M\sin 2\theta\left[\frac{2}{r}I(1,1;0) - I(1,0;1)\right],$$
$$= B_{yz}(\mathbf{r};\mathbf{M}=M\hat{\mathbf{x}}) = B_{xz}(\mathbf{r};\mathbf{M}=M\hat{\mathbf{y}}). \tag{A5.3.2}$$

$$B_{xz}(\mathbf{r};\mathbf{M}=M\hat{\mathbf{z}})$$
$$= -2\pi a\,\mathrm{C_m}\,M\cos\theta\, I(1,1;1)\,, = B_{zz}(\mathbf{r};\mathbf{M}=M\hat{\mathbf{x}}). \tag{A5.3.3}$$

$$B_{yy}(\mathbf{r};\mathbf{M}=M\hat{\mathbf{z}})$$
$$= \pi a\,\mathrm{C_m}M\left\{-\cos 2\theta\left[\frac{2}{r}I(1,1;0) - I(1,0;1)\right] - I(1,0;1)\right\},$$
$$= B_{yz}(\mathbf{r};\mathbf{M}=M\hat{\mathbf{y}}). \tag{A5.3.4}$$

$$B_{yz}(\mathbf{r};\mathbf{M}=M\hat{\mathbf{z}})$$
$$= -2\pi a\,\mathrm{C_m}\,M\sin\theta\, I(1,1;1)\,, = B_{zz}(\mathbf{r};\mathbf{M}=M\hat{\mathbf{y}}). \tag{A5.3.5}$$

$$B_{zz}(\mathbf{r};\mathbf{M}=M\hat{\mathbf{z}}) = 2\pi a\,\mathrm{C_m}M_z\, I(1,0;1). \tag{A5.3.6}$$

The expressions for $\mathbf{B}(\mathbf{r};\mathbf{M}=M\hat{\mathbf{x}})$ in equations (A5.1.1)-(A5.1.6) represent those for the magnetic gradient tensor $\mathbf{B}(\mathbf{r})$ reduced to the equator (RTE) while the expressions for $\mathbf{B}(\mathbf{r};\mathbf{M}=M\hat{\mathbf{z}})$ in equations (A5.3.1)-(A5.3.6) represent those

for the magnetic gradient tensor $\mathbf{B}(\mathbf{r})$ reduced to the north magnetic pole (RTP).

In addition to the symmetry relations derived here and detailed previously in this paper, I also note that it is possible to define six symmetry classes for the set of tensor elements (18 in all) shown in Equations (A5.1.1)–(A5.1.6), (A5.2.1)–(A5.2.6), (A5.3.1)–(A5.3.6). The characteristics of these six symmetry classes are outlined in detail in Table 4.

Table 4. Image symmetry classes for the gradient tensor elements $B_{xx}, B_{xy}, B_{xz}, B_{yy}, B_{yz}, B_{zz}$ due to a semi-infinite right circular vertical cylinder with magnetisation intensity $M = 1\ \mathrm{Am}^{-1}$ along three orthogonal directions, i.e. $\mathbf{M} = \mathrm{M}\hat{\mathbf{x}}, \mathbf{M} = \mathrm{M}\hat{\mathbf{y}}, \mathbf{M} = \mathrm{M}\hat{\mathbf{z}}$ respectively. The notation is B_{xx}^{Mx} short for tensor element $B_{xx}(\mathbf{r}; \mathbf{M} = \mathrm{M}\hat{\mathbf{x}})$ and so on.

Image symmetry class	Gradient tensor elements	Lines of symmetry	Moment direction	Min–Max range (nT/m)	Image pattern
1A	B_{xx}^{Mx}	0°	0°	±2.4704	S–N dipole antisymmetric across the centre
1B	B_{yy}^{My}	090°	090°	±2.4704	W–E dipole antisymmetric across the centre
2A	B_{yy}^{Mx} , B_{xy}^{My}	0°	0°	±0.9345	S–N major dipole antisymmetric across centre with a pair of N–S minor dipoles equidistant from the centre
2B	B_{xx}^{My} , B_{xy}^{Mx}	090°	090°	±0.9345	W–E major dipole antisymmetric across centre with a pair of E–W minor dipoles equidistant from the centre
3A	B_{xz}^{Mx} , B_{xx}^{Mz}	0°, 090°	0°, 180°	−2.2479, 1.3372	Pair of S–N and N–S opposed dipoles which emanate from a global minimum at the centre
3B	B_{yz}^{My} , B_{yy}^{Mz}	0°,090°	090°, 270°	−2.2479, 1.3372	Pair of W–E and E–W opposed dipoles which emanate from a global minimum at the centre
4	B_{yz}^{Mx} , B_{xz}^{My} , B_{xy}^{Mz}	045°, 135°	0°, 180°; 090°, 270°	±1.2443	Quadrupole: pairs of opposed S–N and W–E dipoles equidistant from the centre
5A	B_{zz}^{Mx} , B_{xz}^{Mz}	0°	180°	±3.3135	N–S dipole antisymmetric across the centre
5B	B_{zz}^{My} , B_{yz}^{Mz}	090°	270°	±3.3135	E–W dipole antisymmetric across the centre
6	B_{zz}^{Mz}	all	all	−0.4550, 4.9509	Point pole with radial symmetry about a central maximum